



NOVEL CATALYTIC MATERIALS AND STRATEGIES FOR HYDROGEN PRODUCTION AND HYDROGENATION REACTIONS BASED ON PEM ELECTROLYSIS

Jordi Ampurdanés Vilanova

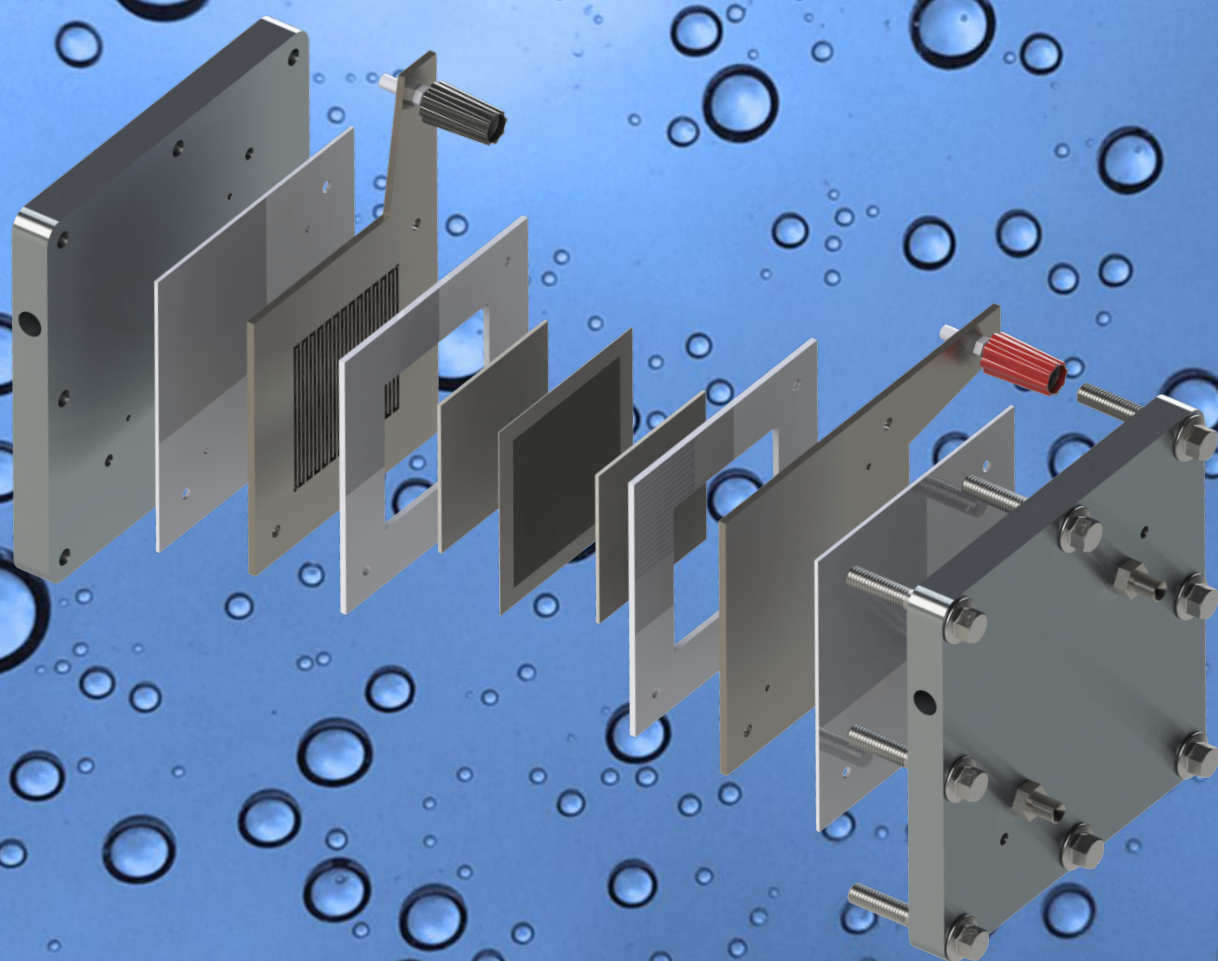
Dipòsit Legal: T 85-2015

ADVERTIMENT. L'accés als continguts d'aquesta tesi doctoral i la seva utilització ha de respectar els drets de la persona autora. Pot ser utilitzada per a consulta o estudi personal, així com en activitats o materials d'investigació i docència en els termes establerts a l'art. 32 del Text Refós de la Llei de Propietat Intel·lectual (RDL 1/1996). Per altres utilitzacions es requereix l'autorització prèvia i expressa de la persona autora. En qualsevol cas, en la utilització dels seus continguts caldrà indicar de forma clara el nom i cognoms de la persona autora i el títol de la tesi doctoral. No s'autoritza la seva reproducció o altres formes d'explotació efectuades amb finalitats de lucre ni la seva comunicació pública des d'un lloc aliè al servei TDX. Tampoc s'autoritza la presentació del seu contingut en una finestra o marc aliè a TDX (framing). Aquesta reserva de drets afecta tant als continguts de la tesi com als seus resums i índexs.

ADVERTENCIA. El acceso a los contenidos de esta tesis doctoral y su utilización debe respetar los derechos de la persona autora. Puede ser utilizada para consulta o estudio personal, así como en actividades o materiales de investigación y docencia en los términos establecidos en el art. 32 del Texto Refundido de la Ley de Propiedad Intelectual (RDL 1/1996). Para otros usos se requiere la autorización previa y expresa de la persona autora. En cualquier caso, en la utilización de sus contenidos se deberá indicar de forma clara el nombre y apellidos de la persona autora y el título de la tesis doctoral. No se autoriza su reproducción u otras formas de explotación efectuadas con fines lucrativos ni su comunicación pública desde un sitio ajeno al servicio TDR. Tampoco se autoriza la presentación de su contenido en una ventana o marco ajeno a TDR (framing). Esta reserva de derechos afecta tanto al contenido de la tesis como a sus resúmenes e índices.

WARNING. Access to the contents of this doctoral thesis and its use must respect the rights of the author. It can be used for reference or private study, as well as research and learning activities or materials in the terms established by the 32nd article of the Spanish Consolidated Copyright Act (RDL 1/1996). Express and previous authorization of the author is required for any other uses. In any case, when using its content, full name of the author and title of the thesis must be clearly indicated. Reproduction or other forms of for profit use or public communication from outside TDX service is not allowed. Presentation of its content in a window or frame external to TDX (framing) is not authorized either. These rights affect both the content of the thesis and its abstracts and indexes.

NOVEL CATALYTIC MATERIALS AND STRATEGIES FOR HYDROGEN PRODUCTION AND HYDROGENATION REACTIONS BASED ON PEM ELECTROLYSIS



UNIVERSITAT
ROVIRA I VIRGILI

JORDI AMPURDANÉS VILANOVA
Doctoral Thesis 2014

DOCTORAL THESIS

Novel Catalytic Materials and Strategies for Hydrogen Production and Hydrogenation Reactions based on PEM Electrolysis

JORDI AMPURDANÉS VILANOVA

Supervised by:

Dr. Atsushi Urakawa

ICIQ-URV



UNIVERSITAT ROVIRA I VIRGILI

Tarragona

2014

UNIVERSITAT ROVIRA I VIRGILI

NOVEL CATALYTIC MATERIALS AND STRATEGIES FOR HYDROGEN PRODUCTION AND HYDROGENATION REACTIONS BASED ON PEM ELECTROLYSIS

Jordi Ampurdanés Vilanova

Dipòsit Legal: T 85-2015



UNIVERSITAT
ROVIRA I VIRGILI

DEPARTAMENT DE QUÍMICA FÍSICA
I INORGÀNICA

Campus Sescelades
Marcel·lí Domingo, s/n
43007 Tarragona
Tel. +34 977 55 81 37
Fax +34 977 55 95 63
www.quimica.urv.es



I STATE that the present study, entitled “Novel Catalytic Materials and Strategies for Hydrogen Production and Hydrogenation Reactions based on PEM Electrolysis”, presented by Jordi Ampurdanés Vilanova for the award of the degree of Doctor, has been carried out under my supervision at the Institute of Chemical Research of Catalonia.

Tarragona, 16th October 2014

Doctoral Thesis Supervisor

浦川 篤

Atsushi Urakawa

UNIVERSITAT ROVIRA I VIRGILI

NOVEL CATALYTIC MATERIALS AND STRATEGIES FOR HYDROGEN PRODUCTION AND HYDROGENATION REACTIONS BASED ON PEM ELECTROLYSIS

Jordi Ampurdanés Vilanova

Dipòsit Legal: T 85-2015

ACKNOWLEDGEMENTS

Firstly, I would like to thank my supervisor, Dr. Atsushi Urakawa, for giving me the chance to undertake my doctoral studies in his new-born group in 2010. Since I started he has always supported me and my work without hesitating. I am really glad to have been under his guidance during this time. My deepest gratitude to him for trusting in me and in my capabilities even when I didn't, for all the knowledge that I acquired, for the scientific and non-scientific discussions we had and, most importantly, for his sincerity and optimism. Moreover, I would like to give him thanks for the opportunity I had to visit Japan during my PhD.

Secondly, thanks to all former/current lab-mates I had during this long journey, without their help and support this work wouldn't have been possible. Most importantly, I will never forget their unlimited human qualities; I don't have enough words to describe their unique capabilities. Starting from the very beginning, Antonio "Chut" Bazzo (my non-recognized Italian brother) and Atul Bansode (the most unique Indian guy I have ever met), many thanks from the bottom of my heart, you have been like my second family during this time, all I have learnt from you is my real PhD. Many thanks also to Noelia "Mami" Barrabés since without her mediation and power of conviction I would have never started the PhD and also for sharing her scientific and life experience. On this huge podium of very special people, (Piri)Dina Fakhrnasova (the little sister I never had) has a very special position; although small in size, a great person is inside her, thank you very much for your help, knives, Russian lessons, amazing dinners and pizza times we shared together. I also would like to express my gratitude to another very special lady; in fact, the smartest lady I have ever met, Tachmajal Corrales,

Ta; since part of this work was built hand in hand with her, suffering together in tough situations as well as enjoying as much as possible in the good moments. A special mention also to all the new generation of PhD and postdocs I had the chance to meet and work with: Sergio Lima, Luis, Dragos (great man and best friend), Sergio (small) Roso, Rezza, Marta and Tsuyoshi Hyakutake (Donquixote Doflamingo); it has been my pleasure to work with you. Furthermore, my only desk-neighbour during these 4 years, Rohit (aka "Happyman" or "Anna"), requires Cum Laude score because of his human skills and his unbeatable way to enjoy life. I will never forget our very unique Korean colleague, Jong-Ki Choi, either.

I would like to express my sincere gratitude to the ICIQ and its staff as a whole (scientific and non-scientific). Special thanks go to the technical/scientific support for accommodating the most unusual requests and providing constant support. In particular, I am really grateful to Miguel Gonzalez for his support whenever it was required. Also thanks to the Chemical Reaction Technology and Chromatography units crews for their great job and highly professional help.

Les meves gràcies de tot cor als dos grans artesans de l'ICIQ, José Luis León i Xavier Asensio, sens dubte les dues persones més imprescindibles de la família. La seva implicació i ganes d'ajudar a solucionar problemes han estat d'un valor únic i insuperable, és més, han estat capaços de fer possible l'impossible. Sense la seva dedicació res del que s'exposa en aquest treball hagués estat real. Per antiguitat i per amistat, m'agradaria donar encara més les gràcies, si és possible, al José Luis, per totes les hores que hem compartit al taller mecànic (la meva segona residència), ja sigui treballant o comentant la jugada, ets un gran entre els grans!

Matrícula d'honor, també, pels grans mestres del repartiment (logística) dels que disposem al centre, el Marc (Deportivo Curaçao) i el Jesús (4-1), amb els que he tingut el plaer de treballar, i el que és més important, parlar i riure del que sigui, on sigui i quan sigui; gràcies per tot, sou uns cracks!

És un plaer donar la meva gratitud a tots els amics que he fet durant aquests anys a l'ICIQ ja siguin de diferents laboratoris, planta o edifici (Pep, Basti, John, Ximo "Moha" Soriano, Dolores, Isra, Bárbara....); no sé si són molt o pocs, però si que són d'una qualitat única. També, la meva més sincera gratitud tant a l'Aurora com a l'Íngrid per tota la seva implicació en temes no científics i de caire burocràtic, així com la seva continua cordialitat i predisposició a ajudar. Gràcies al Raúl Calavia per la seva ajuda incondicional i desinteressada sempre que ha estat requerida; al mateix temps, gràcies al servei de microscòpia de la URV per tota la seva col·laboració.

Menció fora de categoria per a tots els amics de Tarragona (David, Jordi-Enric, Juanmi, Ferran, Jose, Katie, Pili, Adri, Rabas, Víctor, Luci....) que m'han acompanyat tant en els bons com en els mals moments durant aquests darrers 4 anys; senyors/es va per vosaltres! Wan De Fu forever! Mil milions de gràcies també al grup d'amics més autèntic de la història, *el Lokal*, i a la totalitat dels seus components, especialment, al Rossi, Ariadna, Guille, Albert, Sabas, Naxo, Pol, Pepu, Chema, Teti, Meri i Ori per sempre estar allà quan se us ha necessitat, quan un gest val més que mil paraules es el vostre lema! Mini gràcies a la petita Janna també.

No me olvido de la comunidad científico-lúdica residente en Ginebra liderada por Gastón A. Crespo, al que nunca podré agradecer todo el apoyo, consejos y

amistad que me ha dado desde que, por casualidades de la vida, se cruzaron nuestros caminos. Gracias, otra vez, a Noe (y a la pequeña Valentina) por ser de estas pocas personas que te dan la mano sin pedir nada a cambio.

Finalment, però no menys important, gràcies a la meva família composta per mare (Dolors), tiet (Ramón), àvia (Núria), germà (Marc) i cunyada (Elena) per confiar en mi, animar-me i ajudar-me sempre que ho he necessitat. Part d'aquesta tesis també és vostra.

ICIQ foundation and Ministerio de Economía y Competitividad (MINECO) are greatly acknowledged for financial support, making this doctoral project possible.



UNIVERSITAT ROVIRA I VIRGILI

NOVEL CATALYTIC MATERIALS AND STRATEGIES FOR HYDROGEN PRODUCTION AND HYDROGENATION REACTIONS BASED ON PEM ELECTROLYSIS

Jordi Ampurdanés Vilanova

Dipòsit Legal: T 85-2015

UNIVERSITAT ROVIRA I VIRGILI

NOVEL CATALYTIC MATERIALS AND STRATEGIES FOR HYDROGEN PRODUCTION AND HYDROGENATION REACTIONS BASED ON PEM ELECTROLYSIS

Jordi Ampurdanés Vilanova

Dipòsit Legal: T 85-2015

Table of contents

CHAPTER 1: INTRODUCTION	1
1.1 Hydrogen as Alternative Fuel	2
1.1.1 The Hydrogen Economy	2
1.1.2 Steam Reforming of Fossil Fuels for Hydrogen Production	4
1.2 Water Splitting for Large Scale Hydrogen Production	6
1.2.1 Thermochemical Water Splitting	7
1.2.2 Electrochemical Water Splitting	9
1.2.2.1 Thermodynamics & Electrochemistry of Water Splitting	11
1.2.2.2 Applications of H ₂ Produced via Electrolysis	15
1.3 PEM Electrolysis Technology	16
1.3.1 Background	16
1.3.2 High Temperature Electrolysis	19
1.3.3 Perspectives	19
1.4 Hydrogenation Reactions for Nitrate Abatement	20
1.5 Motivation and Aim of this Thesis	23
BIBLIOGRAPHY	26
CHAPTER 2: METHODS AND SYSTEMS	29
2.1 Catalysts Synthesis	30
2.1.1 Support Preparation	32
2.1.1.1 Tin (IV) Oxide (SnO ₂)	32
2.1.1.2 Carbon Support (Vulcan)	34
2.1.2 Catalyst Preparation	34
2.1.2.1 Wet Impregnation	34
2.1.2.2 Ultrasonic Metal Reduction and Deposition	37
2.1.2.3 Mechanical Mixing	39

2.2 MEA Preparation.....	39
2.2.1 Polymer Electrolyte Membrane Pre-Treatment.....	39
2.2.2 Catalyst Ink Preparation	40
2.2.3 Catalyst Deposition.....	41
2.3 Electrochemical Reaction Setup	45
2.3.1 Background.....	45
2.3.2 Electrocatalytic (PEM) Reactor	46
2.3.3 Reaction Systems and Methods	48
2.3.3.1 PEM Electrolyser Configuration	48
2.3.3.2 Electrolysis-Assisted Nitrate Reduction Configuration	50
2.4 Analytical System.....	52
2.4.1 Ion Chromatography (IC)	53
2.4.2 Mass Spectrometry (MS)	55
BIBLIOGRAPHY.....	56

CHAPTER 3: MoS₂-BASED MATERIALS AS ALTERNATIVE CATHODE CATALYST FOR PEM ELECTROLYSIS

59

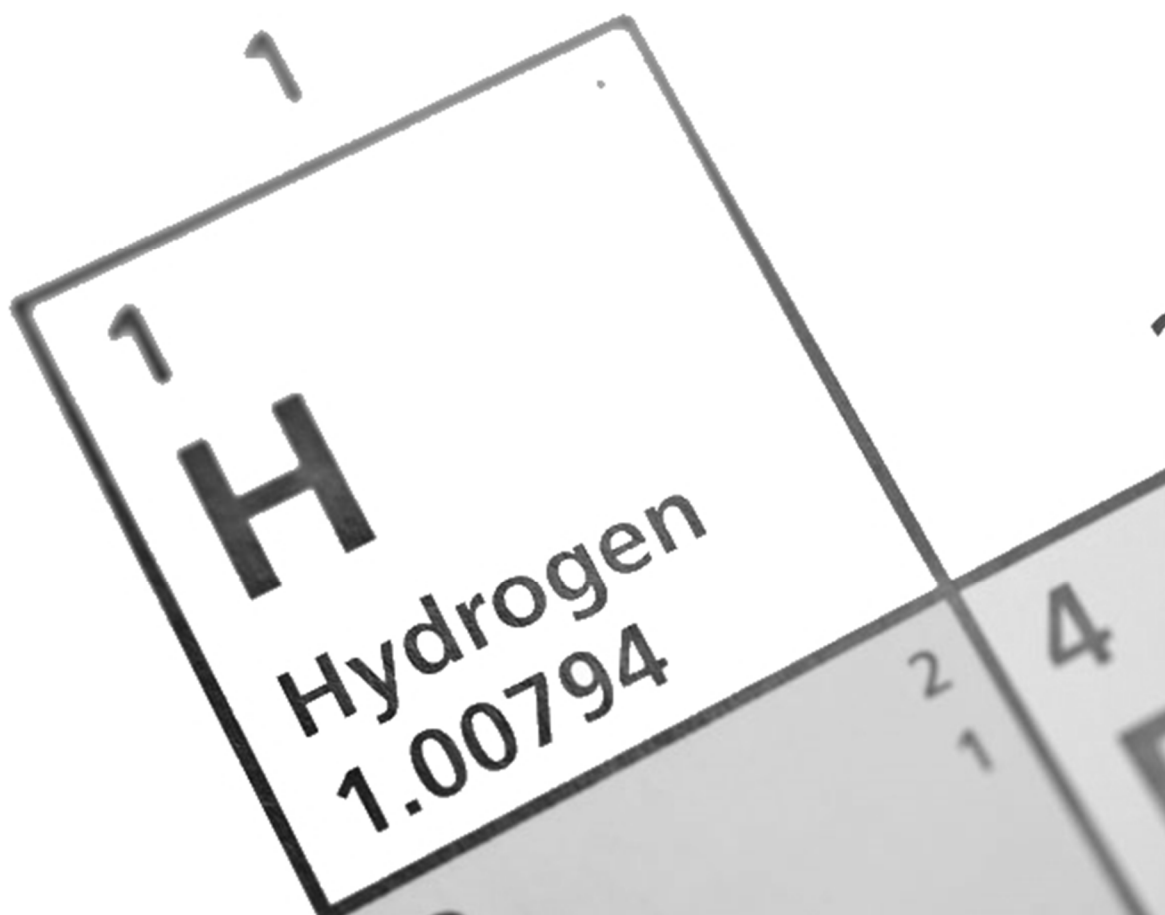
3.1 Introduction.....	60
3.1.1 Aim of the Study	61
3.2 From Electrical Current to H₂ and O₂ Production.....	62
3.3 Materials	64
3.3.1 MoS ₂ Mixed with Carbon Material.....	64
3.3.2 MoS ₂ Nanoparticles Deposited on Reduced Graphene Oxide (MoS ₂ /RGO).....	64
3.4 MEA Preparation and PEM Electrolysis	66
3.5 Electrolyser Performance.....	66
3.5.1 Hybrid MoS ₂ /RGO Characterization	66
3.5.2 Performance of MoS ₂ /Carbon.....	67
3.5.3 Performance of MoS ₂ /RGO	70
3.5.4 Effect of Hot-Press.....	71
3.5.5 Stability Tests	73

3.6 Conclusions	75
BIBLIOGRAPHY	77
CHAPTER 4: CO₃O₄ FOR HIGH POTENTIAL PEM ELECTROLYSIS	79
4.1 Introduction	80
4.1.1 Aim of the Study	82
4.2 Materials	83
4.2.1 Co ₃ O ₄ Mixed with Carbon Material	83
4.3 MEA Preparation.....	84
4.4 System Configuration.....	84
4.5 Results.....	85
4.5.1 Performance of Co ₃ O ₄ /Carbon.....	85
4.5.1.1 Low Potential Electrolysis.....	86
4.5.1.2 High Potential Electrolysis.....	88
4.5.2 Stability Tests	91
4.6 Conclusions	93
BIBLIOGRAPHY	95
CHAPTER 5: CONTINUOUS ELECTROLYSIS-ASSISTED NITRATE REDUCTION ____	97
5.1 Introduction.....	98
5.1.1 Catalytic and Electrocatalytic Nitrate Reduction	98
5.1.2 Reaction Mechanism and Theoretical Basis.....	101
5.1.3 Aim of the Study	104
5.2 Experimental Section	105
5.2.1 Materials	105
5.2.2 Reaction Setup	107
5.3 System Flexibility	109
5.4 System Performance	110

5.4.1 Catalytic Nitrate Reduction	110
5.4.1.1 Catalytic Activity with pH Buffering	112
5.4.1.2 Catalytic Activity of PdCu/SnO ₂ without pH Buffering	115
5.4.2 Continuous Flow Electrocatalytic Tests	117
5.4.2.1 Potential Sweep Study	117
5.4.2.2 System Flexibility Evaluation	127
5.5 Conclusions	132
BIBLIOGRAPHY	134
CHAPTER 6: ADVANCING NITRATE MITIGATION STRATEGIES	137
6.1 Introduction	138
6.2 Low-Potential Electrolysis-Assisted Batch Operation	139
6.3 NH₄⁺ Abatement Strategies	144
6.3.1 Electrolysis-Assisted Ammonium Oxidation	144
6.3.2 Photocatalytic Ammonium Oxidation	147
6.4 Reduction-Oxidation Cycle	151
6.5 Conclusions	154
BIBLIOGRAPHY	156
CHAPTER 7: SUMMARY AND OUTLOOK	157
7.1 Summary	158
7.2 Outlook	163
7.2.1 Background on CO ₂ Conversion	163
7.2.2 Electrolysis-Assisted CO ₂ Reduction	165
BIBLIOGRAPHY	168
SHORTHANDS AND GLOSSARY	171
LIST OF PUBLICATIONS	175
CURRICULUM VITAE	179

CHAPTER 1

INTRODUCTION



1.1 Hydrogen as Alternative Fuel

Nowadays, in response to population growth and the fast industrialization of developing countries the world's demand for energy is projected to double by 2050 as reported by Hoffert and co-workers in 1998 [1]. The supply of fossil fuels is limited and serious shortage of oil and gas is anticipated within the next decades [2, 3]. With the increasing global energy demand as well as climate changes, suggested to be largely induced by CO₂ emission originating from burning fossil fuels, there is an imminent necessity to find an alternative chemical energy carrier with less carbon footprint to replace fossil fuels.

1.1.1 The Hydrogen Economy

Hydrogen (in Greek “water-former”) is one of the most promising chemical energy carriers [3-6] because it is an energetically rich molecule and only water is produced upon burning. It was first artificially produced in the early 16th century by mixing metals with acids. H₂ is abundant and distributed over the world and it can also serve as raw material to synthesize conveniently transportable liquid fuel such as methanol [7]. However, hydrogen does not naturally occur in nature and efficient hydrogen production is the critical factor towards the “hydrogen economy” which is an energy system based on hydrogen [3]. The chemical energy per mass of hydrogen (142 MJ/kg) is at least three times larger than that of other common chemical fuels (for example, the equivalent value for liquid hydrocarbons is about 47 MJ/kg).

Hydrogen oxidation, producing only water as only by-product, and efficient extraction of its chemical energy in the form of heat and/or electricity are the key

processes to utilize hydrogen as energy carrier. Thus-produced water can be further used as a feedstock for the production of hydrogen with the co-production of high purity oxygen.

Even though hydrogen is the chemical of central importance in the current chemical industry, greater efforts are required to use it as common fuel. Global efforts towards hydrogen economy have been witnessed, particularly in Japan where hydrogen fuel-cell cars will be on the market from 2014. However, the complex issues of safety, transportation and lower energy density of hydrogen in comparison to the common liquid carbon based fuels are the bottlenecks to be solved for the wider implementation of H₂ as energy vector. Also, hydrogen produces only water in principle upon burning, but due to the high combustion temperature and utilisation of hydrogen-lean mixtures, formation of nitrogen oxides (NO_x) can occur, although in small quantities [8].

The environmental friendliness depends on the primary energy that is used for its production. [Figure 1.1](#) shows the world H₂ production and use in 2008, according to *International Energy Agency* (IEA) [9], categorized by the technology employed for its production and field of application, respectively. About 50 Mt/year of H₂ are produced over the world. As evident from [Figure 1.1](#), hydrogen is most commonly produced by steam reforming of fossil fuels such as natural gas (48%), oil (30%) and coal (18%). These technologies are, however, destined to be (or rather should be) obsolete in a long run due to the depletion of fossil fuels and associated emission of CO₂. Therefore, environmentally and economically sustainable H₂ production technologies have been sought for over the past decades.

Large quantity of H_2 is needed in the petroleum and chemical industries. The major applications of H_2 are the production of ammonia (*Haber-Bosch* process) and the processing ("upgrading") of fossil fuels (Figure 1.1). The key consumers of H_2 in petrochemical industry are hydrodealkylation, hydrodesulphurization (HDS), and hydrocracking processes. H_2 has several other important uses mainly in hydrogenation reactions to produce methanol and to enhance the level of saturation of unsaturated fats and oils (Figure 1.1).

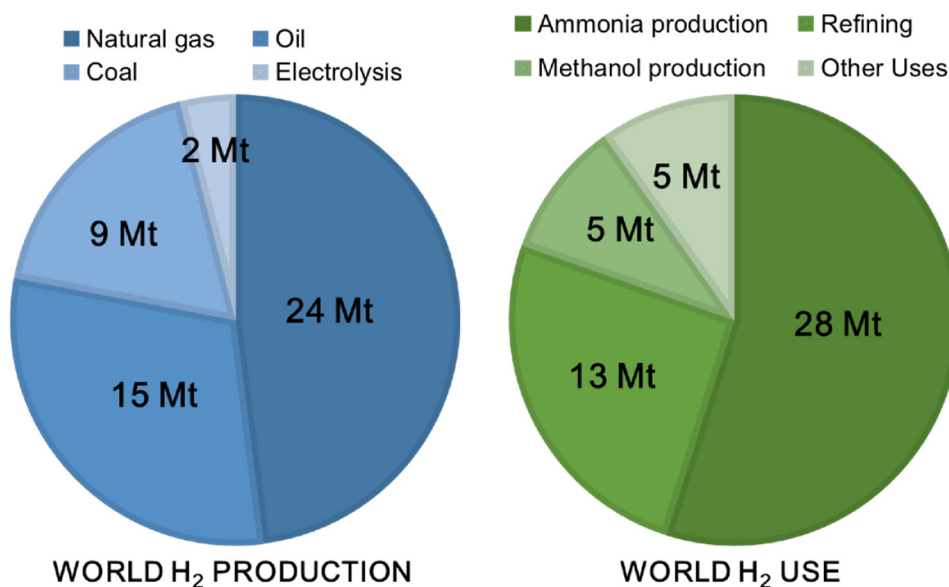
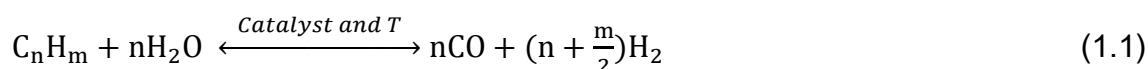


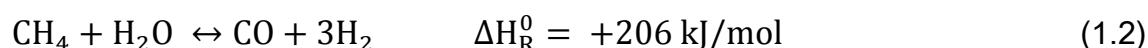
Figure 1.1. World hydrogen production and use in 2008 according to *International Energy Agency* (IEA) [9].

1.1.2 Steam Reforming of Fossil Fuels for Hydrogen Production

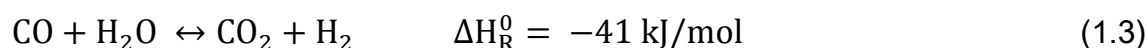
Steam reforming is achieved in a processing device called reformer which reacts steam at high temperature with fossil fuel in the presence of a catalyst. The typical standard reaction for steam reforming of any kind of fossil fuel can be written as follows (eq. 1.1):



Among all kinds of available fuels, steam reforming of natural gas to produce syngas - sometimes referred to as steam methane reforming (SMR) - is the most common method of producing commercial bulk hydrogen. It is also the least expensive method to produce hydrogen at present [3]. At high temperatures (700 – 1100 °C) and in the presence of a metal-based catalyst (nickel), steam reacts with methane to yield carbon monoxide and hydrogen. These two reactions are reversible in nature. In case of methane, eq. 1.1 becomes [10-12]:



Additional hydrogen can be produced by a lower-temperature gas-shift reaction with the carbon monoxide produced by SMR (eq. 1.3).



The first reaction (eqs 1.1 and 1.2) is strongly endothermic (consumes heat), the second reaction is mildly exothermic (produces heat). The efficiency for this process is approximately 65-75%. However, CO₂ formation as side-product, energetically demanding process and the continuous depletion of fossil fuels make this approach unsustainable. Furthermore, purification of hydrogen produced by steam reforming reaction is cumbersome and costly. Therefore, a great efforts have been made in order to stepwise replace steam reforming by sustainable, efficient and environmental friendly techniques [13-19]. Among them

water splitting stands out since only water is required as raw material and at same time oxygen is obtained as a useful by-product. Water splitting can be performed by means of three main routes, namely, thermolysis [20-22] (also known as thermal decomposition or thermochemical water splitting), electrolysis [13-16] (also referred as electrochemical water splitting) and photolysis [23-27] (most commonly known as photochemical water splitting, where water is directly dissociated by means of either UV or visible light stimulus and in presence of catalyst). The photolysis route is still at the premature level of development as a process, although significant steps have been made forward by year towards commercialisation. At present, the hydrogen production rates by photolysis are at least a few orders of magnitude lower than those achieved by thermolysis and electrolysis. Therefore, in the next sections hydrogen production by means of either thermochemical or electrochemical routes (Figure 1.2) will be presented and briefly discussed as feasible candidates for industrial scale water splitting.

1.2 Water Splitting for Large Scale Hydrogen Production

Water splitting is the general term for a chemical reaction in which water is separated into oxygen (O_2) and hydrogen (H_2). The standard enthalpy of formation of water at 25 °C and 1 atm is $\Delta H_f^0 = -285.8$ kJ/mol (positive sign for water decomposition/splitting, ΔH_d^0). Then, it is obvious that water decomposition/splitting process is not spontaneous and does not occur without an energy input (Figure 1.2). Hence, enabling efficient and economical water splitting technologies would be the key element to achieve sustainable hydrogen economy.

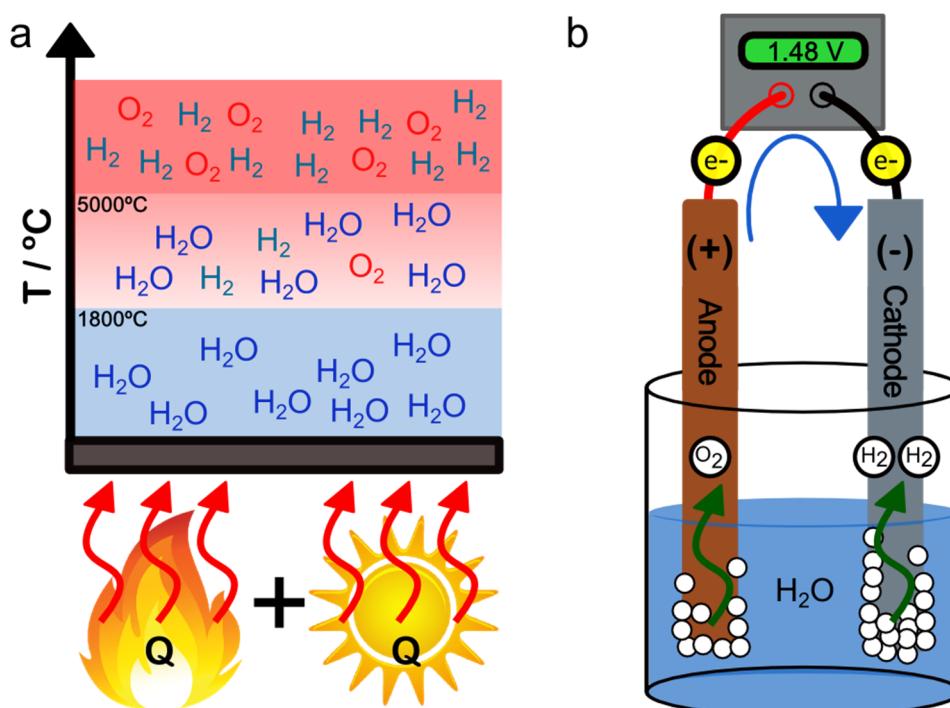
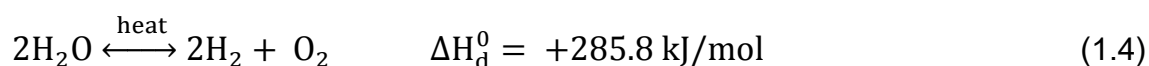


Figure 1.2. Two main routes for industrial scale water splitting: (a) Thermal decomposition (thermochemical water splitting) and (b) electrochemical water splitting commonly performed in an electrolytic cell.

1.2.1 Thermochemical Water Splitting

When water is heated above 1800 °C, dissociation starts. A small percentage of it decomposes into its constituent elements (eq. 1.4). However, if temperature is lowered, the components recombine very quickly.



Harsh conditions are required to carry out thermochemical water splitting, and this fact is not favourable for large scale operation, although solar energy can be potentially employed as the energy source for the reaction by harvesting the

thermal energy directly from sunlight [28]. Unfortunately, extremely high temperatures (ca. 5000 °C) have to be reached in order to obtain 100% conversion of water into hydrogen and oxygen. Solar furnace system that concentrates sunlight using large mirrors is the only conceivable source of heat. The industrial feasibility of this method remains unclear.

There are innovative ideas to make use of thermochemical approach by combining multiple reaction steps. One example is thermochemical water-splitting cycles (TCWSCs), which can lower the reaction temperature and help separate oxygen and hydrogen products to produce pure hydrogen gas. TCWSCs can improve the efficiency of hydrogen production from 30%, for conventional thermochemical electrolysis, to around 40-50%. Regarding such approaches, one of the most promising ones is the sulphur-iodine (S-I) cycle [18, 29]. In this cycle (Figure 1.3), sulphur dioxide (SO₂) and iodine (I₂) are used as catalysts lowering the reaction temperatures and also assisting the formation of pure hydrogen and oxygen [18, 29].

Although thermolysis is achievable and considered as a possible path for large-scale hydrogen production, generally its current limitations in terms of operation temperature and gas separation make this approach less feasible and attractive. In these respects, electrochemical routes have advantages, since the splitting reaction can take place at low temperature and, at same time, the product gases can be produced directly in the pure form as described in the next sections.

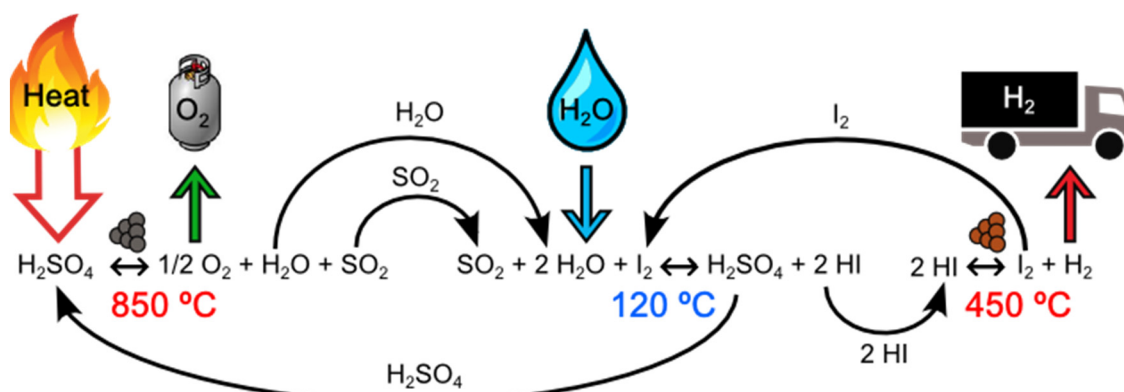


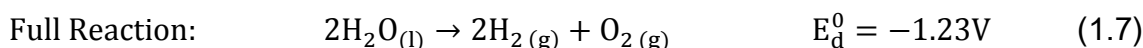
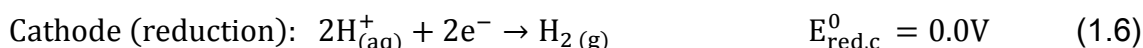
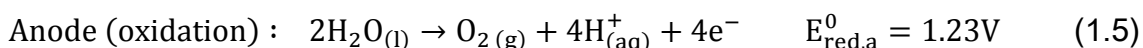
Figure 1.3. Sulphur-Iodine (S-I) cycle for low temperature thermochemical water splitting.

1.2.2 Electrochemical Water Splitting

Electrolysis phenomenon was discovered by Troostwijk and Diemann in 1789 [30]. Soon later in 1800 Alessandro Volta invented the voltaic pile, and a few weeks later William Nicholson and Anthony Carlisle used it for the electrolysis of water. Water electrolysis is the technical term referring to the action of using electricity to split water into its constituent elements, H₂ and O₂ [31]. The overall splitting is accomplished by passing a direct electric current (DC) through electrodes immersed in water. Thus, electron flow from positive (anode) to negative (cathode) terminal allows simultaneous Red-Ox reaction over electrodes surface. Hydrogen is collected at cathode and the oxygen is collected at anode. Electrolysis can produce very pure hydrogen for use in the electronics, pharmaceutical and food industries among other applications.

Electrochemical decomposition of water into hydrogen and oxygen at standard condition is not favourable in thermodynamic terms, since the overall standard potential value for water dissociation (E°_d) into H₂ and O₂ is -1.23 V (eqs. 1.5, 1.6 and 1.7), where $E^{\circ}_d = E^{\circ}_{\text{red,c}} - E^{\circ}_{\text{red,a}}$ and E°_{red} refers to standard reduction

potential either at cathode ($E_{\text{red,c}}^0$) or anode ($E_{\text{red,a}}^0$). Thus, electrical potential equal or higher than $|E_{\text{d}}^0|$, has to be supplied for triggering the decomposition.



From eqs. 1.5 and 1.6, at anode and cathode, the oxidation and reduction reactions take place, respectively. Specifically, water oxidation is performed at anode and this reaction is called oxygen evolution reaction (OER) since oxygen is evolved from the electrode. On the other hand, at cathode a reduction reaction called hydrogen evolution reaction (HER) occurs because of evolution and release of hydrogen from the electrode surface. In water electrolysis, the molar ratio of product gases ($\text{H}_2:\text{O}_2$) is stoichiometric (2:1).

Pure water behaves as insulator since its autoionization constant at room temperature, K_w defined as $[\text{H}^+][\text{OH}^-]$, is equal to $1.0 \cdot 10^{-14}$ and its electrical conductivity is poor (ca. $0.055 \mu\text{S}/\text{cm}$). Thus, pure water is not a suitable medium for ion transport, that is, for H^+ or OH^- to travel towards cathode and anode, respectively. Consequently, water splitting using pure water is rather difficult, demanding higher potential condition than thermodynamic one. To overcome this issue, electrolyte is often added. Strong acids such as sulphuric acid (H_2SO_4) and strong bases like potassium hydroxide (KOH) and sodium hydroxide (NaOH) are frequently used as electrolytes due to their strong conducting abilities.

On the other hand, the most common electrode material (both cathode and anode) is Pt due to its excellence in electrical conductivity (higher than gold) and high resistance to corrosion. Usually, it is employed in a form of wire or foil. However, its low abundance on Earth's crust and extremely high price restrict its use and implementation in large-scale industrial electrolysis processes.

1.2.2.1 Thermodynamics & Electrochemistry of Water Splitting

Electrolysis (or dissociation) of liquid water in the standard condition (P and T) requires a theoretical minimum of 237.2 kJ as work input (ΔG^0_d), in form of electrical energy (cell potential, E_{cell}) to dissociate every mole of water. Furthermore, heat input is also required in order to overcome the thermal barrier imposed by $T\Delta S^0_d$, ca. 48.6 kJ/mol. Thus, standard enthalpy of liquid water dissociation (ΔH^0_d) is obtained from $\Delta H^0_d = \Delta G^0_d + T\Delta S^0_d$, giving as final result, an endothermic reaction of 285.8 kJ/mol (section 1.2.2). This amount of demanded energy can be supplied by means of electrical + thermal energy combination or only applying electrical energy.

ΔH^0_d for liquid water is also referred to as higher heating value (HHV). Gibbs free energy of water dissociation is connected to electrical potential (E^0_d) according to eq. 1.8.

$$\Delta G^0_d = -nE^0_d F \quad (1.8)$$

Where n is the moles of electrons involved in the reaction and F is the Faraday constant ($96.485 \cdot 10^3$ C/mol). Assuming that overall water splitting is a 2 electron

transfer reaction, taking ΔG_d^0 and rearranging eq. 1.8, theoretical potential of water electrolysis (E_d^0) is -1.23 V in the standard condition (eq. 1.9). Therefore to activate the reaction, $E_{\text{cell}} \geq |E_d^0|$ condition must be accomplished. This potential (E_d^0) is known specifically as reversible standard potential (E_{rev}^0) and it is of great importance for more advanced calculations and assumptions.

$$E_{d(\text{rev})}^0 = -\frac{\Delta G_d^0}{nF} = -\frac{\Delta H_d^0 - T\Delta S_d^0}{nF} = -1.23 \text{ V} \quad (1.9)$$

However, electrolysis will not generally proceed at this voltage shown in eq. 1.9, since the electrical input must provide the full amount of enthalpy of the H_2 and O_2 products (285.8 kJ/mol) formation. This leads to the threshold potential of electrolysis to -1.48 V ($E_{\text{cell}} \geq |E_{\text{th}}^0|$) commonly known as thermoneutral potential, E_{th}^0 (E_{th} in non-standard condition) (eq. 1.10). For latter occurrence both E_{rev} and E_{th} will be taken in their absolute value.

$$E_{\text{th}}^0 = -\frac{\Delta H_d^0}{nF} = -1.48 \text{ V} \quad (1.10)$$

Voltage efficiency ($\epsilon_{\Delta H}$) [16, 17, 32], either in standard or real conditions, of a water electrolysis cell (eq. 1.11) is defined by the thermoneutral potential (E_{th}) over the cell operating voltage (E_{cell}) or also the HHV (ΔH_d) divided by the cell energy consumption in terms of Gibbs free energy (ΔG_{cell} calculated from eq. 1.8 using E_{cell} instead of E_d) [13, 14, 16]. Since electrical energy is proportional to voltage under constant current, the efficiency can be equally calculated in both ways (eq. 1.11).

$$\varepsilon_{\Delta H} = \frac{E_{th}}{E_{cell}} = \frac{\Delta H_d}{\Delta G_{cell}} \quad (1.11)$$

Analogously, ε can be also expressed as energy efficiency ($\varepsilon_{\Delta G}$), using E_{rev} (or ΔG_d) instead of E_{th} (or ΔH_d) in eq. 1.11. Energy efficiency will be always lower than voltage efficiency since $E_{rev} < E_{th}$.

From eq. 1.11 the efficiency trend can be elucidated while increasing potential, that is, the higher the cell voltage, the lower the efficiency ($\varepsilon_{\Delta H}$ or $\varepsilon_{\Delta G}$). It should be noted that, at same time, the higher the cell voltage the higher is the current density through electrodes and the production rate of both H_2 and O_2 is enhanced. Therefore, in reality a good balance between cell voltage, current density and efficiency (usually $\varepsilon_{\Delta H}$) has to be established in order to achieve high rate of H_2 and O_2 production while minimising electrical power input.

Isothermal operation at the thermoneutral potential ($E_{cell} = E_{th}$), that is supplying ΔH_d (or ΔH^0_d in standard condition) completely from electrical source, corresponds to 100% voltage efficiency in electricity-to-chemical energy conversion. Theoretical voltage efficiencies greater than 100% are possible when the cell operates at a lower potential than the thermoneutral potential. In such a case, external heat would be required to supply the remaining energy necessary ($T\Delta S_d$) by operating electrolysis at temperature higher than standard condition (25 °C). Furthermore, this thermal contribution to overall process energy consumption is of great importance in solid oxide electrolyser cell (SOEC) technology (voltage efficiencies higher than 100%), since it allows to work at electrical potentials even lower than reversible potential ($E_{cell} \leq 1.23$ V).

Moreover, eq. 1.11 shows the overall electrolysis efficiency which already includes all irreversibility and non-ideality, termed overpotentials (η in Volts). Overpotentials, are defined as the part that exceeds 1.23 V (reversible condition), i.e., $\eta = E_{\text{cell}} - E_{\text{rev}}$. Overpotentials are always affecting the overall system efficiency. Therefore, in a non-ideal case $\epsilon_{\Delta H}$ is defined as in eq. 1.12. Where, ΔG_{rev} refers to Gibbs free energy at reversible potential (ΔG_d), $\Delta G_{\text{overpot}}$ to energy change due to overpotentials ($\Delta G_{\text{cell}} = \Delta G_{\text{rev}} + \Delta G_{\text{overpot}}$ or $E_{\text{cell}} = E_{\text{rev}} + \eta_t$) and η_t to overall overpotential (in Volt).

$$\epsilon_{\Delta H} = \frac{E_{\text{th}}}{E_{\text{rev}} + \eta_t} = \frac{\Delta H_d}{\Delta G_{\text{rev}} + \Delta G_{\text{overpot}}} \quad (1.12)$$

In an electrolytic cell, existence of η results in more energy input than that expected thermodynamically to drive the reaction. Overpotential is specific to each cell design and varies across cells and operational conditions. The most important contributions to the overall overpotential (η_t) are related with (i) ohmic losses within the cell and its components, that is, Joule heating due to electron flow through a conductor (calculated by means of Ohm's law, $I \cdot R_{\text{tot}}$ in Volts, or $I^2 \cdot R_{\text{tot}}$ in Watts when refers to heat), (ii) ionic transport through electrolyte (η_{ionic} , conductivity (σ) dependent), (iii) concentration or mass transport overpotentials (η_{conc} , mass transport limitations due to diffusion and involving charge-carriers depletion over electrode surface), (iv) activation overpotential at cathode (η_c) and (v) activation overpotential at anode (η_a). Thus, the complete expression for defining the real potential applied on an electrolysis cell corresponds with eq. 1.13 (same calculation can be done using E_{th} analogously).

$$E_{\text{cell}} = E_{\text{rev}} + \underbrace{IR_{\text{tot}} + \eta_{\text{ionic}} + \eta_{\text{conc}} + \eta_{\text{c}} + \eta_{\text{a}}}_{\eta_{\text{t}}} \quad (1.13)$$

Large R+D efforts have been spent in reducing such overpotentials at the minimum level possible, but there are important innovations to be made to reduce the overpotentials further.

The key quantity of an electrolysis system characterising the performance is the current which passes through the system. The goal is to reach the highest current densities (j , A/cm) at the lowest possible voltages thermodynamically allowed (1.23 V with thermal contribution). For example, 1 A/cm² was fixed as standard current density in some scientific works [16, 32] in order to evaluate voltage/energy efficiency. As mentioned above, current density through the electrodes (anode-cathode system) is directly related with both H₂ and O₂ formation ([Chapter 3](#)); therefore, linear scaling of current density with electrolysis cell voltages is an important factor in electrolyser design.

1.2.2.2 Applications of H₂ Produced via Electrolysis

Currently about five percent of hydrogen gas produced worldwide is created by electrolysis ([section 1.1](#)). The majority of this hydrogen is the side product in the production of chlorine in water-alkaline electrolysis, which is the most common electrolytic approach for H₂ and Cl₂ production at once ([eq. 1.14](#)).



Water electrolysis is also used to generate oxygen for the International Space Station [33, 34].

Efficiency of modern electrolyzers is measured by power consumed per standard volume of hydrogen produced (MJ/m^3 or kWh/m^3), assuming standard temperature and pressure of H_2 . At 100% efficiency, 39 kWh of electricity and 8.9 L of water are required to produce 1 kg of hydrogen at 25 °C and 1 atm [19]. Moreover, over the past decades the ever-increasing price of electricity has hindered and/or postponed the production of electrolytic hydrogen [35]. This figure is about to change with the recent growth in energy capacity based on renewable sources like photovoltaics and wind turbines [36]. The U.S. Department of Energy (U.S. DOE) has set a cost goal for the renewable hydrogen at \$2.00–\$3.00/kg; including production, delivery, and dispensing [37].

1.3 PEM Electrolysis Technology

Conventional water splitting (in acidic or alkaline conditions) described in previous section is the first stepping stone on the way towards the large scale H_2 electrochemical production. However, several drawbacks exist related with conventional electrolysis, namely, higher overpotentials to be overcome, use of electrolytes like SO_4^{2-} to improve water conductivity, low current density and gas separation issues.

1.3.1 Background

To overcome aforementioned engineering bottlenecks of conventional electrolysis, in 1960s a new electrolysis technology/approach was born. This

novel technology was called polymer electrolyte membrane (PEM) electrolysis [14, 15, 38]. PEM electrolysis was first introduced by General Electric in 1966 [14, 15] using a solid PEM. The PEM was coated with a heterogeneous electrode catalyst on each side of the membrane. The system could efficiently split water molecules at low potential [14, 38] and solve the issues described above. Such electrolyzers were initially developed for special purposes like spacecrafts, submarines, and also for needs of the civil industry.

The concept of PEM electrolysis (Figure 1.4) is the same as in case of electrolytic cells (Figure 1.2). The red-ox reactions take place, but with a physical separation between anode (OER) and cathode (HER). This physical separation enabled by a thin PEM allows efficient separation of H_2 and O_2 and cell operation at high current densities with a low potential input.

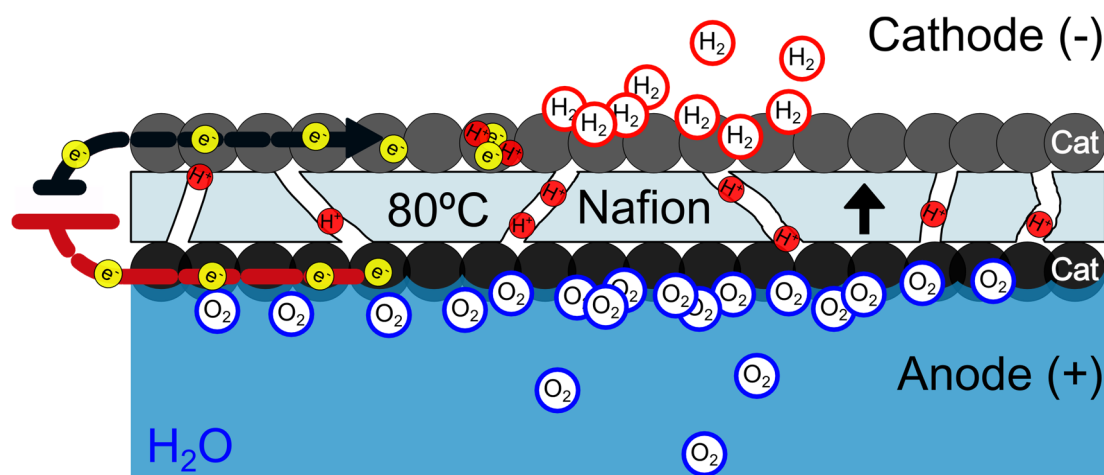


Figure 1.4. PEM electrolysis working principle. Proton exchange membrane (Nafion®) coated with catalyst layer on each side. Water oxidation takes place at anode side (+). Proton recombination to hydrogen occurs at cathode side (-).

Development of PEM electrolyzers is historically related to the development of perfluorinated ion exchange membranes (Nafion®) discovered by Walther Grot

(DuPont®). The main feature of such material, also called ionomer, is its unique capability for proton (H⁺) transport through its internal channels (Figure 1.4) as a result of incorporating perfluorovinyl ether groups terminated with sulfonate groups onto a tetrafluoroethylene (Teflon®) backbone [39, 40]. Nafion® (Figure 1.5, hereafter it is denoted as “Nafion”) has received considerable attention because of its excellent thermal and mechanical stability. These features made this material suitable for both fuel cell and electrolyser systems. Its optimal working temperature is about 80 °C, where the proton conductivity reaches the maximum value (ca. 0.1 ± 0.02 S/cm for Nafion 117, 175 μm) [14, 41, 42].

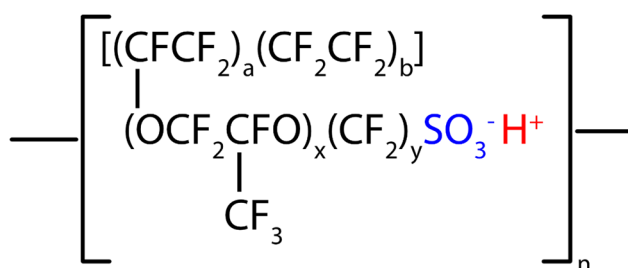


Figure 1.5. Sulfonated tetrafluoroethylene based fluoropolymer-copolymer (Nafion®) molecule chemical structure. Sulfonate group depicted in blue and free proton in red.

In PEM electrolyzers, high-purity hydrogen can be generated, promoted by heterogeneous catalysts with a voltage efficiency ($\epsilon_{\Delta H}$) reaching around 67-82% (calculated from HHV) [14], and the efficiency keeps improving year by year. Furthermore, PEM electrolyser technology can overcome the drawbacks observed in alkaline electrolyzers, such as low partial load range (evolved gases cross-diffusing through anode and cathode compartments), limited current density and low operating pressure [14]. Noble metals such as platinum (Pt black)

and iridium (IrO_2 or Ir black) are widely chosen as the catalyst because of their superior performance.

1.3.2 High Temperature Electrolysis

High-temperature electrolysis is the technology arising from high-temperature fuel cells (HTFC). The electrical energy needed to split water at 1000 °C is considerably less than that at 80-100 °C. This means that a high-temperature electrolyser (HTE) can operate at significantly higher overall process efficiencies than regular low-temperature electrolyser. A typical technology related with high temperature electrolysis is the solid oxide electrolyser cell (SOEC). This electrolyser is based on the design identical to that of the solid oxide fuel cell (SOFC) [43], which normally operates at 500 to 1000 °C. At these temperatures, the electrode reactions are more reversible and the fuel cell reaction can more easily be reversed to the electrolysis reactions. Attempts are currently underway to develop systems in which some of the electricity consumed by the electrolyser can be supplemented by the heat available from geothermal, solar or natural gas sources, thus reducing the consumption of electricity significantly.

1.3.3 Perspectives

One of the remarkable advantages of PEM electrolysis is its ability to operate at high current densities (ca. $2 \text{ A}\cdot\text{cm}^{-2}$) at low potentials (ca. 1.7 V) [14, 16, 44], without apparent degradation for a long period of time. PEM, due to its solid structure, exhibits a low gas crossover rate resulting in very high purity gas product (>99.999%) [14, 15, 17, 32]. Thus, hydrogen generated by means of

electrolysis e.g. using PEM electrolyzers is a very promising. The technology has been shown to be a viable (5 Mt H₂/year) alternative for large-scale production, although the gap in the production quantity is considerable compared with methane steam reforming (24 Mt H₂/year) as the leader in global H₂ production.

Utilization of green hydrogen, obtained from water by electrolysis and sourced by renewable energies, as reagent in industrial processes like hydrogenation reactions is a very attractive future strategy [3]. Such hydrogenation reactions with great importance in environmental and energetic impacts are for example CO₂ hydrogenation to produce liquid fuels [45-47] and abatement of aqueous nitrates (NO₃⁻) and nitrites (NO₂⁻) to harmless nitrogen molecule [48-50].

In the following section, the latter reaction, namely nitrates hydrogenation, will be presented as a potential application to directly use sustainable H₂ produced within PEM electrolysis cell.

1.4 Hydrogenation Reactions for Nitrate Abatement

Hydrogenation is a chemical reaction between molecular hydrogen and another compound or element, usually in the presence of a catalyst such as nickel (Ni), copper (Cu), palladium (Pd) or platinum (Pt). Such catalytic reaction can be either in homogeneous or heterogeneous phase depending on the catalyst employed and reaction to be performed. Heterogeneous catalytic hydrogenation is more common on a large scale industrially.

On the other hand, among several pollutants as well as harmful compounds, nitrate (NO₃⁻) is the most common chemical contaminant in the world's groundwater aquifers, and pollution of ground and surface water by nitrate is a

common environmental problem [51]. Furthermore, intake of such anion and derivatives may cause human health problems [52]. As an example, high nitrate amount in blood can lead to generalized lack of oxygen in organ tissue and to a dangerous condition called methemoglobinemia. Besides that, formation of nitrosamines from nitrite (derived from nitrates) can give rise to cancer of the digestive tract since they are the most efficacious carcinogens in mammals. Therefore, nitrate removal from waste water has become considerable importance during the last decades. Since nitrate is regarded as potentially harmful to human health, *European Environment Agency* (EEA) established the limit for nitrate in drinking water (98783/EC) to 11 mg NO_3^- - N/L (or 50 mg NO_3^- /L or ppm) [53, 54]. Moreover, *World Health Organization* (WHO) recommendation is even stricter, suggesting the limit allowable for nitrate in drinking water to 10 ppm NO_3^- .

Several physical and chemical NO_3^- removal strategies have been employed including reverse osmosis, ion exchange, and biological denitrification among others. Main drawbacks of these methodologies are related to the fact that nitrates are not transformed into harmless compounds but they are only concentrated, thus becoming even more dangerous than the raw wastes upon disposal [55]. Obviously, the most attractive strategy is to convert nitrate to harmless gaseous nitrogen (N_2) avoiding the formation of nitrite or ammonium ions, the most common by-products after hydrogenation reaction, which are regarded more toxic than nitrates. Thus, the limits for NO_2^- and NH_4^+ concentration in drinking water, established by EEA (98783/EC), are 0.1 ppm NO_2^- and 0.5 ppm NH_4^+ , respectively, even harder than the limit for nitrate.

The requirement for a chemically sustainable route for nitrate transformation led to the study and further implementation of nitrate catalytic hydrogenation as one of the most effective way for nitrate abatement. Thus, hydrogenation of nitrate and nitrite over noble metal catalysts was reported for the first time in 1989 by Vorlop et al. [56]. Catalytic hydrogenation (Figure 1.6) has been considered as one of the most effective methods for nitrate reduction to nitrogen [57]. The major problem of the approach is the usage, storage, and infrastructure needed for hydrogen gas that is dissolved in the aqueous solution containing nitrate ion, besides poor N_2 selectivity in some cases producing even more harmful NO_2^- and NH_4^+ by-products.

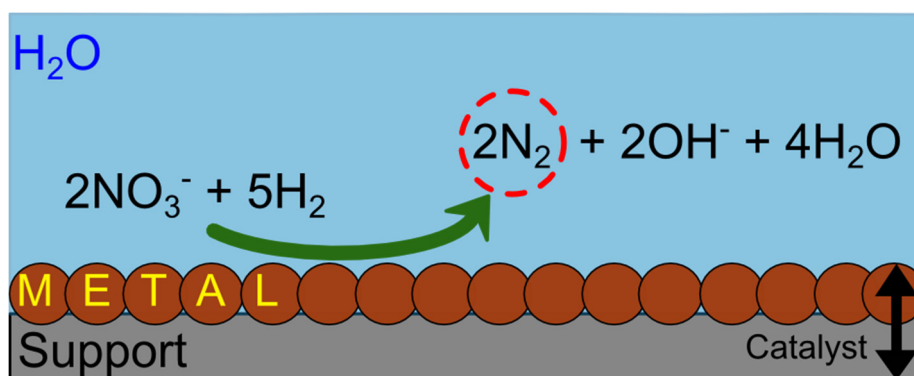


Figure 1.6. Catalytic nitrate hydrogenation towards harmless nitrogen scheme. Aqueous phase and supported catalyst.

Catalytic hydrogenation using bimetallic catalysts [48, 56, 58-60] supported on a variety of materials like Al_2O_3 , TiO_2 , SiO_2 , ZrO_2 , zeolites and carbon-based materials [48] is the most common process employed, although hydrogenation reactions using monometallic supported catalysts [57, 58, 61, 62] and photocatalytic processes [48] have been demonstrated to remove nitrates efficiently.

In the light of these backgrounds, electrolysis-assisted nitrate reduction (Chapter 5) is a promising approach due to possible process simplicity and the generation of H_2 or H^+ used for nitrate reduction in situ by electrolysis of water. Recently, Machida and co-workers reported the possibility of selective electrocatalytic hydrogenation of NO_3^- to N_2 using electrochemical reactors [63, 64]. The use of a PEM allowed the transport of in situ generated protons on the anode side to the surface of the catalyst deposited at the cathode (Figure 1.4), enabling nitrate reduction at surface. Among others, some advantages of this approach include high system efficiency, near ambient operating conditions, small equipment sizes, high purity oxygen production, no external hydrogen source and rapid start-up.

1.5 Motivation and Aim of this Thesis

Electrolysis of water and PEM technology play very important roles towards industrial hydrogen production, but still some technical and economic issues have to be solved for further technological spread and establishment. Hurdles like low efficiency and performance compared with H_2 production via steam reforming are expected to be overcome in the near future thanks to the continuous advances and improvements of electrolysis technologies and also greater availability of renewable energies. Still there is one hurdle which needs to be lowered greatly. That is economic one closely related to the abundance of specific chemical elements. The most effective and efficient materials in PEM electrolysis are precious/noble metals, namely Ir-based materials (IrO_2 or Ir black) for OER and Pt (raw or Pt black) for HER. Even though the amount of these metals in the

catalysts are minimized by dispersing on inexpensive support materials (e.g. carbon), their use and low abundance make PEM electrolysis extremely expensive [65], unsustainable and particularly unfavoured in a large scale production [14]. The quest for non-precious metal alternatives started a long time ago and several candidates have been reported as a replacement for HER and OER materials. For HER finding alternatives to Pt are increasingly reported [66, 67], whereas for OER no good alternative has been found and the trend in R+D is still trying to decrease the loading of IrO₂ as much as possible by supporting it on SnO₂, Ta₂O₅ or Sb₂O₅ [68, 69]. In this thesis, efficient, alternative HER catalysts made of abundant, inexpensive and non-precious chemical elements were sought for. The performance and stability of such catalytic materials in PEM electrolysis was compared with the standard reference catalyst, Pt black.

The second major challenge of this project was to exploit PEM electrolysis as a mean to perform hydrogenation reactions using H⁺/H₂ generated in situ. This approach, we call “electrolysis-assisted hydrogenation”, has an obvious advantage over ordinary hydrogenation because of process simplicity and flexibility, avoiding the use of hydrogen gas source (e.g. cylinders) and producing hydrogen on demand by applying electrical potential. As our target reaction, nitrate reduction was chosen and the effect of active metals and operation conditions, such as constant current or potential, on reaction performance and selectivity were examined.

In order to enhance conversion and selectivity of electrolysis-assisted nitrate hydrogenation approach, some technical modifications of the PEM cell configuration were made and their effectiveness was evaluated for the nitrate reduction. Moreover, aiming at further abatement of undesired side products

formed during the reaction, the combination of electrolysis-assisted hydrogenation setup with secondary techniques (e.g. electrochemical or photochemical) was also examined.

Finally, as an outlook of this multidisciplinary project and particularly related to the electrolysis-assisted hydrogenation, initial attempts for continuous CO₂ reduction and possible reactor configurations using our electrolysis-assisted approach are discussed.

BIBLIOGRAPHY

1. M. I. Hoffert, K. Caldeira, A. K. Jain, E. F. Haites, L. D. Harvey, S. D. Potter, M. E. Schlesinger, S. H. Schneider, R. G. Watts, T. M. Wigley, *Nature* **395**, 881, **1998**.
2. P. B. Weisz, *PHYSICS TODAY* **57**, 47, **2004**.
3. G. W. Crabtree, M. S. Dresselhaus, M. V. Buchanan, *Physics Today* **57**, 39, **2004**.
4. L. Barreto, A. Makihiro, K. Riahi, *International journal of hydrogen energy* **28**, 267, **2003**.
5. S. Penner, *Energy* **31**, 33, **2006**.
6. J. Rifkin, *The hydrogen economy: The creation of the worldwide energy web and the redistribution of power on earth*, Penguin, **2003**.
7. G. A. Olah, A. Goepfert, G. S. Prakash, *Beyond oil and gas: the methanol economy*, John Wiley & Sons, **2009**.
8. P. De Boer, W. McLean, H. Homan, *International journal of hydrogen energy* **1**, 153, **1976**.
9. International Energy Agency, *Key World Energy Statistics 2008*, **2008**.
10. K. Aasberg-Petersen, C. S. Nielsen, S. L. Jørgensen, *Catalysis Today* **46**, 193, **1998**.
11. G. Marigliano, G. Barbieri, E. Drioli, *Catalysis Today* **67**, 85, **2001**.
12. J. Tong, Y. Matsumura, *Applied Catalysis A: General* **286**, 226, **2005**.
13. F. Barbir, *Solar Energy* **78**, 661, **2005**.
14. M. Carmo, D. L. Fritz, J. Mergel, D. Stolten, *International journal of hydrogen energy* **38**, 4901, **2013**.
15. S. Grigoriev, V. Porembsky, V. Fateev, *International journal of hydrogen energy* **31**, 171, **2006**.
16. P. Millet, N. Mbemba, S. A. Grigoriev, V. N. Fateev, A. Aukauloo, C. Etievant, *International Journal of Hydrogen Energy* **36**, 4134, **2011**.
17. P. Millet, R. Ngameni, S. Grigoriev, N. Mbemba, F. Brisset, A. Ranjbari, C. Etievant, *International Journal of Hydrogen Energy* **35**, 5043, **2010**.
18. K. Onuki, S. Kubo, A. Terada, N. Sakaba, R. Hino, *Energy & Environmental Science* **2**, 491, **2009**.
19. J. Turner, G. Sverdrup, M. K. Mann, P. C. Maness, B. Kroposki, M. Ghirardi, R. J. Evans, D. Blake, *International Journal of Energy Research* **32**, 379, **2008**.
20. R. B. Diver, J. E. Miller, M. D. Allendorf, N. P. Siegel, R. E. Hogan, *Journal of Solar Energy Engineering* **130**, 041001, **2008**.
21. J. Norman, G. Besenbruch, L. Brown, D. O'keefe, C. Allen, *GA-A16713*, **1982**.
22. M. Roth, K. Knoche, *International journal of hydrogen energy* **14**, 545, **1989**.
23. H. Kato, K. Asakura, A. Kudo, *Journal of the American Chemical Society* **125**, 3082, **2003**.

24. A. Kudo, Y. Miseki, *Chemical Society Reviews* **38**, 253, **2009**.
25. K. Maeda, T. Takata, M. Hara, N. Saito, Y. Inoue, H. Kobayashi, K. Domen, *Journal of the American Chemical Society* **127**, 8286, **2005**.
26. Y. Sakata, Y. Matsuda, T. Nakagawa, R. Yasunaga, H. Imamura, K. Teramura, *ChemSusChem* **4**, 181, **2011**.
27. Y. Sakata, T. Nakagawa, Y. Nagamatsu, Y. Matsuda, R. Yasunaga, E. Nakao, H. Imamura, *Journal of Catalysis* **310**, 45, **2014**.
28. A. Steinfeld, *Solar Energy* **78**, 603, **2005**.
29. S. Kubo, H. Nakajima, S. Kasahara, S. Higashi, T. Masaki, H. Abe, K. Onuki, *Nuclear Engineering and Design* **233**, 347, **2004**.
30. S. Trasatti, *Journal of Electroanalytical Chemistry* **476**, 90, **1999**.
31. R. De Levie, *Journal of Electroanalytical Chemistry* **476**, 92, **1999**.
32. P. Millet, R. Ngameni, S. Grigoriev, V. Fateev, *International Journal of Hydrogen Energy* **36**, 4156, **2011**.
33. R. Roy, *ASME (American Society of Mechanical Engineers)*, **2012**.
34. P. L. Barry, *NASA Science*, **2012**
35. G. Naterer, M. Fowler, J. Cotton, K. Gabriel, *International journal of hydrogen energy* **33**, 6849, **2008**.
36. K. Hedegaard, P. Meibom, *Renewable Energy* **37**, 318, **2012**.
37. O. o. E. E. a. R. E. W. Department of Energy, DC, **2006**.
38. J. Russell, L. Nuttall, A. Fickett, *Hydrogen generation by solid polymer electrolyte water electrolysis*, in *Am. Chem. Soc. Div. Fuel Chem. Meeting, Chicago (August 1973)*, **1973**.
39. C. Heitner-Wirguin, *Journal of Membrane Science* **120**, 1, **1996**.
40. K. A. Mauritz, R. B. Moore, *Chemical reviews* **104**, 4535, **2004**.
41. S. Slade, S. Campbell, T. Ralph, F. Walsh, *Journal of The Electrochemical Society* **149**, A1556, **2002**.
42. Y. Sone, P. Ekdunge, D. Simonsson, *Journal of The Electrochemical Society* **143**, 1254, **1996**.
43. R. M. Ormerod, *Chemical Society Reviews* **32**, 17, **2003**.
44. J. Xu, G. Liu, J. Li, X. Wang, *Electrochimica Acta* **59**, 105, **2012**.
45. A. Bansode, A. Urakawa, *Journal of Catalysis* **309**, 66, **2014**.
46. P. G. Jessop, T. Ikariya, R. Noyori, *Chemical reviews* **95**, 259, **1995**.
47. B. Tidona, C. Koppold, A. Bansode, A. Urakawa, P. Rudolf von Rohr, *The Journal of Supercritical Fluids* **78**, 70, **2013**.
48. N. Barrabes, J. Sa, *Applied Catalysis B-Environmental* **104**, 1, **2011**.
49. F. Epron, F. Gauthard, C. Pineda, J. Barbier, *Journal of Catalysis* **198**, 309, **2001**.
50. U. Prüsse, M. Hähnlein, J. Daum, K.-D. Vorlop, *Catalysis Today* **55**, 79, **2000**.

51. M. Duca, M. T. M. Koper, *Energy & Environmental Science* **5**, 9726, **2012**.
52. J. W. Peel, K. J. Reddy, B. P. Sullivan, J. M. Bowen, *Water Research* **37**, 2512, **2003**.
53. M. H. Ward, T. M. deKok, P. Levallois, J. Brender, G. Gulis, B. T. Nolan, J. VanDerslice, *Environmental Health Perspectives* **113**, 1607, **2005**.
54. M. Zhou, W. Wang, M. Chi, *Bioresource Technology* **100**, 4662, **2009**.
55. N. Barrabes, J. Just, A. Dafinov, F. Medina, J. L. G. Fierro, J. E. Sueiras, P. Salagre, Y. Cesteros, *Applied Catalysis B-Environmental* **62**, 77, **2006**.
56. K. D. Vorlop, T. Tacke, *Chemie Ingenieur Technik* **61**, 836, **1989**.
57. M. D'Arino, F. Pinna, G. Strukul, *Applied Catalysis B-Environmental* **53**, 161, **2004**.
58. F. Gauthard, F. Epron, J. Barbier, *Journal of Catalysis* **220**, 182, **2003**.
59. S. Hörold, K.-D. Vorlop, T. Tacke, M. Sell, *Catalysis Today* **17**, 21, **1993**.
60. F. A. Marchesini, S. Irusta, C. Querini, E. Miro, *Catalysis Communications* **9**, 1021, **2008**.
61. J. Sá, T. Berger, K. Föttinger, A. Riss, J. A. Anderson, H. Vinek, *Journal of Catalysis* **234**, 282, **2005**.
62. A. Shukla, J. V. Pande, A. Bansiwale, P. Osiceanu, R. B. Biniwale, *Catalysis letters* **131**, 451, **2009**.
63. M. A. Hasnat, M. R. Karim, M. Machida, *Catalysis Communications* **10**, 1975, **2009**.
64. M. Machida, K. Sato, I. Ishibashi, M. Abul Hasnat, K. Ikeue, *Chemical Communications*, 732, **2006**.
65. N. N. Greenwood, A. Earnshaw, *Chemistry of the Elements*, Elsevier, **1997**.
66. B. Hinnemann, P. G. Moses, J. Bonde, K. P. Jørgensen, J. H. Nielsen, S. Horch, I. Chorkendorff, J. K. Nørskov, *Journal of the American Chemical Society* **127**, 5308, **2005**.
67. Y. Li, H. Wang, L. Xie, Y. Liang, G. Hong, H. Dai, *Journal of the American Chemical Society* **133**, 7296, **2011**.
68. S. Ardizzone, C. Bianchi, G. Cappelletti, M. Ionita, A. Minguzzi, S. Rondinini, A. Vertova, *Journal of Electroanalytical Chemistry* **589**, 160, **2006**.
69. G. Chen, X. Chen, P. L. Yue, *The Journal of Physical Chemistry B* **106**, 4364, **2002**.

CHAPTER 2

METHODS AND SYSTEMS



2.1 Catalysts Synthesis

The research work summarized in this thesis unifies two main research fields, namely, (i) electrochemistry and (ii) heterogeneous catalysis. Hence, the suitable choice of catalysts plays a crucial role, since such materials should be able to perform electrochemical as well as catalytic function at the same time. Thus, an exhaustive literature survey was initially performed to make correct choice/combination of catalyst materials.

The heterogeneous (electro)catalysts used in this research work can be categorised in two main types: unsupported and supported (or mixed) catalysts. In the first category of unsupported ones, the materials employed were: IrO₂, Pt black, MoS₂ and cobalt (II, III) oxide (Co₃O₄) whereas supported ones, the most relevant for our study, were (i) Pt, Pd, Cu and PdCu supported over SnO₂ high surface area or (ii) MoS₂ and Co₃O₄ mixed with electrically conducting carbon material (e.g. Vulcan[®]-XC72, for later occurrence it is denoted as “Vulcan”) [1]. [Table 2.1](#) summarises the most important catalysts employed and their applications in this doctoral thesis project. Furthermore, the distinction between anode material (performing oxidation reaction) and cathode material (reduction reaction) is also provided. In all the tests performed the anode side of the electrochemical reactor was used as a proton (in addition to oxygen) generation source by means of water oxidation reaction ([section 2.3](#)).

Table 2.1. Catalysts employed in this thesis work and their function. (i) Anode materials for oxidation reactions (OER) and (ii) cathode for reduction reactions. (✓) Tested and (✗) not tested for the purpose.

	Electrode	Catalyst	Water Splitting	Nitrate Reduction
Unsupported	Anode	IrO ₂	✓	✓
	Cathode	Co ₃ O ₄	✓	✗
	Cathode	Pt black	✓	✗
	Cathode	MoS ₂	✓	✗
	Cathode	SnO ₂	✗	✓
Supported on SnO ₂	Cathode	Pt/ SnO ₂	✗	✓
	Cathode	Pd/ SnO ₂	✗	✓
	Cathode	Cu/ SnO ₂	✗	✓
	Cathode	PdCu/ SnO ₂	✗	✓
Mixed with Vulcan	Cathode	MoS ₂ /Vulcan	✓	✗
	Cathode	Co ₃ O ₄ /Vulcan	✓	✗

All materials employed in this study (supported and unsupported/mixed catalysts) were carefully characterized using various techniques. XRD, BET and H₂ & CO pulse-chemisorption studies were performed in order to identify the catalyst crystal structure and calculate the dispersion of precious metal over support material. Furthermore, catalyst layer characterization over Nafion was performed to find out the true state of catalyst on top of polymeric membrane. As clearly seen from [Table 2.1](#), Iridium (IV) oxide (IrO₂, >99%, powder, Alfa Aesar) was used as the only anode catalyst due to its unique and superior ability for

water oxidation reaction (oxygen evolution reaction, OER) compared to other materials [2, 3]. Because of the acidic environment and high anode potential during water electrolysis, non-noble catalytic metals like Ni, Co, and Cu are subject to corrosion [4]. Among noble metal electrocatalysts, Pt forms a poorly conducting oxide film and shows a high overpotential for OER. However, electrocatalysts consisting of Ir, Ru, or their oxides (which are reported to have the rutile structure and to be very good conductors (metallic type, ca. 10^4 S/cm)) [5] have been shown to possess very high electrocatalytic activities for OER [6]. Therefore, based on the information available in literature, IrO_2 was selected for both water electrolysis tests (section 2.3.3.1) as well as electrochemical (electrolysis-assisted) reduction reaction studies (section 2.3.3.2) to make a straightforward comparison among all cathodes materials and configurations screened.

2.1.1 Support Preparation

2.1.1.1 Tin (IV) Oxide (SnO_2)

High surface area tin (IV) oxide (BET area of ca. $230 \text{ m}^2/\text{g}$, cassiterite crystal structure), synthesized by urea ($\text{CH}_4\text{N}_2\text{O}$, Sigma-Aldrich) precipitation methodology [7], was used as a support to enhance the metal dispersion over its microporous surface and to benefit from its capabilities as semiconductor-type material as well as its durability under harsh operating conditions (e.g. pH and electrical current) [8].

High surface SnO_2 was synthesized by following the procedure described elsewhere [7]. In brief, an aqueous solution of 0.1 M SnCl_4 and 10-fold excess of

urea was refluxed at 90 °C for 15 h in a round bottom flask. The precipitate was isolated and washed by centrifugation, dried at 120 °C for 16 h and calcined at 200 °C for 4 h in air. [Figure 2.1](#) shows the XRD patterns of the synthesized SnO₂ and the commercial SnO₂ sample (Alfa Aesar, 99.9% metals basis, <10 μm powder).

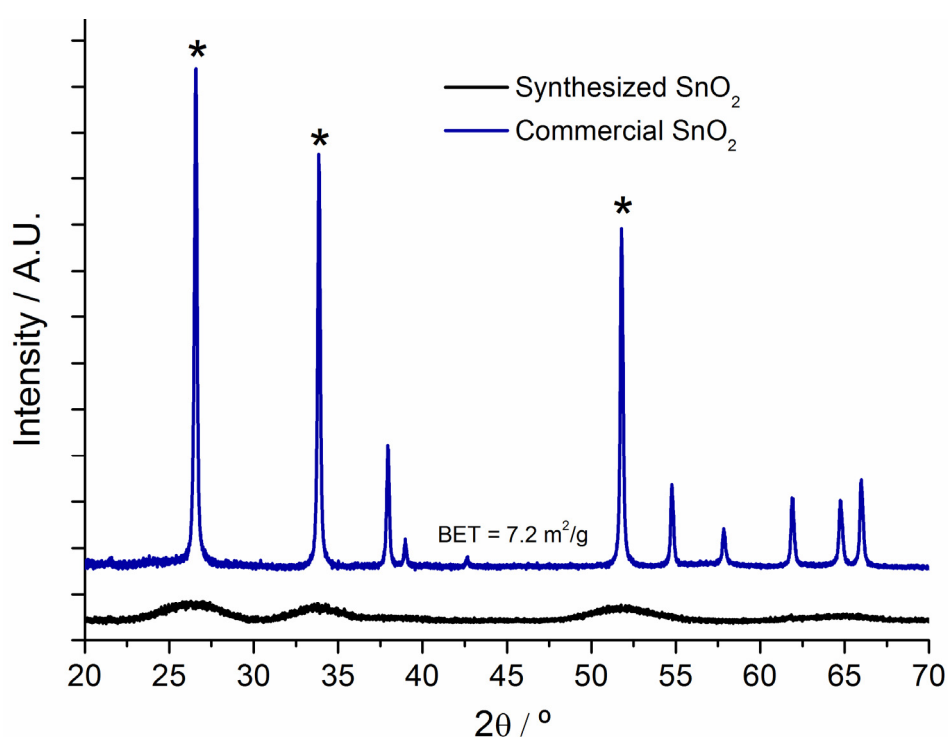


Figure 2.1. XRD pattern of commercial (blue line) and in-house synthesized SnO₂ (black line) with BET area of ca. 7 m²/g and 230 m²/g respectively. (*) refers to the most relevant peaks of the cassiterite phase crystal structure.

The crystalline structure commonly described in literature and database, cassiterite phase, was confirmed for both materials with the intense diffraction peaks located at $2\theta = 26.6, 33.9$ and 51.8° (highlighted with *) corresponding to (110), (101) and (211) diffraction planes, respectively. The powder XRD pattern of the synthesized SnO₂ ([Figure 2.1](#), black line) exhibited broad characteristic

diffraction peaks indicating much smaller crystallite size than that of commercial one (blue line, narrow peaks). This observation was also confirmed by transmission electron microscope (TEM) investigation, whose results are shown in Chapter 5.

2.1.1.2 Carbon Support (Vulcan)

Vulcan (carbon black, Fuel Cell Store) was used as received. Its surface area is around ca. 250 m²/g and the electrical conductivity ca. 70 S/m. Vulcan has amorphous crystalline structure and commonly acts as a conductive support or substrate on which typically platinum (Pt) is deposited in case of Fuel Cell technology. Moreover, it is widely used in plastic compounds for electrostatic discharge products.

2.1.2 Catalyst Preparation

2.1.2.1 Wet Impregnation

Impregnation is the simplest and the most popular technique in solid catalyst preparation [9] (Figure 2.2a). Catalysts are prepared by adding a metal salt solution (typically aqueous solution) over a pre-shaped support, followed by drying and calcination treatments to remove excess solvent and decompose the precursor to form metal and metal oxide (nano)particles over the support material. If the volume of the solution is equal to the pore volume of the support, the process is called incipient wetness impregnation. Active component (e.g. metal) can be well dispersed and no loss of active material within the support phases is

generally observed. The advantage of this method is that catalyst support can be prepared separately, allowing for higher temperature treatments than the case where the active metal is already incorporated on/in the support. The distribution of the active species on the support varies, depending on the preparation conditions. Various factors such as type, concentration of precursor salt, solvent, temperature, type of support and contact time with support can be controlled to obtain optimum dispersion of catalytically active components.

In this project tin (IV) oxide support was decorated with some kinds of metals, mainly Pt, Pd, Cu, and PdCu by means of the wet impregnation method (Figure 2.2a). Aqueous solutions of the metal precursors were prepared and poured over the catalyst support, drop by drop, while mechanically mixing the generated mixture and until whole support is properly impregnated with solution. The most common metal precursor salts used were those of nitrate, namely $\text{Cu}(\text{NO}_3)_2$, $\text{Fe}(\text{NO}_3)_3$ and $\text{Pd}(\text{NO}_3)_2$ since nitrate decomposition temperature is lower than chloride based salts, besides its cleanliness upon decomposition (no residual halogen atoms on the surface). On the other hand, Pt precursor used was chloroplatinic acid $\text{H}_2\text{PtCl}_6 \cdot 6\text{H}_2\text{O}$ (ACS reagent, $\geq 37.50\%$ Pt basis, Sigma-Aldrich).

After impregnation, the samples were dried for 12 h in an oven at $100\text{ }^\circ\text{C}$, once elapsed drying time, samples were cooled and crushed using pestle and mortar until they become fine powder. Last step was calcination using a high temperature furnace in order to remove all the water and decompose the remaining metal precursors from the surface of catalyst. For all the catalysts prepared by the impregnation method, calcination temperature was set at $500\text{ }^\circ\text{C}$ for 4 h in air with a temperature ramp (β) of $5\text{ }^\circ\text{C}/\text{min}$.

Initially we performed measurements using catalysts prepared via wet impregnation and they gave good results in terms of stability and performance as catalyst. However, several drawbacks were found to use these materials in PEM system. Among them, the most problematic one is catalyst activation by pre-reduction, because all the metals over the supports are in oxidized state after the calcination treatment. Therefore, along this research we tried other ways for catalyst preparation although wet impregnation is one of the most employed techniques for supported catalyst preparation.

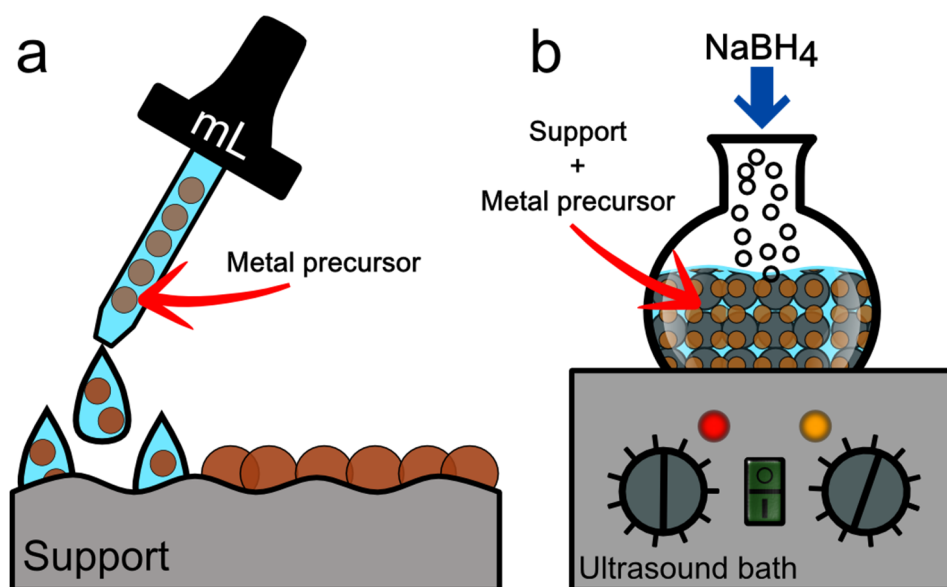


Figure 2.2. Catalyst preparation methods carried out: (a) wet impregnation and (b) ultrasonic metal deposition and reduction.

Among other possible preparation methods of supported metal catalysts, as a promising one we have identified a method based on in situ chemical reduction of metal precursors using NaBH_4 and while maintaining continuous sonication in order to keep a well dispersion of support and metal (Figure 2.2b). A brief description of this procedure is explained in the following section [10].

2.1.2.2 Ultrasonic Metal Reduction and Deposition

In the ultrasonic metal deposition method (Figure 2.2b), catalyst preparation was accomplished as follows: (1) Catalyst support together with metal precursor (same than those used for wet impregnation) aqueous solution were taken in a round bottom flask and stirred for 10 min, (2) homogenous solution in the flask was moved to an ultrasonic bath where reduction of target metal precursor(s) was performed by stepwise NaBH_4 (sodium borohydride, >97%, 10-40 mesh granules, Alfa Aesar) addition [10] and left for 1h under continuous sonication, (3) powder was filtrated using a vacuum funnel, (4) cleaned with excess of milliQ H_2O (10:1 volume ratio of water compared to the nitrate solution used for the synthesis) for complete Na^+ removal and (5) dried at 100 °C for 12 h in the oven. Consistent sonication is important for homogeneity of the metal deposition by maximising the contact between all the metal precursor and support particles. Moreover, material precipitation at bottom of the synthesis flask has to be avoid.

Using this procedure we avoided metal oxides formation (no calcination and further reduction required) while enhancing metal surface area ($\text{m}^2 \text{ cat}/\text{g}_{\text{sample}}$) and thus degree of metal dispersion over the support calculated by means of pulse chemisorption measurements and further mathematical treatment. Figure 2.3 shows an example of pulse chemisorption profile obtained for 40 wt% Pt supported over SnO_2 catalyst synthesized via this technique. Metal dispersion and metal surface are also shown.

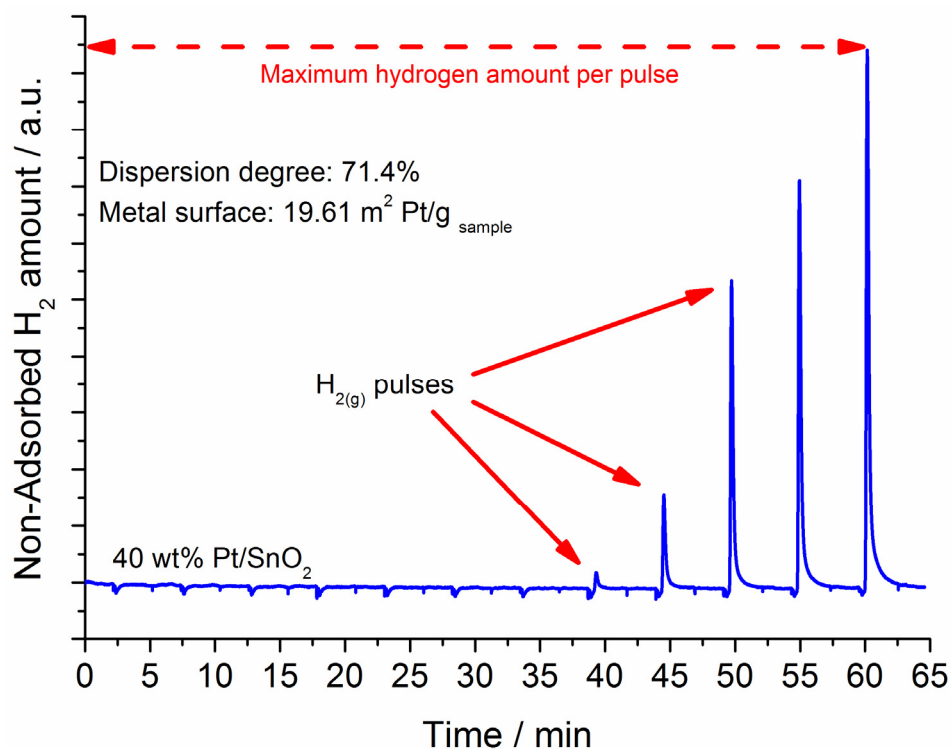


Figure 2.3. Pulse chemisorption profile for 40 wt% Pt/SnO₂ catalyst prepared by the NaBH₄ procedure. H₂ was used as probe gas. A known amount of hydrogen (0.34 cm³) was pulsed every 5 minutes. Degree of metal dispersion and metal surface are shown.

Pulse chemisorption measurements were carried out using H₂ as a probe molecule which adsorbs over Pt surface. Each H₂ pulse contained the same amount of H₂ (0.34 cm³) and injected to the system (passed over the sample) every 5 minutes. H₂ uptake was calculated from the amount of H₂ adsorbed over platinum surface. Figure 2.3 shows one representative profile. From the 1st to the 7th pulse all the hydrogen passed over the sample was adsorbed, showing a complete uptake of H₂ and indicating high metal surface area and high degree of dispersion of Pt. The degree of metal dispersion was ca. 71.5% and the available metal surface for catalytic processes was ca. 20 m² Pt/g_{sample}. This excellent

results led us to use the sonication- NaBH_4 method to prepare SnO_2 -supported metal catalysts throughout this thesis project.

2.1.2.3 Mechanical Mixing

Chemical reduction using NaBH_4 was established as a default procedure for catalyst preparation, but in some cases another preparation route was chosen. In the case of MoS_2 and Co_3O_4 catalysts the metal salt was mixed with Vulcan. In these catalysts, Vulcan was used in order to enhance the electrical conductivity without modifying metal oxides structure and oxidation state. Either molybdenum(IV) sulphide (>99%, powder, <2 μm , Sigma Aldrich) or Co_3O_4 (>99.5%, nanopowder, <50 nm, Sigma Aldrich) were physically mixed [1] with Vulcan flakes using a mortar and pestle during the preparation of the cathode catalyst inks. No further step was required prior to deposition over the PEM (section 2.2.2).

2.2 MEA Preparation

2.2.1 Polymer Electrolyte Membrane Pre-Treatment

Nafion 117 membrane (175 μm thick, Ion-Power) was used as the proton transport medium. Prior to use, the Nafion membrane was treated [11] by washing in 5 vol% H_2O_2 aqueous solution for 1 h at 80 $^\circ\text{C}$ to eliminate residual organic impurities [12], then in 0.5 M sulphuric acid for 1 h at 80 $^\circ\text{C}$ to incorporate water molecules and to activate the membrane by hydration [13]. The membrane was further treated with boiling water for 1 h in order to remove possible impurities

remaining from previous treatments. The pre-treated membranes were stored in water at ambient temperature prior to deposition of the catalyst materials. Furthermore, treated membranes were kept in flat shape so that further catalyst deposition would be easier, avoiding possible problems related to membrane bending and fixation over the holder used for catalyst deposition.

2.2.2 Catalyst Ink Preparation

As a solid particles, catalysts cannot be coated over the membrane since there would not be any physical binding force between catalyst and membrane surface and as a result catalysts could get easily removed from the Nafion surface. In order to avoid this, the catalyst should be prepared in the form of either paste (for screen printing) or ink (for decal transfer, spray coating, inkjet printing or electroless deposition).

Typical ink formulation contains dry catalyst, Nafion solution and solvent (e.g. methanol, ethanol, isopropanol or water) [14, 15]. Catalyst ink composition varies depending on the purpose and the amount of the material to be deposited over the membrane, referred as a dry catalyst loading per unit of surface area or most commonly known as loading ($\text{mg}_{\text{cat}}/\text{cm}^2$). In order to provide ionic transport to catalytic active sites [16, 17], addition of Nafion solution (resulting in dry Nafion after deposition) to the catalyst ink is required. Nafion helps to form a thin layer of catalyst after the deposition over the membrane surface ensuring a proper H^+ transport between the catalyst surface (which are not in close contact with PEM) and the membrane (Figure 2.6). Lee and co-workers investigated the effect of Nafion addition on commercial low PEM fuel cell electrodes and they conclude

that without the addition of some Nafion, the majority of the catalyst sites were inactive [11].

In our studies, catalyst inks were made of a mixture of catalyst powder (amount depending on catalyst loading over membrane surface, $\text{mg}_{\text{cat}}/\text{cm}^2$), isopropanol (4 mL) and Nafion solution (Nafion D-521 dispersion, 5 wt% in water and 1-propanol, ≥ 0.92 meq/g exchange capacity, Alfa Aesar), in a ratio of 15.4 wt% dry Nafion in total dry solid. The ink was sonicated for 1 h using an ultrasound bath (120W/ 60Hz, BANDELIN SONOREX).

2.2.3 Catalyst Deposition

Catalyst deposition over PEM can be accomplished by means of several techniques such as screen printing [18], decal transfer [19], spray coating [20, 21], electrospray coating [22, 23], inkjet printing [24, 25] and electroless deposition [26]. As a default methodology to produce our membrane electrode assemblies (MEAs) we chose spray deposition method (Figure 2.4) due to its ease of implementation (only airbrush and carrier gas are required), operation and amount of resources required.

Using spray coating, catalyst inks can be either deposited over membrane or on diffusion layer (porous material which allows suitable management of gas-liquid interphase, section 2.3.2) depending on electrolyser configuration. In our studies all the membranes were prepared by catalyst deposition over the membrane, by the so called catalyst coated membrane approach (CCM).

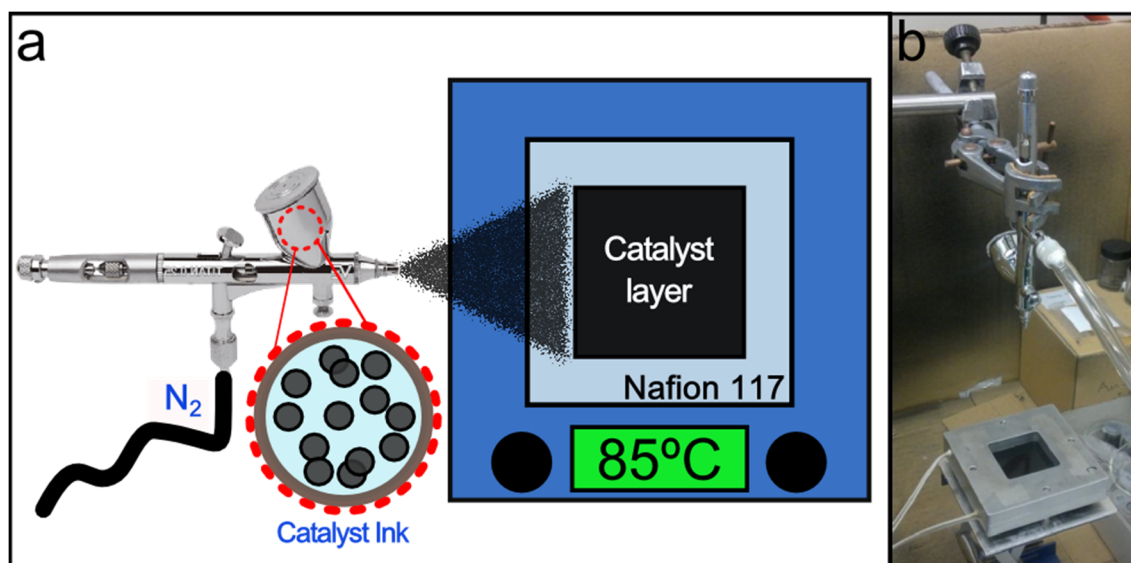


Figure 2.4. Spray (airbrush) catalyst deposition method over Nafion membranes. (a) Schematic representation of the methodology employed and (b) actual deposition system built in the lab: Airbrush connected to a N_2 line + heating plate kept at 85 °C with an inner 2x2 or 4x4 cm² frame to ensure reproducibility in the active area dimension.

Figure 2.4a shows a schematic representation of the catalyst coating procedure. Figure 2.4b shows actual catalyst deposition system installed in our lab. The deposition procedure was as follows. Catalysts were coated over the Nafion membrane (active area of either 2x2 or 4x4 cm², depending on final application) by using a common airbrush ($\varnothing_{\text{nozzle}}$: 0.5 mm, Ventus Titan) and fixing Nafion membrane in a heated holder with open window (Figure 2.4b). Deposition temperature was set at 85 °C to evaporate the solvent during the deposition avoiding membrane swelling and allowing the formation of a homogeneous and uniform catalyst layer on both sides of Nafion membrane (Figure 2.5). The total membrane surface covered by catalyst is termed as active area, this is the portion of area which is used to determine the catalyst loading. The final catalyst layer will act as an electrode (i.e., anode or cathode depending on catalyst).

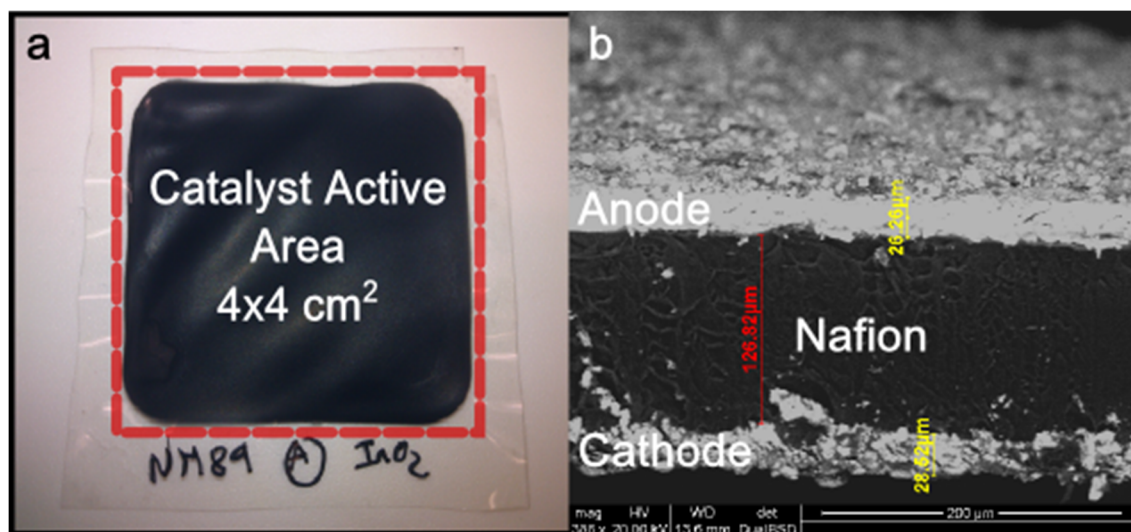


Figure 2.5. MEA produced by spray deposition. (a) Image taken right after catalyst deposition (fresh membrane), (b) ESEM image of the cross-section of same MEA (in red Nafion 117 membrane thickness, in yellow thickness of catalyst layers).

Ready to work MEAs prepared in our laboratory look like the one shown on [Figure 2.5a](#). Furthermore, the thickness of the catalyst layer over membrane was measured by means of environmental scanning electron microscopy (ESEM) using a FEI Quanta 600 (equipped with EDX from Oxford Systems) by focusing the electron beam towards the cross section of an entire MEA ([Figure 2.5b](#)). The thickness of catalyst layers at both anode and cathode side was ca. 25 μm.

An effective electrode is the one that correctly balances the various transport processes required for the operation of PEM system, as shown in [Fig. 2.6](#). Three processes are required for the transport of (1) protons from the membrane to the catalyst; (2) electrons from the current collector to the catalyst through the gas diffusion layer (GDL); and (3) the reactant and evolved gases to/from the catalyst layer/gas channels [16], respectively.

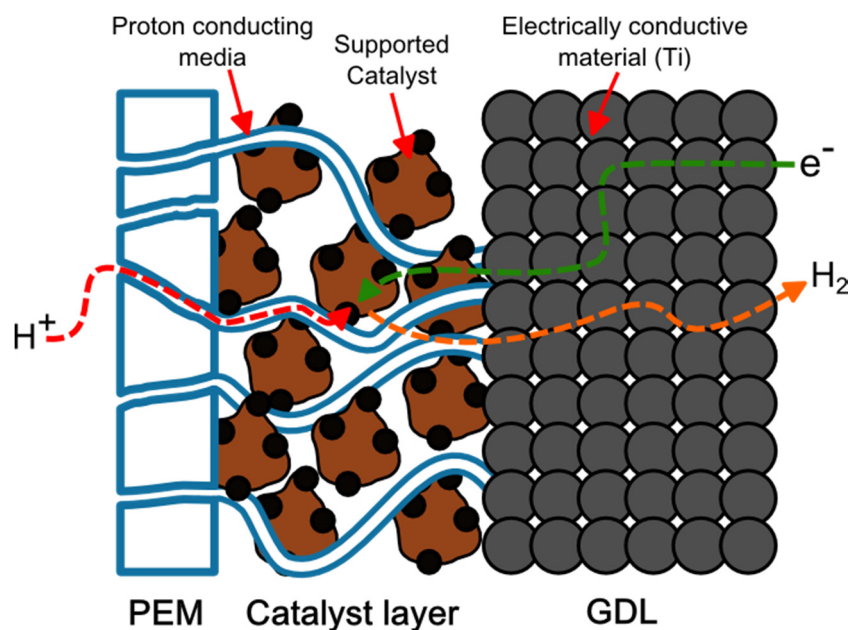


Figure 2.6. Transport of gases, protons, and electrons at cathodic electrode of a PEM water electrolyser, where HER takes place. Dashed arrows show schematic proton (red), electron (green) and gas (orange) pathways.

Protons (H^+), electrons (e^-), and gases are often referred to as the three phases found in a catalyst layer [16]. Part of the optimization of an electrode is the attempt to minimize transport losses. Besides, an intimate connection of these transport processes at the catalyst particles surface is crucial for efficient operation of a PEM cell. Figure 2.6 gives a graphical representation of what has been explained above, taking as an example the cathode of a PEM electrolyser where HER takes place continuously. All the required reagents (protons and electrons) must be provided to the catalyst surface in order to produce hydrogen. If there is no good path and contact among them, the process will fail and efficiency will dramatically drop.

2.3 Electrochemical Reaction Setup

Typically, electrochemical reactions and characterization measurements are performed in a 3-electrodes cell approach (working, counter and reference electrodes) [27, 28]. Such configuration is currently mainly used for determination of redox potentials, reaction overpotentials, as well as for electrochemical sensors testing. Nevertheless such a methodology is only valid for lab-scale measurements, with no feasible possibility of scaling-up. In this research project, a PEM based electrochemical reactor approach has been used instead, due to its simplicity and scale up potential. In all the cases either hydrogen formation (HER) or hydrogenation reactions were studied.

2.3.1 Background

This doctoral project was initiated as a new line in the research group, without specific and direct previous experience on active materials and also appropriate reaction systems. Equipment and strategies for electrocatalytic reaction systems were designed and improved throughout the project in order to solve technical issues as well as to meet the demands of the scientific challenges arising.

The goal of this research line was at its first stage (1) hydrogen production via PEM electrolysis strategy using novel materials, and at its second stage (2) using the produced hydrogen (in the form of atom, molecule, or ion) to trigger hydrogenation reactions. In order to accomplish the first stage, a PEM based electrolysis reactor (PEM electrolyser) was designed and manufactured, using previously reported designs [29, 30]. PEM reactors have well-optimised structure and components that were substantially standardised in the last years [29-31].

This leaves relatively limited room for design improvement and thus most of our efforts have been focused on catalysts testing and optimization.

In the following sections, electrocatalytic homemade cells will be described more in detail to give a general idea about the tools we developed to accomplish our targets.

2.3.2 Electrocatalytic (PEM) Reactor

Overall assembly of the electrocatalytic cell is represented in [Figure 2.7a](#), and its layer by layer components are shown in [Figure 2.7b](#).

A PEM cell is based on a multilayer arrangement where the most important parts are (i) membrane electrode assembly (MEA), (ii) diffusion layers and (iii) current collectors with internal flow field. In our design, we made use of: (1) Nafion 117 MEA, coated with electrode catalysts (anode and cathode), (2) porous titanium (Ti) gas diffusion layers (GDL, 2x2 or 4x4 cm², 1 mm thick, $\varnothing_{\text{pores}}$: 50 μm , Sintered-Filter, XINXIANG FILTER TECHNOLOGY CO., LTD) and (3) Ti current collectors (2 mm thick) with a CNC machined flow field (1 cm³ of total channel volume, with face filling single serpentine groove as shown in [Figure 2.8](#)).

Grade 1 titanium (GR1Ti) was used to avoid corrosion of (ii) and (iii). The MEA and GDL were sandwiched between the current collectors, which were held together by 8 screws aluminium cell housing plates (1 cm thick). Sealing and internal electrode insulation was provided by PTFE gaskets ([Figure 2.7b](#)). Screw torque was set at 5 N·m, providing a gas and liquid leak-free system.

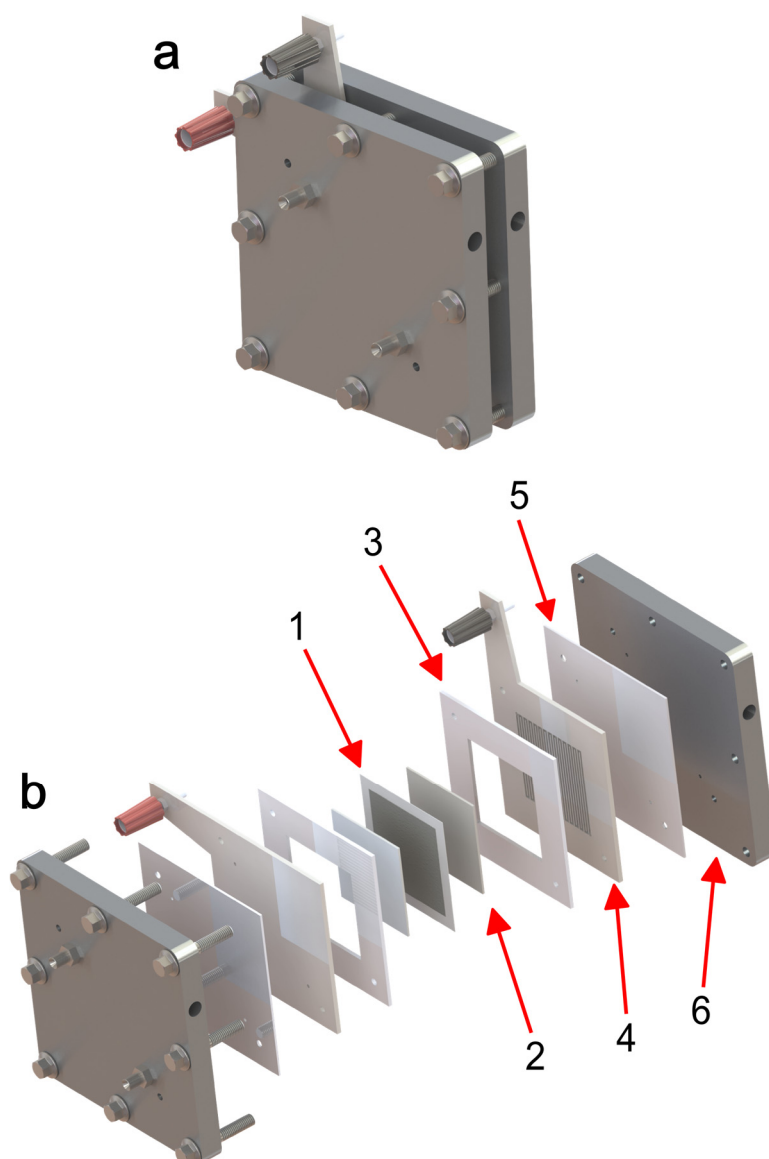


Figure 2.7. Flow-through PEM reactor for water electrolysis and electrolysis-assisted reactions. It can be operated either in gas phase or liquid phase. (a) Electrochemical cell fully assembled and (b) layer-by-layer reactor components, from membrane to back plate: (1) MEA, (2) gas diffusion layer (GDL), (3) PTFE gasket, (4) current collector, (5) PTFE back gasket and (6) front or end plate.

Power supply electrical connectors were directly plugged to the current collector plates through the connections pins shown in [Figure 2.7](#) (red and black for anode (+) and cathode (-), respectively).

MEA is the heart of the system and current collectors (Figure 2.8) are the arteries distributing the electrons through or from the diffusion layer depending whether acting in the cathode or anode side. Furthermore, due to their flow-field, they allow a proper and continuous water flow through the cell. At the same time GDL allows optimum liquid (water) - gas (H_2 , O_2) interface management.

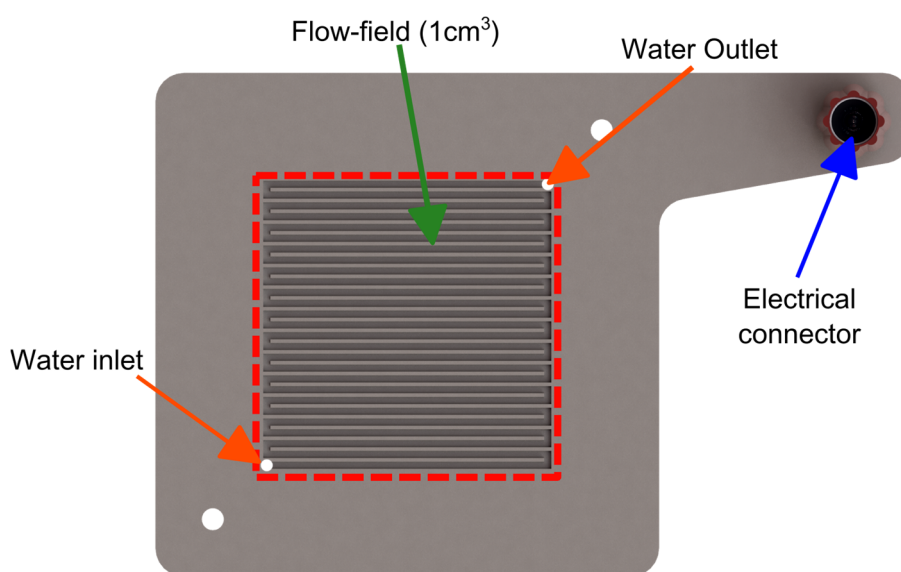


Figure 2.8. In-house designed current collector plate (Ti Grade1). Inside the dashed rectangle serpentine flow field can be observed. Water inlet, outlet and current connector are also shown.

2.3.3 Reaction Systems and Methods

2.3.3.1 PEM Electrolyser Configuration

Figure 2.9 shows a scheme of the PEM electrolysis reactor, described in detail in the previous section (Figure 2.7), integrated in our flow system for water splitting (Chapters 3 and 4). This system consists of four main components, namely (1) PEM electrolyser, (2) peristaltic pump system and water reservoir, (3) temperature controller and (4) computer controlled potentiostat.

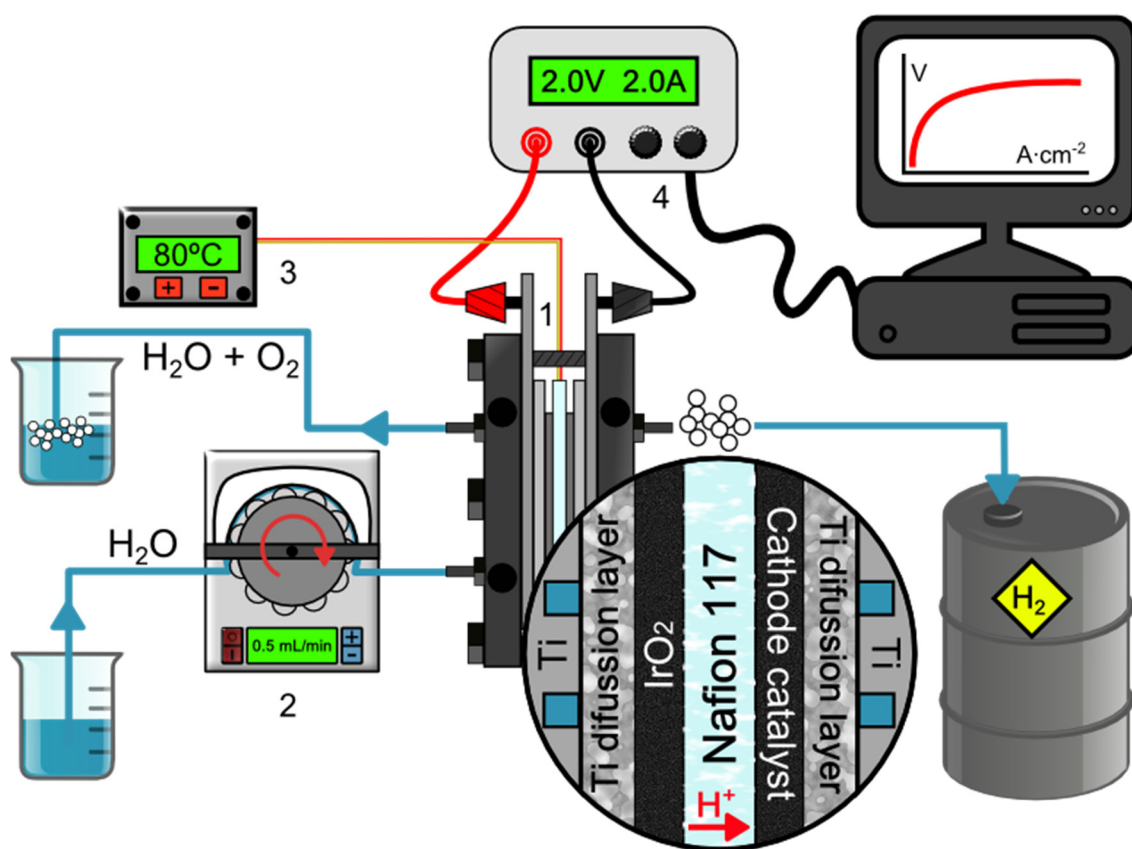


Figure 2.9. Continuous electrocatalytic reaction system configuration for water electrolysis. (1) PEM cell (electrolyser), (2) peristaltic pump and water reservoir, (3) temperature controller and (4) computer controlled potentiostat. The inset of the PEM cell shows the multilayer configuration.

A peristaltic pump (Ismatec Reglo Digital, 2 channels) was employed to continuously supply water to the system. The temperature controller was used to set the desired working temperature (80 °C, optimum value for Nafion membrane operation) inside the electrochemical reactor. Voltage (EMF, V), current (I, A) and current density (j , A/cm^2) values, were controlled, measured and recorded using a power supply/potentiostat system (CPX400DP, 420 DC Power Supply, 60 V max, 20 A max), controlled by a custom LabVIEW based interface. Evolved gases (O_2 from anode and H_2 from cathode) were released to the atmosphere.

The flow system described above allows to work in several ranges of water flow, temperature and either potential or current. Similar systems are described in literature [29-31]. MEA layer-by-layer composition for all water electrolysis tests was IrO₂ | Nafion | CC, where CC refers to cathode catalyst (Pt black, MoS₂, Co₃O₄, MoS₂/Vulcan and Co₃O₄/Vulcan).

Polarization curves were performed from 1.2 V up to 2.7 V by means of potential sweep measurements with $\Delta V = 0.05$ V/step. Liquid water flow rate of 0.5 mL/min was found to be optimum for our studies.

2.3.3.2 Electrolysis-Assisted Nitrate Reduction Configuration

Electrocatalytic tests employed for electrolysis-assisted nitrate reduction (Chapter 5) were performed using the same PEM cell described above (Figure 2.7). Figure 2.10 shows a scheme of electrochemical reaction cell and flow reaction system configuration. Nitrate solution reservoir and auxiliary peristaltic pump were added as main feature compared with the electrolyser system.

The pH of the effluent stream at the cathodic side was constantly evaluated with a Crison pH meter (model 5028, probe $\varnothing = 3$ mm). Peristaltic pumps (Reglo Digital, 2 channels; Ismatec) were used to feed either milliQ H₂O or nitrate solution to the electrochemical cell. Working temperature and flow rate of nitrate solution were set at 80 °C, and 160 μ L/min, respectively. Pure water was passed through the anode compartment at flow rate of 0.5 mL/min. All NO₃⁻ reduction tests, except potential sweeps (Chapter 5), were evaluated using a 100 ppm initial concentration solution prepared from NaNO₃ as precursor salt. MEA layer-by-

layer composition for all NO_3^- reduction tests was IrO_2 | Nafion | 40 wt% M/ SnO_2 , where M = Pt, Pd, Cu and PdCu.

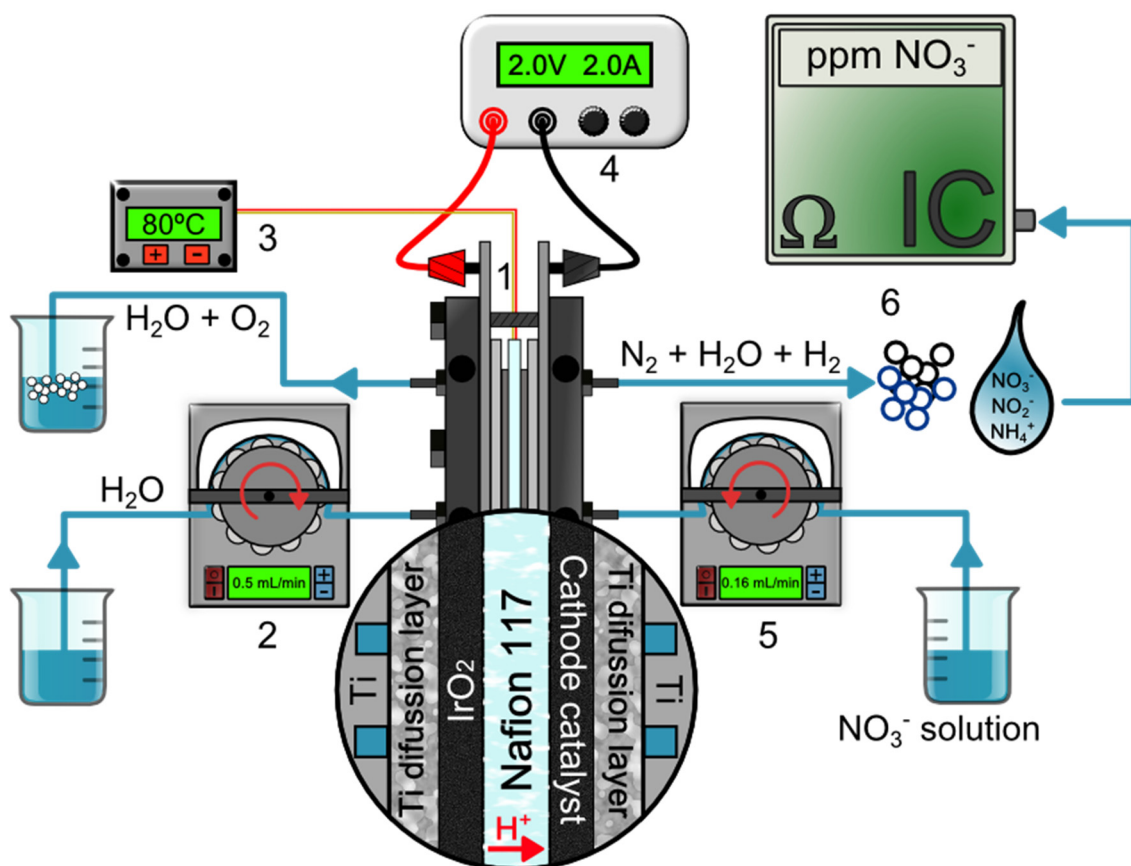


Figure 2.10. Continuous electrocatalytic reaction system configuration for electrolysis-assisted nitrate hydrogenation in aqueous media. (1) PEM cell, (2) peristaltic pump and water reservoir, (3) temperature controller, (4) computer controlled potentiostat, (5) peristaltic pump and nitrate solution reservoir, (6) ion chromatograph (IC) system for final product analysis.

Potentiostat (SP-150, from 10 nA to 1 A / ± 10 V; BioLogic Science Instruments) was used as an external power source with fine V-I control. For high potential measurements (ca. 2.1-2.7 V) combination of potentiostat + Booster (VMP3B-5, 5A/20V, BioLogic Science Instruments) was used. By applying a DC current to

the MEA, the evolution of H_2 and the reduction of nitrate/nitrite took place simultaneously at the cathode surface.

Automated programmable sample collection was done by using an in-house built autosampler (Figure 2.11). It was computer controlled through a LabVIEW based interface allowing custom frequency of sampling in each of the 48 available sample positions (2 mL vials).

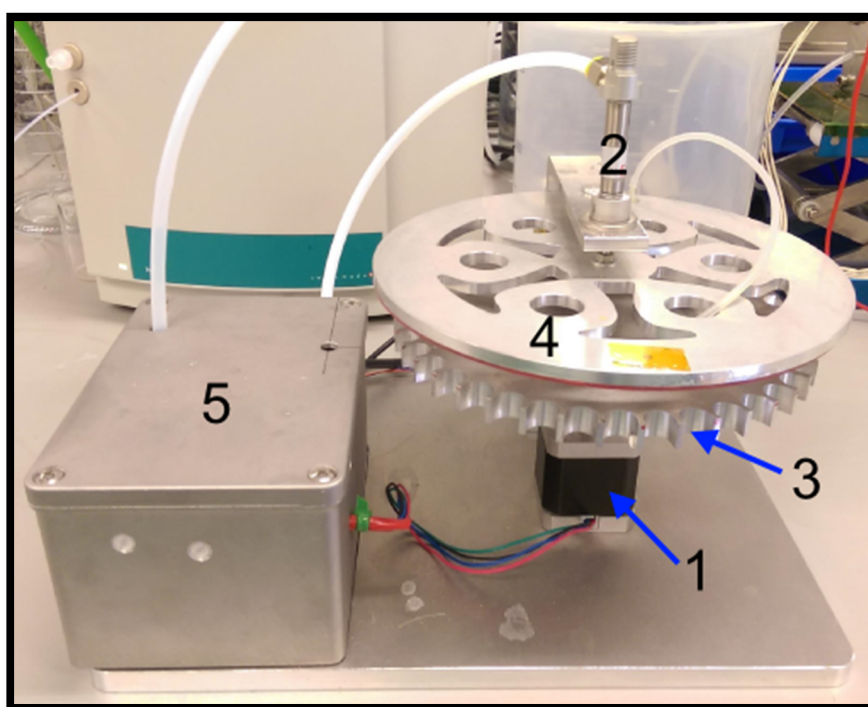


Figure 2.11. In-house designed autosampler. (1) Stepper motor, (2) piston, (3) rotatory stage, (4) moving lid and (5) electronics.

2.4 Analytical System

In nitrate reduction mode, Ion chromatography (IC, section 2.4.1) and mass spectroscopy (MS, section 2.4.2) were employed to analyse the compositions of product streams, during and after reaction.

2.4.1 Ion Chromatography (IC)

Ion-exchange chromatography (or ion chromatography) is an analytical system that allows the separation of ions and polar molecules based on the charge properties of the ions/molecules. Any kind of charged molecule, including large proteins, small nucleotides and amino acids can be separated and detected. This type of chromatography is further subdivided into: anion or cation exchange chromatography. Generally, it is used in water analysis. IC provided an easy-to-use and robust methodology for quantification of aqueous product from NO_3^- electrochemical reduction tests.

An 883-IC Basic device (Metrohm AG, Switzerland, [Figure 2.12a](#)) was used for ions (NO_3^- , NO_2^- and NH_4^+) quantification. Metrosep A-Supp4 (250/4.0) and C6 (250/4.0) IC columns were used for anion and cation detection, respectively. All the samples were purged using a Nylon syringe filter (0.45 μm porous diameter, FilterLab) before injection to a 20 μL sample loop. Samples were manually injected and subsequently analysed while they were collected from the reaction system ([Figure 2.12b](#)). All the analyses were performed at room temperature and ambient pressure. All concentration values have been corrected taking in account the dilution effect at cathode compartment due to the electro-osmotic drag of water [32-34] induced by the potential applied in our electrochemical reactors.

Electro-osmosis is the water flux accompanying the proton flux, and can be characterized by the electro-osmotic drag coefficient ($\eta_d = \text{H}_2\text{O}/\text{H}^+$), which is defined as the number of water molecules moving with each proton in the absence of the concentration gradient. For a Nafion 117 membrane (175 μm

thick), operating at 80 °C, for each H⁺ travelling from anode to cathode, 1.5 to 3 water molecules will be also transported [34, 35]. Thus, cathode side will be partially wet, humidifying the gas evolved from cathode.

Ammonium analysis is pH sensitive, being the concentration of the cationic form of the NH₃/NH₄⁺ pair (pK_a = 9.26) dependant on the basicity of the solution, The pH of our product outlet stream is ca. 10-11, i.e. only the uncharged NH₃ can be present. For analytical purpose, ion chromatograph mobile phase is acidic. Under these conditions ammonia equilibrium is completely shifted to NH₄⁺ in order to be detected by IC. In our final results (Chapter 5) we refer to ammonium as NH₃/NH₄⁺ pair total concentration.

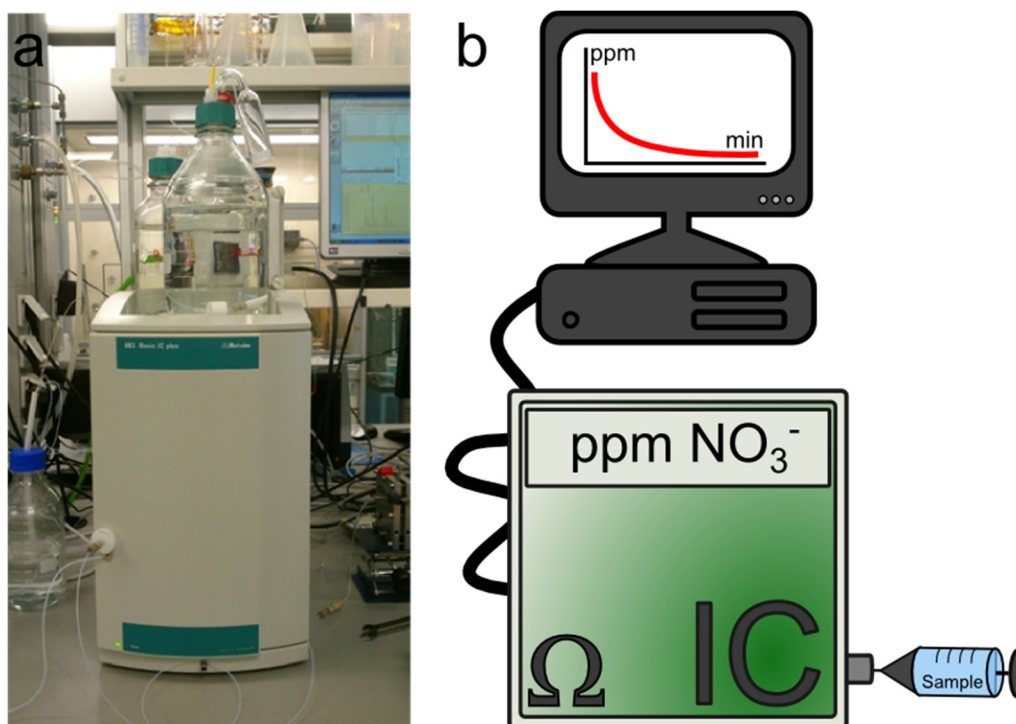


Figure 2.12. Ion chromatography system for water analysis. (a) 883-IC device (Metrohm AG, Switzerland) and (b) schematic view of ion chromatograph (IC) injection procedure. Nitrates, nitrites and ammonium containing solutions from reaction system were manually injected.

2.4.2 Mass Spectrometry (MS)

Mass spectrometer (MS) was used in order to analyse the gas product coming from cathode outlet of the electrolysis-assisted reaction cells. MS allows to detect compounds at very low concentration (typically as low as few ppm) and with a very high time resolution (seconds), allowing real time continuous flow gas analysis.

Continuous flow of gas products was fed into the MS prior drying, by means of gas-liquid separation, since cathode products are wet due to the electro-osmotic drag (section 2.4.1) phenomena that takes place inside the cell [32, 33].

The MS (Pfeiffer Vacuum, Omnistar GSD 320) was equipped with a quadrupole mass analyser capable of separating fragments with molecular mass to charge ratio (m/z) up to 100. It is designed exclusively for the analysis of gases. The analysis chamber is kept under high vacuum ($\approx 10^{-9}$ bar) by a turbomolecular pump. Before the sampling capillary, a flow splitting device (essentially a T-piece open to atmospheric pressure), must be placed to avoid overpressure at the inlet of the MS. Capillary temperature was fixed at 200 °C and multiple ion detection mode (MID) was selected as the standard method for detection. Electrolysis-assisted nitrate reduction gaseous side products (N_2 , H_2 , N_2O , NO , NH_3 and NH_2OH) were online monitored when it was required. The target fragments were N_2 ($m/z = 28, 14$), H_2 ($m/z = 2$), N_2O ($m/z = 44, 30$), NO ($m/z = 30, 14$), NH_3 ($m/z = 17, 16$) and NH_2OH ($m/z = 33, 32, 16$). Argon (Ar, $m/z = 40$) or Helium (He, $m/z = 4$) fragments were also followed as reference standards.

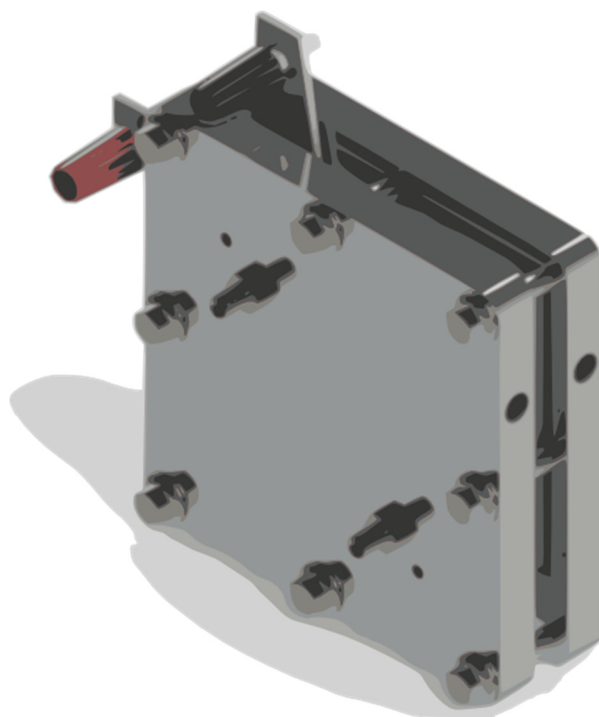
BIBLIOGRAPHY

1. J. C. TOKASH, B. E. LOGAN, *INTERNATIONAL JOURNAL OF HYDROGEN ENERGY* **36**, 9439, **2011**.
2. E. RASTEN, G. HAGEN, R. TUNOLD, *ELECTROCHIMICA ACTA* **48**, 3945, **2003**.
3. S. SONG, H. ZHANG, X. MA, Z. SHAO, R. T. BAKER, B. YI, *INTERNATIONAL JOURNAL OF HYDROGEN ENERGY* **33**, 4955, **2008**.
4. P. MILLET, *ELECTROCHIMICA ACTA* **39**, 2501, **1994**.
5. S. TRASATTI, G. LODI, *ELECTRODES OF CONDUCTIVE METALLIC OXIDES*, ELSEVIER AMSTERDAM, **1981**.
6. L. KRUSIN-ELBAUM, M. WITTMER, *JOURNAL OF THE ELECTROCHEMICAL SOCIETY* **135**, 2610, **1988**.
7. A. HAGEMEYER, Z. HOGAN, M. SCHLICHTER, B. SMAKA, G. STREUKENS, H. TURNER, A. VOLPE, H. WEINBERG, K. YACCATO, *APPLIED CATALYSIS A-GENERAL* **317**, 139, **2007**.
8. K. SASAKI, F. TAKASAKI, Z. NODA, S. HAYASHI, Y. SHIRATORI, K. ITO, *ECS TRANSACTIONS* **33**, 473, **2010**.
9. J. T. RICHARDSON, M. TWIGG, M. SPENCER, *PRINCIPLES OF CATALYST DEVELOPMENT*, PLENUM PRESS NEW YORK, **1989**, VOL. 1.
10. O. ILINICH, F. P. CUPERUS, R. VAN GEMERT, E. GRIBOV, L. NOSOVA, *SEPARATION AND PURIFICATION TECHNOLOGY* **21**, 55, **2000**.
11. S. LEE, S. MUKERJEE, J. MCBREEN, Y. RHO, Y. KHO, T. LEE, *ELECTROCHIMICA ACTA* **43**, 3693, **1998**.
12. C. YANG, P. COSTAMAGNA, S. SRINIVASAN, J. BENZIGER, A. BOCARSLY, *JOURNAL OF POWER SOURCES* **103**, 1, **2001**.
13. Z. LU, G. POLIZOS, D. D. MACDONALD, E. MANIAS, *JOURNAL OF THE ELECTROCHEMICAL SOCIETY* **155**, B163, **2008**.
14. S. SIRACUSANO, A. DI BLASI, V. BAGLIO, G. BRUNACCINI, N. BRIGUGLIO, A. STASSI, R. ORNELAS, E. TRIFONI, V. ANTONUCCI, A. ARICÒ, *INTERNATIONAL JOURNAL OF HYDROGEN ENERGY* **36**, 3333, **2011**.
15. M. CARMO, D. L. FRITZ, J. MERGEL, D. STOLTEN, *INTERNATIONAL JOURNAL OF HYDROGEN ENERGY* **38**, 4901, **2013**.
16. S. LITSTER, G. MCLEAN, *JOURNAL OF POWER SOURCES* **130**, 61, **2004**.
17. G. SASIKUMAR, J. IHM, H. RYU, *ELECTROCHIMICA ACTA* **50**, 601, **2004**.
18. J. IHM, H. RYU, J. BAE, W. CHOO, D. CHOI, *JOURNAL OF MATERIALS SCIENCE* **39**, 4647, **2004**.
19. J. H. CHO, J. M. KIM, J. PRABHURAM, S. Y. HWANG, D. J. AHN, H. Y. HA, S.-K. KIM, *JOURNAL OF POWER SOURCES* **187**, 378, **2009**.
20. L. SUN, R. RAN, G. WANG, Z. SHAO, *SOLID STATE IONICS* **179**, 960, **2008**.

21. L. SUN, R. RAN, Z. SHAO, *INTERNATIONAL JOURNAL OF HYDROGEN ENERGY* **35**, 2921, **2010**.
22. S. MARTIN, P. GARCIA-YBARRA, J. CASTILLO, *JOURNAL OF POWER SOURCES* **195**, 2443, **2010**.
23. A. CHAPARRO, M. FOLGADO, P. FERREIRA-APARICIO, A. MARTÍN, I. ALONSO-ÁLVAREZ, L. DAZA, *JOURNAL OF THE ELECTROCHEMICAL SOCIETY* **157**, B993, **2010**.
24. S. TOWNE, V. VISWANATHAN, J. HOLBERY, P. RIEKE, *JOURNAL OF POWER SOURCES* **171**, 575, **2007**.
25. A. D. TAYLOR, E. Y. KIM, V. P. HUMES, J. KIZUKA, L. T. THOMPSON, *JOURNAL OF POWER SOURCES* **171**, 101, **2007**.
26. K. BEARD, M. SCHAAL, J. VAN ZEE, J. MONNIER, *APPLIED CATALYSIS B: ENVIRONMENTAL* **72**, 262, **2007**.
27. I. KATSOUNAROS, D. IPSAKIS, C. POLATIDES, G. KYRIACOU, *ELECTROCHIMICA ACTA* **52**, 1329, **2006**.
28. I. KATSOUNAROS, G. KYRIACOU, *ELECTROCHIMICA ACTA* **52**, 6412, **2007**.
29. P. MILLET, R. NGAMENI, S. GRIGORIEV, V. FATEEV, *INTERNATIONAL JOURNAL OF HYDROGEN ENERGY* **36**, 4156, **2011**.
30. P. MILLET, R. NGAMENI, S. GRIGORIEV, N. MBEMBA, F. BRISSET, A. RANJBARI, C. ETIEVANT, *INTERNATIONAL JOURNAL OF HYDROGEN ENERGY* **35**, 5043, **2010**.
31. S. GRIGORIEV, V. POREMBSKY, V. FATEEV, *INTERNATIONAL JOURNAL OF HYDROGEN ENERGY* **31**, 171, **2006**.
32. X. M. REN, S. GOTTESFELD, *JOURNAL OF THE ELECTROCHEMICAL SOCIETY* **148**, A87, **2001**.
33. T. A. ZAWODZINSKI, C. DEROUIN, S. RADZINSKI, R. J. SHERMAN, V. T. SMITH, T. E. SPRINGER, S. GOTTESFELD, *JOURNAL OF THE ELECTROCHEMICAL SOCIETY* **140**, 1041, **1993**.
34. T. A. ZAWODZINSKI, J. DAVEY, J. VALERIO, S. GOTTESFELD, *ELECTROCHIMICA ACTA* **40**, 297, **1995**.
35. S. GE, B. YI, P. MING, *JOURNAL OF THE ELECTROCHEMICAL SOCIETY* **153**, A1443, **2006**.

CHAPTER 3

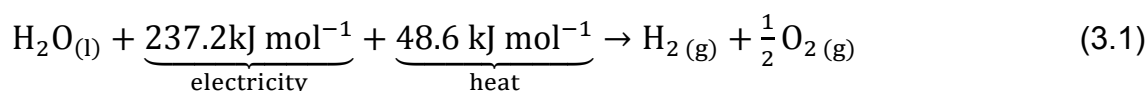
MOS₂-BASED MATERIALS AS ALTERNATIVE CATHODE CATALYST FOR PEM ELECTROLYSIS



3.1 Introduction

Hydrogen is considered as one of the most promising future chemical energy carriers, because it is energetically rich and clean; and only water is produced upon burning as described in [Chapter 1](#). However, hydrogen does not naturally occur in nature and its production is one of the greatest challenges towards the so-called, hydrogen economy [1].

Among available technologies for hydrogen production, electrochemical water splitting ([eq. 3.1](#)) stands out as a cleaner and more advantageous approach in performance, reliability, and scalability [2-4].



The approach is also favourable in the light of increasingly available renewable energy. PEM electrolysis has great advantages over other electrolysis technologies ([Chapter 1](#)). Noble metals such as platinum (Pt black) and iridium (IrO₂ or Ir black) are widely chosen as electrode catalysts because of their high performance, but their low abundance on Earth's crust [5] as well as their high price make them unsustainable for future use and unfavoured on a large scale [6]. Moreover, Pt can be poisoned by chemical species adsorbed on its surface affecting the cathodic potential, resulting in decreased performance of HER [7].

In the quest for non-precious metal alternatives, molybdenum disulphide (MoS₂) has been found to be a promising catalyst for HER [8-10]. MoS₂ is remarkably more economical than Pt and more importantly Mo is about 10⁴ times more abundant than Pt [5]. MoS₂-based catalysts have been used as

hydrogenation catalysts in industrial processes like hydrodesulphurisation (HDS) of crude oil [11-13]. Thus, Mo-based materials are interesting alternatives, becoming a trending material for researchers during the last few years [10].

MoS₂ is classified as a metal dichalcogenide and it behaves as a semiconductor similar to silicon with good chemical stability and laminar structure, showing great benefits in the performance when used in electrochemical systems [7]. Electrocatalytic activity of MoS₂ catalysts correlates linearly with the number of edges in its substructure [8]. Amorphous MoS₂ is consequentially not as catalytically active as its nanoparticle-sized or hybrid-supported counterparts [14]. Recently, MoS₂ has been shown to exhibit competent performance in microbial electrolysis cells, outperforming stainless steel which is the leading low cost HER catalyst [7, 15]. Also, MoS₂ chemically bound to graphene oxide (GO) or reduced GO (RGO) was reported as a novel and advanced catalyst [14], exhibiting a high electrocatalytic activity in HER.

3.1.1 Aim of the Study

The aim of this study was to evaluate the performance of MoS₂-based materials as cathode HER catalyst in PEM electrolysis. We selected three different forms of MoS₂-based materials for this purpose: (1) Bare pristine MoS₂, (2) MoS₂ physically mixed with an electrically conducting carbon material (Vulcan) [7] and (3) MoS₂ nanoparticles chemically bound to reduced graphene oxide (MoS₂/RGO). The performance of these materials was evaluated by means of polarization curves and compared with that of Pt black, serving as a highly performing cathode reference catalyst in HER (Figure 3.1) [16].

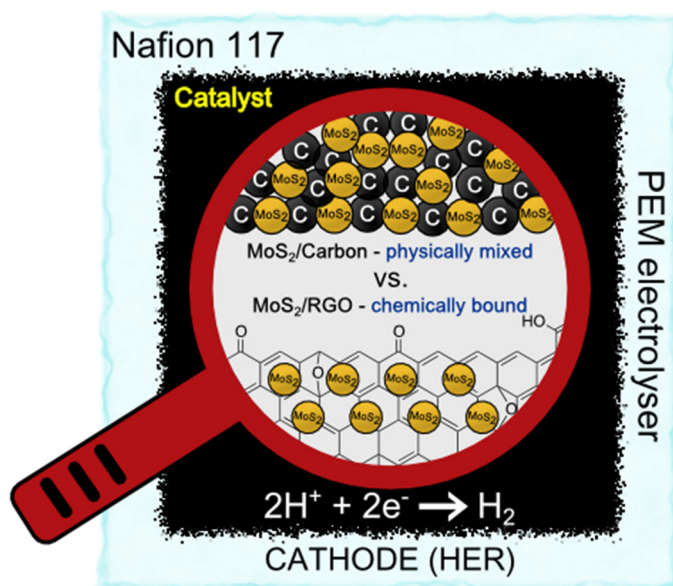
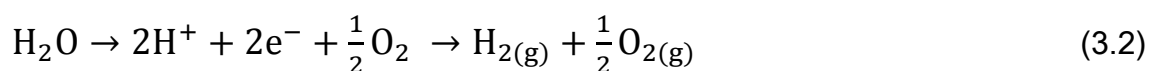


Figure 3.1. Schematic view of MoS₂ composites investigated in this study. Top part MoS₂/Carbon and bottom part MoS₂/RGO [16].

3.2 From Electrical Current to H₂ and O₂ Production

There is a linear relation between the current passing in a PEM electrolyser and the hydrogen and oxygen produced (e.g. mL/min). The higher the current, the higher the gas production. Oxidation of a water molecule generates 2 protons (H⁺) and 2 electrons (e⁻) (eq. 3.2). Two H⁺ recombine with two e⁻, generating H₂ at cathode. Therefore, for each two flowing electrons, one H₂ molecule is formed (eq. 3.2).



It is rather straightforward to calculate the amount of H₂ and O₂ theoretically produced as a function of electrical current (I, A) or current density (j, A/cm²) for an electrolyser. Hence, the mass of H₂ produced (m_{H₂}) over time can be calculated from Faraday's law of electrolysis, eq. 3.3.

$$m_{H_2} = \frac{Q \cdot M}{F \cdot Z} \quad (3.3)$$

Where F is the Faraday constant (96485 C/mol e⁻), Q is the total charge transferred (I·t) during reaction, Z the amount of electrons transferred per each mol of H₂ produced (i.e., 2:1) and M molecular mass of H₂. At same time, if eq. 3.3 is combined with ideal gas law (PV=nRT, R = 0.082 atm·L/K·mol) together and later rearranged, flow rate of H₂ produced inside the electrolyser (F_{H₂} in L/s) can be elucidated for any condition of I (A), P (atm) and T (K) (eq. 3.4).

$$F_{H_2} \left(\frac{L}{s} \right) = \frac{I \cdot R \cdot T}{Z \cdot F \cdot P} \quad (3.4)$$

Similarly, from the stoichiometry of the water splitting reaction (eqs. 3.1 and 3.2), O₂ production rate (F_{O₂}) can be calculated as well. Table 3.1 shows several values for H₂ and O₂ flow rates at different electrical current standards.

Table 3.1. Theoretical H₂ and O₂ production rate (mL/min) versus electrical current through membrane. T = 80 °C and P = 1 atm.

Current / A	H ₂ production / mL·min ⁻¹	O ₂ production / mL·min ⁻¹
0.00	0.00	0.00
0.10	0.90	0.45
0.50	4.50	2.25
1.00	9.00	4.50
2.00	18.0	9.00
3.00	27.0	13.5
5.00	45.0	22.5
10.0	90.0	45.0

3.3 Materials

3.3.1 MoS₂ Mixed with Carbon Material

Molybdenum(IV) sulphide (MoS₂) was physically mixed [7] with Vulcan during the preparation of the cathode catalyst inks. No further preparation was required prior to deposition over the PEM (section 3.4). Four different weight percentages of MoS₂ in the mixture of MoS₂ with Vulcan, 9, 33, 47, and 70 wt% were examined.

3.3.2 MoS₂ Nanoparticles Deposited on Reduced Graphene Oxide (MoS₂/RGO)

Graphene oxide (GO) was synthesized using the improved Hummers method [17] using graphite flakes (natural, 325 mesh, >99.8% metals basis, Alfa Aesar) as the starting material. The hybrid MoS₂/RGO material was synthesized according to the method described by Li et al. [14]. In short, 10 mg of the obtained GO were suspended in *N,N*-dimethylformamide (DMF) by sonication for 30 min. 22 mg of ammonium tetrathiomolybdate ((NH₄)₂MoS₄, >99.97% trace metals basis, Sigma-Aldrich) was added and the solution was sonicated for 30 min. Then, 0.1 mL of hydrazine (N₂H₄ monohydrate, >99%, Alfa Aesar) was added to the solution, which was further sonicated for 30 min. The resultant solution was transferred to a 40 mL autoclave, heated at 200 °C for 10 h. During this solvothermal reaction, (NH₄)₂MoS₄ precursor was reduced to MoS₂ on GO surface and, at same time, the GO was transformed to RGO by hydrazine reduction, finally yielding MoS₂ dispersed on RGO (MoS₂/RGO).

The synthesised MoS₂/RGO materials were characterised by transmission electron microscopy (TEM) using a JEOL 1011 operated at 80 kV (Figure 3.2a). The sample was dispersed in ethanol, and a drop of the suspension was poured onto carbon coated-copper grids. Furthermore, the starting and final materials were characterised by Raman spectroscopy (Renishaw InVia Raman) using a 633 nm excitation laser to confirm whether the desired materials (GO, RGO, and MoS₂) were properly synthesized (Figure 3.2b). Moreover, energy dispersive X-ray (EDX) analysis was employed to quantify molybdenum to carbon and oxygen (Mo:C:O) ratio. EDX analysis was performed on an FEI Quanta 600 ESEM equipped with an Oxford Instruments EDS Detector.

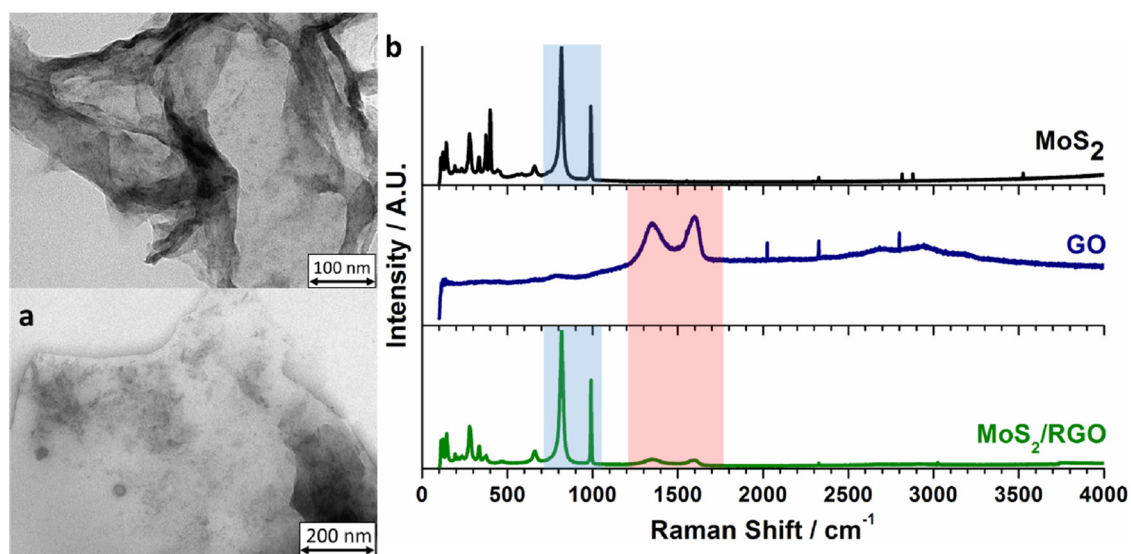


Figure 3.2. MoS₂/RGO characterization: (a) TEM images of as-synthesized MoS₂/RGO, (b) Raman spectra of MoS₂ (characteristic bands are highlighted in blue shadow), GO (characteristic bands are highlighted in red shadow), and chemically bound MoS₂ on reduced GO (MoS₂/RGO).

3.4 MEA Preparation and PEM Electrolysis

MEA were prepared as described in [Chapter 2 \(section 2.2\)](#). Iridium (IV) oxide (IrO_2) was used as the anode catalyst with a fixed loading of 2 mg/cm^2 . Pt black ($\leq 20 \text{ }\mu\text{m}$ powder, surface area $\geq 25 \text{ m}^2/\text{g}$, $\geq 99.97\%$ trace metal basis, Sigma Aldrich) was used as reference cathode catalyst with 0.6 mg/cm^2 loading.

Catalyst materials for anode or cathode were coated over the pre-treated Nafion membrane ($2 \times 2 \text{ cm}^2$ active area, $3.5 \times 3.5 \text{ cm}^2$ total area) by spray deposition. The inks were composed of a mixture of catalyst powder, 2 g of isopropanol, and Nafion solution amounting to 15.4 wt% dry Nafion per total dry solid.

Electrolysis tests were performed at $80 \text{ }^\circ\text{C}$ using a home-made PEM electrolyser cell shown in [Figure 2.7](#) integrated in a flow system shown in [Figure 2.9](#) with the procedure described in [Chapter 2 \(section 2.3.3.1\)](#).

3.5 Electrolyser Performance

3.5.1 Hybrid MoS_2/RGO Characterization

[Figure 3.2a](#) shows the TEM images of the as-synthesized MoS_2/RGO . From [Figure 3.2a](#) (top) we can recognize the characteristic folding of graphene oxide sheets and from [Figure 3.2a](#) (bottom) the MoS_2 (darker spots) deposited onto the graphene oxide sheet can be clearly observed. The Raman spectrum of MoS_2/RGO ([Figure 3.2b](#)) confirms the co-presence of GO (two bands around 1500 cm^{-1}) and MoS_2 (bands in $100\text{-}1000 \text{ cm}^{-1}$ with the prominent bands at 819 and 991 cm^{-1}), in agreement with the spectra of the respective reference materials (MoS_2 and GO, [Figure 3.2b](#)). Mo:C:O atomic ratio of the MoS_2/RGO

sample was found to be 1:13.5:2.7, corresponding to approximately 43.8 wt% MoS₂ in MoS₂/RGO. The characterization results were similar to those reported in literature [14]; therefore we concluded that the hybrid MoS₂/RGO material was successfully synthesized.

3.5.2 Performance of MoS₂/Carbon

First, the effect of mixing MoS₂ with electrically conducting carbon material (Vulcan) on PEM electrolysis performance was investigated by means of polarization curves. The physically-mixed materials with various amounts of MoS₂ namely 9, 33, 47, 70 and 100 wt%, with respect to the total weight of MoS₂/Vulcan were evaluated as the cathode catalyst. In the MoS₂/Vulcan composite, the amounts of Vulcan (5 mg/cm²) and the Nafion binder were kept constant; therefore the amount of MoS₂ was changed to vary the loading of MoS₂.

Although the performance of MoS₂/Vulcan at 9 wt% MoS₂ is rather poor (Figure 3.3 curve a), increasing the amount of MoS₂ in the cathode catalyst remarkably improved the HER activity and electrolysis performance (Figure 3.3, curves b (33 wt%) and c (47 wt%)). However, further increase of MoS₂ in the catalyst (curve d (70 wt%)) resulted negatively, decreasing the HER activity. Pure MoS₂ without Vulcan (curve e) exhibited HER activity, but the performance was poor and lower than that of the sample where the least amount of MoS₂ was mixed with Vulcan (9 wt% MoS₂/Vulcan, curve a).

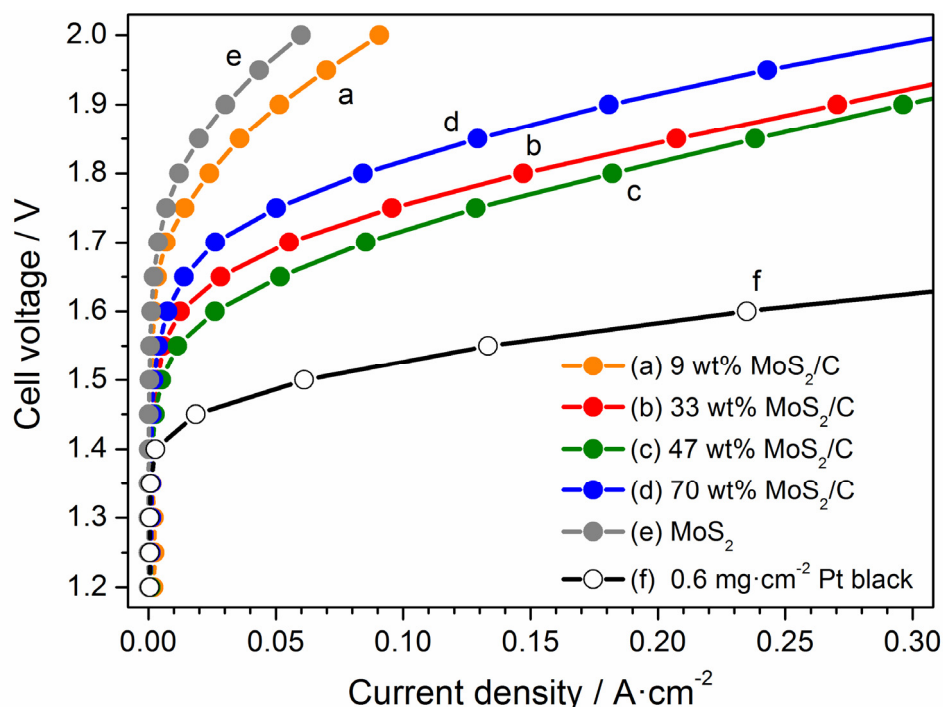


Figure 3.3. Polarization curves (potential sweep from 1.2 to 2.0 V, $\Delta V = 0.05$ V) for PEM electrolysis using MoS₂/Vulcan as the cathode catalyst with varying amount of MoS₂ with respect to total amount of MoS₂/Vulcan: (a) 9 wt%, (b) 33 wt%, (c) 47 wt%, (d) 70 wt%, (e) 100 wt% (i.e. bare MoS₂ without Vulcan). As a reference, the performance of Pt black (f) is also shown. Anode: IrO₂ 2 mg/cm², cathode: Vulcan (5 mg/cm²) mixed with proper amount of MoS₂ or bare Pt black 0.6 mg/cm².

The results indicate the critical importance of the ratio between MoS₂ and carbon material (here Vulcan). The major role of the carbon material is the enhancement of catalyst conductivity, highly beneficial to efficiently utilize electrocatalytic sites distributed over the PEM. This was confirmed by a simple 4-point measurement of the resistance through the cathode catalyst coated on the Nafion membrane using an Agilent 34401A digital multimeter (Figure 3.4). Using such method, resistivity (ρ in $\Omega \cdot \text{m}$, eq. 3.5) of the catalyst layer was evaluated and thus, conductivity (κ in S/m, eq. 3.5) was determined as the reverse of resistivity.

$$\rho = R \frac{A}{L} \rightarrow \kappa = \frac{1}{\rho} \quad (3.5)$$

Where R is the resistance between the electrical contacts, A is the cross section ($25 \cdot 10^{-4} \times 4 \text{ cm}^2$) area of the layer and L is the distance in between contacts. These measurements showed a much higher relative conductivity of the MoS₂/Vulcan membranes, which were between 14 and 20 S/m, than that of the MoS₂ membrane, which showed conductivity values as low as $2 \cdot 10^{-3} \text{ S/m}$. The amount of MoS₂ is also critical because this is the active material of the reaction; therefore, there exists a well-balanced, optimum amount of MoS₂ in the MoS₂/Vulcan mixture. Following the trend observed in [Figure 3.3](#), it can be concluded that the optimum lies around 47 wt% MoS₂ in MoS₂/Vulcan. This is exactly the value reported to be optimum for HER in microbial electrolysis cells and this study confirms that the specific amount of MoS₂ in MoS₂/Vulcan is also beneficial when used for PEM electrolysis.

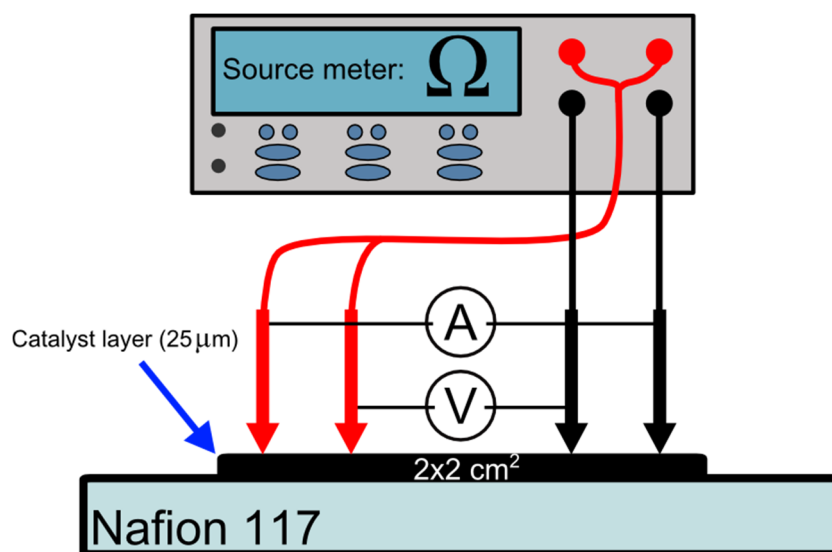


Figure 3.4. 4-point measurement of the resistance through the cathode catalyst coated on the Nafion membrane using a digital multimeter.

3.5.3 Performance of MoS₂/RGO

Furthermore, PEM electrolysis performance of the MoS₂/RGO nano-composite (Figure 3.2) as cathode catalyst was investigated to examine the effect of high dispersion of MoS₂ nanoparticles over the carbon support (RGO) and possible synergetic effects.

Figure 3.5 shows the PEM electrolysis performance of MoS₂/RGO with two different deposition loadings (1 and 3 mg/cm², curves a and b, respectively). It is compared with those of the optimum 47 wt% MoS₂/Vulcan (curve c), pure MoS₂ (curve d) and the reference Pt black cathode catalysts (curve e). Evidently, reasonable HER activities of MoS₂/RGO were observed. Increasing the amount of deposition loading (Figure 3.5, curves a and b) showed that the electrolysis performance was improved by increasing the amount, although the increase in current density was not fully proportional to the amount of the catalyst at higher cell voltage. Also, poorer performance (less prominent increase in current density) at higher cell voltage was noticed compared to the MoS₂/Vulcan composite catalysts prepared by physical mixing. This feature may be originated from the lower conductivity of RGO, which calculated from the 4-point resistance measurement, was between 2 and 5 S/m, much lower than that of MoS₂/Vulcan composites. These can be attributed to the fact that reduced graphene oxide has lower electrical conductivity than that of graphene because of the lost uniformity in its structure after reduction, and also tends to agglomerate [18]. In fact, graphene oxide is known to be an electrical insulator [19], therefore the presence of remaining oxide groups could diminish conductivity.

This conductivity problem may be mitigated by the same approach as shown in Figure 3.3, i.e. physical mixing with carbon materials, or fine-tuning the reduction procedure of GO to increase the degree of reduction and thus the conductivity. This, together with the optimum loading of MoS₂ on RGO, are parameters promising to be optimized.

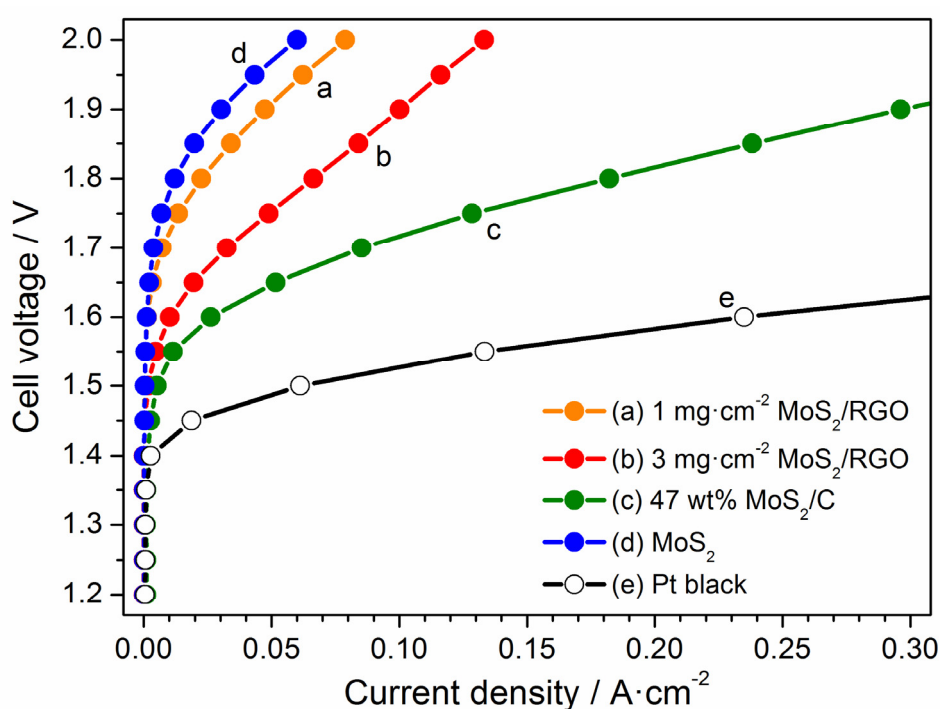


Figure 3.5. Polarization curves (potential sweep from 1.2 to 2.0 V, $\Delta V = 0.05$ V) for PEM electrolysis using two different catalyst loadings of MoS₂/RGO over the membrane (a) 1 mg/cm² and (b) 3 mg/cm². For the sake of better comparison, the performances of (c) 47 wt% and (d) 100 wt% MoS₂/Vulcan as well as (e) Pt black are shown. The loadings of these and the anode catalyst (IrO₂) are presented in the caption of Figure 3.3.

3.5.4 Effect of Hot-Press

Usually when preparing MEAs and before their usage, it is recommended to apply hot-press to properly embed the catalyst layer into the membrane [20],

promoting good contact within the three-phase region [21] and alleviating ohmic losses [18], thus to achieve better PEM electrolysis performance and to avoid catalyst delamination [22]. We investigated the effects of hot-press on PEM electrolysis performance using 9 wt%, 33 wt% and 47 wt% MoS₂/Vulcan. Hot-press was performed at a constant pressure (140 bar) for 5 min at 85 °C. [Figure 3.6](#) presents polarization curves obtained without hot-press (as obtained after spray deposition) and with hot-press. Surprisingly, the MEAs without hot-press gave better electrolysis performance at all cell voltages examined. At the cell voltage of ca. 1.6 V and above, the difference started to become prominent with increasing voltage and amount of MoS₂, even ca. 3 times higher for the MEA without hot-press at 47 wt% MoS₂ content. This suggests that hot-press strategy for MoS₂/Vulcan materials can be detrimental. Although the reason for the decreased performance of hot-pressed membranes is not known and further studies are needed to understand this phenomenon, it can be attributed to a reduction in the size of the pores of the Nafion membrane which diminishes proton conductivity and therefore performance [23]. This effect would become more apparent at higher current densities as observed in the polarization curves shown in [Figure 3.6](#).

It has been shown that the effect of hot-press varies depending on the thickness and tensile strength (among others) of the Nafion membrane [24, 25]. Thinner membranes with lower tensile strength such as Nafion 212 have shown more improvements by hot press than thicker membranes like Nafion 115 [24, 25]. Our data indicates that for Nafion 117 membranes water transport issues are surpassing the improved contact due to hot pressing.

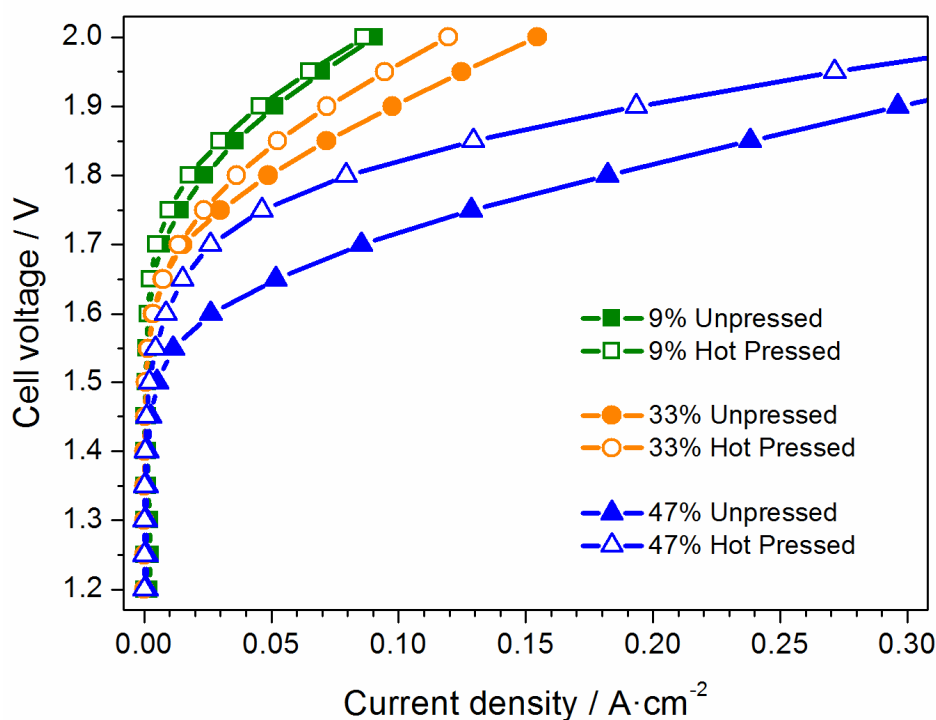


Figure 3.6. Effects of hot-press on polarization curves in PEM electrolysis using the MEA with 9 wt%, 33 wt% and 47 wt% MoS₂/Vulcan. Hot press condition was 140 bar, 85 °C for 5 min.

3.5.5 Stability Tests

The short-term and long-term stability of electrolyzers is of primary importance in practice, especially at a harsh condition such as at high cell voltage and consequently at higher current density. This point has been investigated using the best MoS₂-based cathode catalyst found in this work, 47 wt% MoS₂/Vulcan, at the highest cell voltage investigated in this study (2.0 V).

First, we investigated the reproducibility of polarization curves upon forward (1.2 to 2.0 V) and reverse (2.0 to 1.2 V) potential sweeps without an interval between the two experiments (Figure 3.7a). Almost identical current density values were observed at all the cell voltage points along the sweep, although a slight deviation was observed between 1.65 and 1.90 V. Actually, a performance

improvement was detected upon reverse sweep due to improving stabilization period of the MEA (*vide infra*).

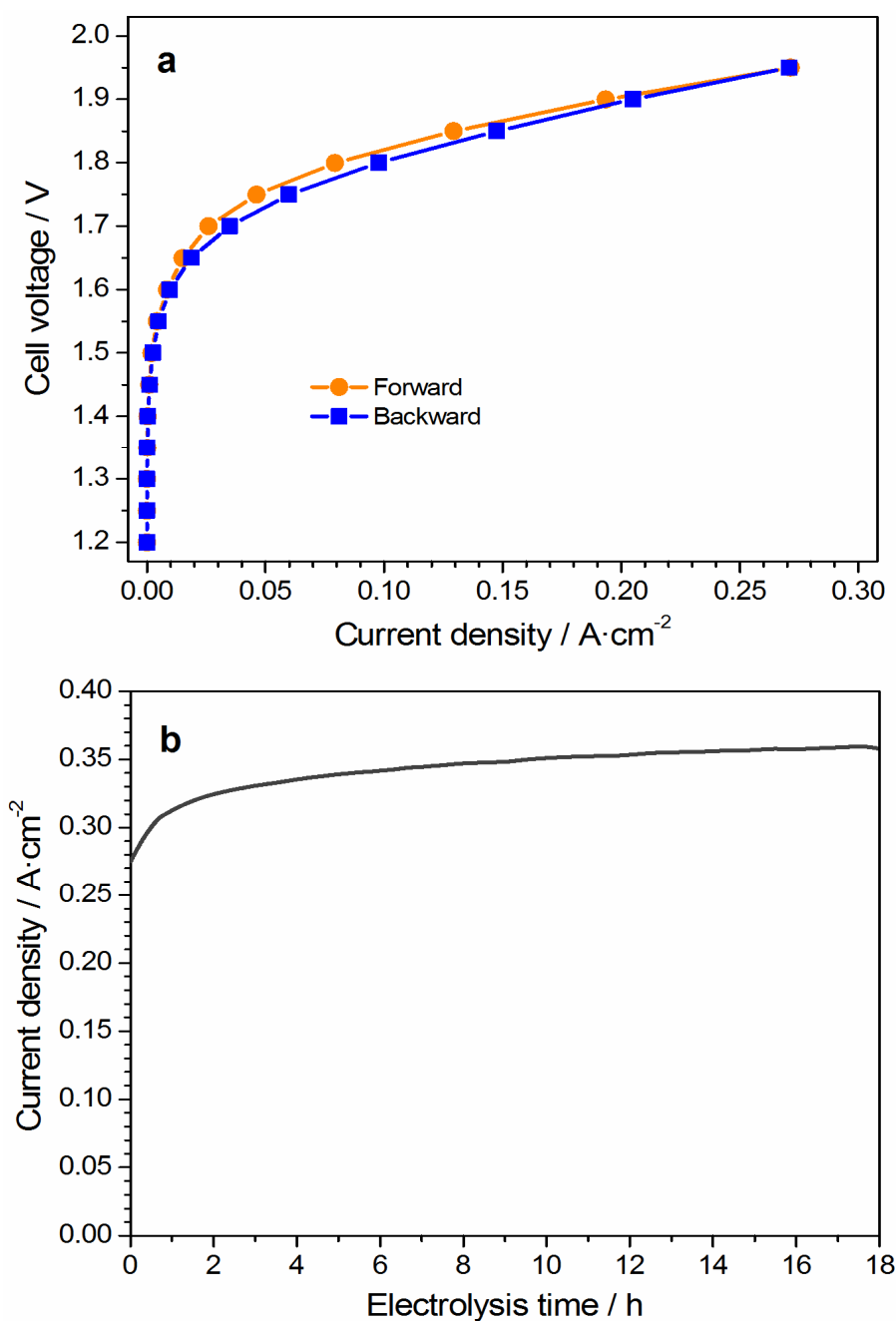


Figure 3.7. Stability tests of 47 wt% MoS₂/Vulcan in PEM electrolysis. (a) polarization curves with forward and reverse potential sweeps and (b) long term stability test at a constant cell voltage of 2.0 V.

Secondly, we investigated the long-term stability of the MEA prepared without hot-press. Figure 3.7b shows the variation of current density profile over 18 h of continuous PEM electrolysis of 47 wt% MoS₂/Vulcan, which was performed immediately after the continuous voltage ramp from 1.2 to 2.0 V (potential sweep, Figure 3.7a). A stable and relatively high current density (ca. 0.35 A/cm²) was reached after 15 h with no indication of performance deterioration over 18 h. The performance slightly increased overtime because of possible hydration effects as the proton and water transport occurred through the membrane [26]. Based on these results, we can conclude that MoS₂/Vulcan catalyst is a stable electrocatalyst for HER in PEM electrolysis.

3.6 Conclusions

MoS₂ was found to be an efficient, inexpensive cathode catalyst in PEM electrolysis when its electrical conductivity is enhanced by simple physical mixing with highly conducting carbon materials (Vulcan) or by finely dispersing MoS₂ over RGO.

The ratio of MoS₂ to carbon highly influenced the performance of the physically mixed MoS₂/Vulcan composites. Best performance among all the materials evaluated in this study was observed with 47 wt% MoS₂/Vulcan, which also showed high long-term stability up to 18 h of continuous operation in a PEM electrolyser. This material's stability, facile preparation and improved performance when compared to pristine MoS₂ are encouraging features for practical application.

MoS₂/RGO was successfully synthesized and characterized. This catalyst showed reasonable and promising activity in PEM electrolysis; however, further investigation is required to evaluate the real value of the nano-composite in HER, e.g. by increasing the conductivity of the material by physical mixing with carbon material and by tuning the reduction procedure of GO together with the amount of MoS₂ deposited on RGO.

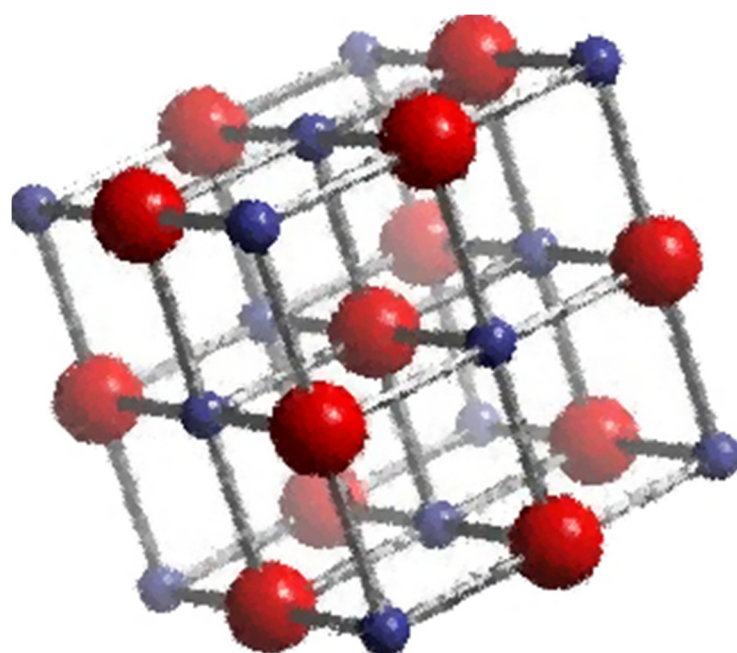
BIBLIOGRAPHY

1. G. W. CRABTREE, M. S. DRESSELHAUS, M. V. BUCHANAN, *PHYSICS TODAY* **57**, 39, **2004**.
2. P. MILLET, N. MBEMBA, S. A. GRIGORIEV, V. N. FATEEV, A. AUKAULOO, C. ETIEVANT, *INTERNATIONAL JOURNAL OF HYDROGEN ENERGY* **36**, 4134, **2011**.
3. P. MILLET, R. NGAMENI, S. GRIGORIEV, V. FATEEV, *INTERNATIONAL JOURNAL OF HYDROGEN ENERGY* **36**, 4156, **2011**.
4. P. MILLET, R. NGAMENI, S. GRIGORIEV, N. MBEMBA, F. BRISSET, A. RANJBARI, C. ETIEVANT, *INTERNATIONAL JOURNAL OF HYDROGEN ENERGY* **35**, 5043, **2010**.
5. A. EARNSHAW, N. GREENWOOD, *CHEMISTRY OF THE ELEMENTS*, ELSEVIER, **1997**.
6. M. CARMO, D. L. FRITZ, J. MERGE, D. STOLTEN, *INTERNATIONAL JOURNAL OF HYDROGEN ENERGY* **38**, 4901, **2013**.
7. J. C. TOKASH, B. E. LOGAN, *INTERNATIONAL JOURNAL OF HYDROGEN ENERGY* **36**, 9439, **2011**.
8. T. F. JARAMILLO, K. P. JORGENSEN, J. BONDE, J. H. NIELSEN, S. HORCH, I. CHORKENDORFF, *SCIENCE* **317**, 100, **2007**.
9. H. I. KARUNADASA, E. MONTALVO, Y. SUN, M. MAJDA, J. R. LONG, C. J. CHANG, *SCIENCE* **335**, 698, **2012**.
10. A. B. LAURSEN, S. KEGNÆS, S. DAHL, I. CHORKENDORFF, *ENERGY & ENVIRONMENTAL SCIENCE* **5**, 5577, **2012**.
11. S. BRUNET, D. MEY, G. PÉROT, C. BOUCHY, F. DIEHL, *APPLIED CATALYSIS A: GENERAL* **278**, 143, **2005**.
12. J. S. CHOI, F. MAUGE, C. PICHON, J. OLIVIER-FOURCADE, J. C. JUMAS, C. PETIT-CLAIR, D. UZIO, *APPLIED CATALYSIS A-GENERAL* **267**, 203, **2004**.
13. G. SCHUIT, B. GATES, *AICHE JOURNAL* **19**, 417, **1973**.
14. Y. LI, H. WANG, L. XIE, Y. LIANG, G. HONG, H. DAI, *JOURNAL OF THE AMERICAN CHEMICAL SOCIETY* **133**, 7296, **2011**.
15. A. KUNDU, J. N. SAHU, G. REDZWAN, M. A. HASHIM, *INTERNATIONAL JOURNAL OF HYDROGEN ENERGY* **38**, 1745, **2013**.
16. T. CORRALES-SÁNCHEZ, J. AMPURDANÉS, A. URAKAWA, *INTERNATIONAL JOURNAL OF HYDROGEN ENERGY* **39**, 20843, **2014**.
17. D. C. MARCANO, D. V. KOSYNKIN, J. M. BERLIN, A. SINITSKII, Z. SUN, A. SLESAREV, L. B. ALEMANY, W. LU, J. M. TOUR, *ACS NANO* **4**, 4806, **2010**.
18. V. MEHTA, J. S. COOPER, *JOURNAL OF POWER SOURCES* **114**, 32, **2003**.
19. S. PEI, H.-M. CHENG, *CARBON* **50**, 3210, **2012**.
20. A. THERDTHIANWONG, P. MANOMAYIDTHIKARN, S. THERDTHIANWONG, *ENERGY* **32**, 2401, **2007**.

21. K. S. LOH, A. B. MOHAMAD, N. HARAHAP, A. A. KADHUM, W. R. DAUD, *CHEMICAL ENGINEERING & TECHNOLOGY* **34**, 439, **2011**.
22. Z. LIANG, T. ZHAO, C. XU, J. XU, *ELECTROCHIMICA ACTA* **53**, 894, **2007**.
23. S. Y. JEONG, O. H. HAN, *BULL. KOREAN CHEM* **30**, 1559, **2009**.
24. A. BAYRAKÇEKEN, S. ERKAN, L. TÜRKER, İ. EROĞLU, *INTERNATIONAL JOURNAL OF HYDROGEN ENERGY* **33**, 165, **2008**.
25. M. GLASSMAN, A. OMOSEBI, R. BESSER, *JOURNAL OF POWER SOURCES* **247**, 384, **2014**.
26. M. CAPPADONIA, J. W. ERNING, S. M. S. NIAKI, U. STIMMING, *SOLID STATE IONICS* **77**, 65, **1995**.

CHAPTER 4

CO₃O₄ FOR HIGH POTENTIAL PEM ELECTROLYSIS



4.1 Introduction

The quest for novel, abundant, non-expensive, and high-performance electrode materials in water electrolysis started several years ago. Our attempt in this direction was demonstrated in [Chapter 3](#) using MoS₂-based materials which exhibited promisingly high performance at the relevant level for practical applications. During the course of the doctoral thesis project, we encountered another type of economical material, Co₃O₄, showing a good HER activity particularly with excellent stability. This chapter describes evaluation of Co₃O₄ and Co₃O₄-based materials in HER.

Cobalt-containing materials are known to be active in electrochemical reactions. Many spinel cobaltite oxides meet the requirement for a wide range of electrochemical reactions, mainly for OER or oxygen reduction reaction (ORR) [1]. The presence of mixed valences of the same cation in such cobaltite spinel systems is known to induce the bifunctional behaviour of the materials towards OER and ORR by providing donor-acceptor chemisorption sites for the reversible adsorption of oxygen. Also, these oxides exhibit relatively high electrical conductivity by electron transfer taking place with relatively low activation energy between cations of different valences by hopping processes.

Cobaltites (e.g. Co₃O₄, NiCo₂O₄, MgCo₂O₄, MnCo₂O₄ spinel oxides) have received great interests and they are used in many industrial applications. Co₃O₄ has been shown to be an effective anode material for various oxidation reactions including Cl⁻ to Cl₂ [2], CO to CO₂ [3], EtOH to AcOH [4] and H₂O to O₂ [5-7]. The same material has also considerable potential for use as electrolytic capacitor [8,

9], as anode in air–metal batteries, and it has also demonstrated high lithium storage capacity and good cycle-ability [10].

Co₃O₄ adopts the normal spinel (Figure 4.1) structure, with Co²⁺ ions in tetrahedral interstices and Co³⁺ ions in the octahedral interstices of the cubic close-packed lattice of oxide anions. Co₃O₄ is also referred as cobalt (II,III) oxide since it has mixed valences; hence, its formula is sometimes written as Co^{II}Co^{III}₂O₄ or CoO·Co₂O₃ [11]. The advantages of using these oxides as electrode materials are associated with their activity, availability, low cost, thermodynamic stability, low electrical resistance and their environmental friendliness [1]. In fact, cobalt (Co) is 10 times more abundant than molybdenum (Mo) in Earth's crust [11]. Furthermore, current market price of bulk MoS₂ or Co₃O₄ is about the same; ca. 0.5 €/g, and this is 400 times cheaper than Pt black, ca. 200 €/g (values taken from common chemical suppliers brochure).

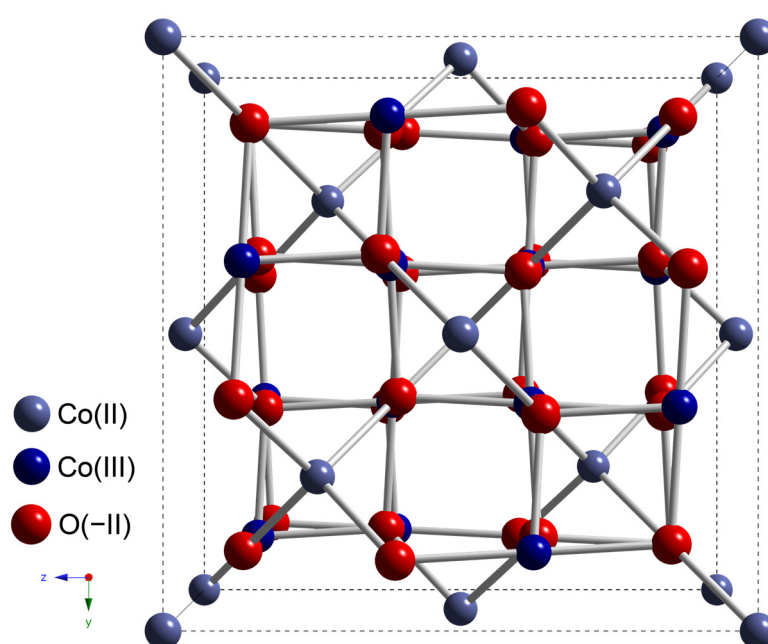


Figure 4.1. Spinel structure (unit cell) of cobalt (II, III) oxide (Co₃O₄).

Our literature survey reveals that many experimental works have focused on the electroactivity of Co_3O_4 in the last two decades [1, 7, 12, 13], all related with OER and ORR [1]. However, the material was never tested as a cathode material for HER.

As already mentioned in [Chapter 1](#), PEM electrolysis research is generally focused on minimizing electrodes overpotentials in order to efficiently work at either thermoneutral (1.48 V, 100% voltage efficiency) or reversible (1.23 V, 120% voltage efficiency) water splitting potentials while reducing the amount of noble metal required [14-16]. From literature, the highest performance values of a PEM electrolyser operating at “low potential” are stacked at ca. 2.0 A/cm² at around 1.7 V using Pt-based cathodes [14].

4.1.1 Aim of the Study

The main goal of this chapter’s work was to evaluate Co_3O_4 as a novel cathode material in PEM electrolysis particularly in a very wide range of cell voltages (1.2 to 2.7 V). We selected two different forms of Co_3O_4 -based materials: (1) Bare commercial Co_3O_4 and (2) Co_3O_4 physically mixed with Vulcan [17]. The latter was chosen because of the previously-shown great benefit of Vulcan addition to another alternative HER active material, MoS_2 ([Chapter 3](#)). The performance of these materials was evaluated by means of polarization curves and compared with those of Pt black and 47 wt% of MoS_2 /Vulcan [18] as reference materials for HER. Moreover, examination of PEM electrolysis stability is of central importance due to possible high cell voltage applications. Therefore, a long-term stability test using the most active HER material up to 24 h was performed.

4.2 Materials

4.2.1 Co₃O₄ Mixed with Carbon Material

Cobalt (II, III) oxide (Figure 4.2) was physically mixed with Vulcan during the preparation of the cathode catalyst inks (Chapter 2, section 2.2.2). No further preparation was required prior to deposition over the polymer electrolyte membrane. Four Co₃O₄-Vulcan composites with different weight percentages of Co₃O₄, namely 9, 33, 47, and 70 wt% were prepared.

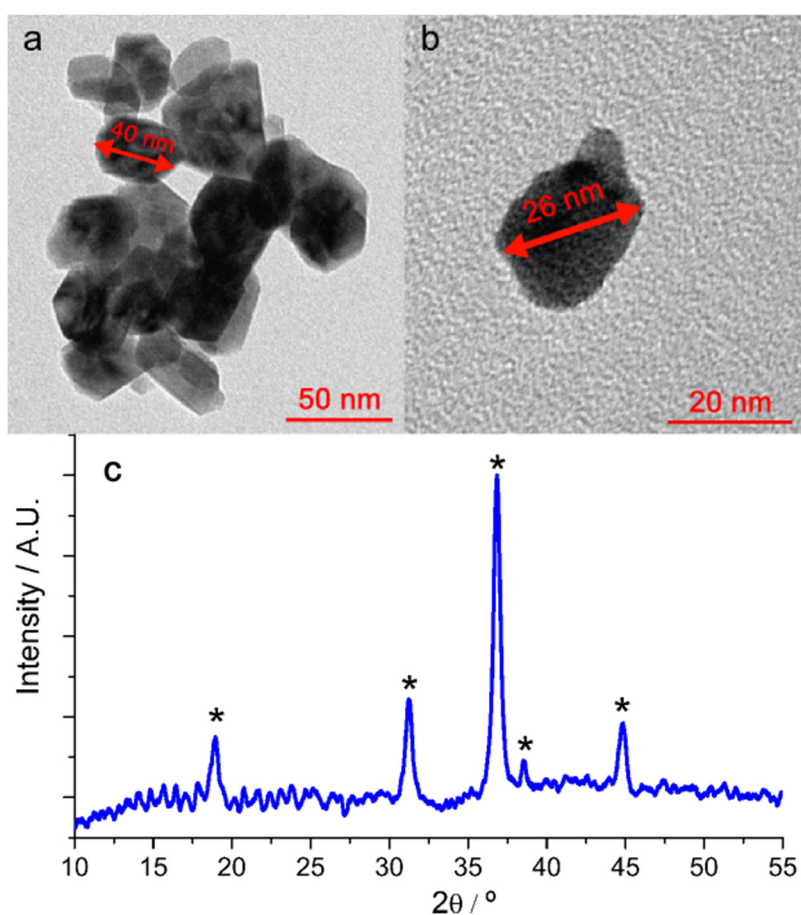


Figure 4.2. Material characterisation: (a) TEM micrograph of commercial cobalt (II,III) oxide nanopowder employed in our studies, agglomerated particles, (b) single particle and (c) Powder XRD pattern of Co₃O₄.

In [Figure 4.2a and b](#), TEM pictures (JEOL 1011 operated at 80 kV) are shown (agglomerated particles and single particle, respectively). The observed particle size of the material was around 20-40 nm, which is in agreement with the specifications on the datasheet (<50 nm). Apparently, the particle shape was not well-defined. [Figure 4.2c](#) shows an XRD profile of the Co_3O_4 where the most characteristic phases of this material are highlighted, confirming the crystalline structure commonly described in literature and database [19, 20].

4.3 MEA Preparation

MEA preparation is extensively described in [Chapter 2 \(section 2.2\)](#). It is important to note that IrO_2 (>99%, powder, Alfa Aesar) was used as the anode catalyst with a fixed loading of 2 mg/cm². This IrO_2 was from same batch as the one we used for MoS_2 studies, in order to allow a proper comparison among different MEAs (depending on the purchase date, the structure of IrO_2 was different, sometimes containing significant amount of metallic Ir). Furthermore, Pt black was used as reference cathode catalyst with 0.6 mg/cm² loading. The anode and cathode catalyst materials were coated over the pre-treated Nafion membrane (2x2 cm² active area, 3.5x3.5 cm² total area) by spray deposition, following the procedure described in [Chapter 2 \(Figure 2.4 and section 2.2.3\)](#).

4.4 System Configuration

The PEM electrolyser system is described in [Chapter 2 \(section 2.3.2 and Figure 2.9\)](#) and the same parameters as for MoS_2 -based electrolysers ([Chapter](#)

3) were used. The only difference was the cathode material (Co₃O₄/Vulcan instead of MoS₂/Vulcan).

Polarization curves were evaluated in a wide range from 1.2 to 2.7 V, because our aims were to study the Co oxides material at the current density (*j*) through the system at non-conventional high cell voltages and to examine electrolysis stability under such conditions. Especially, we focused on the higher cell voltage range from 2.0 to 2.7 V where not only current density is important but also stability plays crucial roles. Thus, the study was summarized in two regions separated by employed cell voltage: (i) Low potential region (1.2-2.0 V) and (ii) high potential (2.0-2.7 V) region.

4.5 Results

4.5.1 Performance of Co₃O₄/Carbon

The effect of mixing Co₃O₄ with electrically conducting carbon material (Vulcan) on PEM electrolysis performance was investigated by means of polarization curves. The physically-mixed materials with various amounts of Co₃O₄ namely 9, 33, 47, 70 and 100 wt%, with respect to the total weight of Co₃O₄/Vulcan were evaluated as the cathode catalyst. In the Co₃O₄/Vulcan composite, the amounts of Vulcan (5 mg/cm²) and the Nafion binder were kept constant (ca. 15.4 wt%); therefore the amount of Co₃O₄ was changed to vary the loading of Co₃O₄.

4.5.1.1 Low Potential Electrolysis

Operating at low potentials (1.2-2.0 V), several features among all set of materials screened were observed. First of all, pure Co_3O_4 without Vulcan (Figure 4.3 curve e) exhibited HER activity, but the performance at this range was poor and the onset potential for PEM electrolysis was >1.8 V, likely determined by the electronic (semiconducting) property of the material.

The addition of Vulcan to the material consistently improved the current density and thus electrolysis performance (Figure 4.3). Curves a, b, c and d show better current density than that of bare Co_3O_4 (curve e), this HER performance enhancement is in well agreement with what we observed in previous studies [18] (Chapter 3), although in case of the lowest Co_3O_4 loading (9 wt%, curve a), the improvement is very small and j values are almost overlapping with those of bare Co_3O_4 towards 2.0 V (curves a and e). Main reason for this is likely due to the small amount of Co_3O_4 dispersed over Vulcan surface which does not efficiently provide sufficient active sites for HER. On the other hand, 33, 47 and 70 wt% Co_3O_4 catalysts performed notably better than bare Co_3O_4 (100 wt%). The same trend as observed in MoS_2 study was recognized. That is, from 9 to 47 wt% Co_3O_4 loading, electrolysis performance improved; however, further increase in Co_3O_4 amount in the Co_3O_4 /Vulcan composites (curve d, 70 wt%) resulted negatively, decreasing the HER activity. Thus, the results indicate the critical importance of balance between the amounts of electrocatalytic material for HER (Co_3O_4) and of the carbon material (Vulcan). The major role of the carbon material is attributed to the enhancement of catalyst conductivity, highly beneficial to efficiently utilize electrocatalytic sites distributed over the PEM.

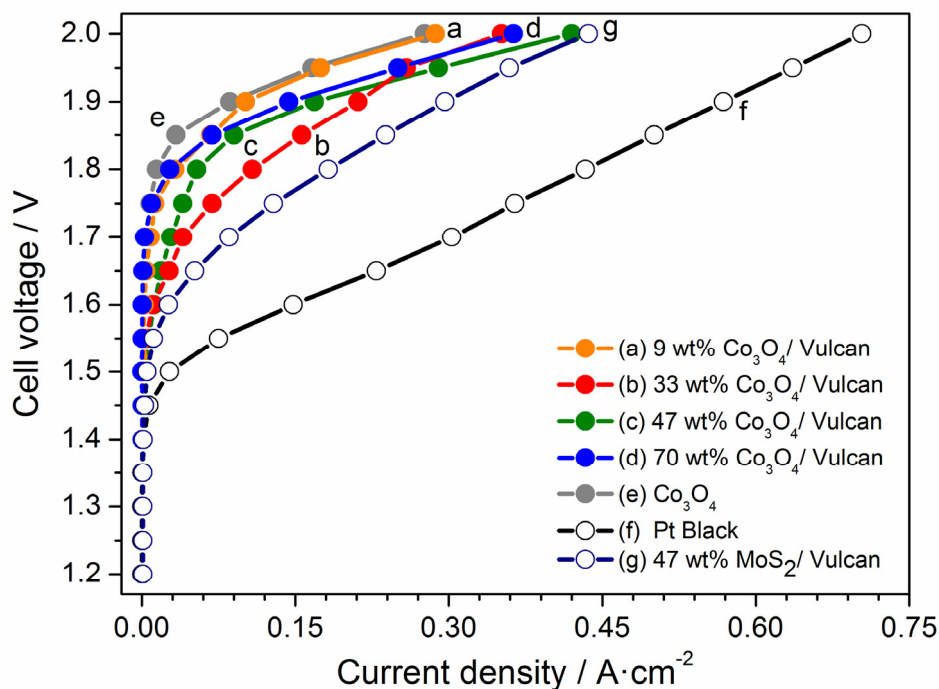


Figure 4.3. Polarization curves (potential sweep from 1.2 to 2.0 V, $\Delta V = 0.05$ V) in low potential region for PEM electrolysis using Co₃O₄/Vulcan as the cathode catalyst with varying amount of Co₃O₄ with respect to total amount of Co₃O₄/Vulcan: (a) 9 wt%, (b) 33 wt%, (c) 47 wt%, (d) 70 wt%, (e) 100 wt% (i.e. bare Co₃O₄ without Vulcan). As references, the performance of Pt black (f) and 47 wt% MoS₂/Vulcan (g) are also shown. Anode: IrO₂ 2 mg/cm², cathode: Vulcan (5 mg/cm²) mixed with proper amount of Co₃O₄ or bare Pt black 0.6 mg/cm².

From 1.6 to 1.9 V, 33 wt% Co₃O₄ performed better than 47 wt% Co₃O₄ which can be attributed to the better dispersion of cobalt oxides over Vulcan surface; but it is interesting to note that as soon as potential is close to the high potential boundary (2 V) 47 wt% Co₃O₄ boosts its performance getting almost closer to that of 47 wt% MoS₂/Vulcan (Figure 4.3, curves c and g). The Co₃O₄/Vulcan catalysts with higher Co₃O₄ loading showed superior performance at higher potentials. Comparing with the performance of our post-Pt reference catalyst, 47 wt% MoS₂/Vulcan (curve g), the reference MoS₂/Vulcan showed superior performance in 1.2 - 2 V range. It should be noted, however, that at the highest

potential range examined 47 wt% $\text{Co}_3\text{O}_4/\text{Vulcan}$ achieved nearly the same level of current density, ca. 0.42 A/cm^2 .

4.5.1.2 High Potential Electrolysis

Figure 4.4 presents the polarization curves evaluated at the higher potential range (2.0-2.7 V) using the same materials examined for the low potential electrolysis (Figure 4.3). Obviously, the trend observed in the higher potential range changed completely compared to that in the lower potential range. The most striking observation was that 47 wt% $\text{Co}_3\text{O}_4/\text{Vulcan}$ (curve c) was the best material in terms of current density at the very high potential region, showing ca. 2 A/cm^2 at 2.7 V. The performance of 47 wt% $\text{Co}_3\text{O}_4/\text{Vulcan}$ (curve c) surpassed that of 47 wt% $\text{MoS}_2/\text{Vulcan}$ (curve g) at ca. 2.05 V and, most remarkably, even that of Pt black (curve f) at 2.3 V. Although the electrolysis performance of the Pt catalyst could be better than the results we report here by further optimizing the Pt loading and conditions for catalyst deposition; nevertheless, it is very significant to observe the higher HER activity than that of the Pt catalyst. Furthermore, 47 wt% $\text{Co}_3\text{O}_4/\text{Vulcan}$ (Figure 4.4, curve c) showed a linear increase in current density proportional to the cell voltages. It is significant that there was no symptom of decelerated current increase at higher potentials in all the range examined (2.0-2.7 V). Similarly linear behaviour of current density increase at higher potential was observed for 9, 33 and 47 wt% $\text{Co}_3\text{O}_4/\text{Vulcan}$ (curves a, b and c). Among the three composite materials, 47 wt% $\text{Co}_3\text{O}_4/\text{Vulcan}$ showed the highest performance followed by 33 wt% and finally 9 wt%

Co₃O₄/Vulcan, confirming the consistent trend between electrolysis performance and loading of active HER material with respect to the carbon material.

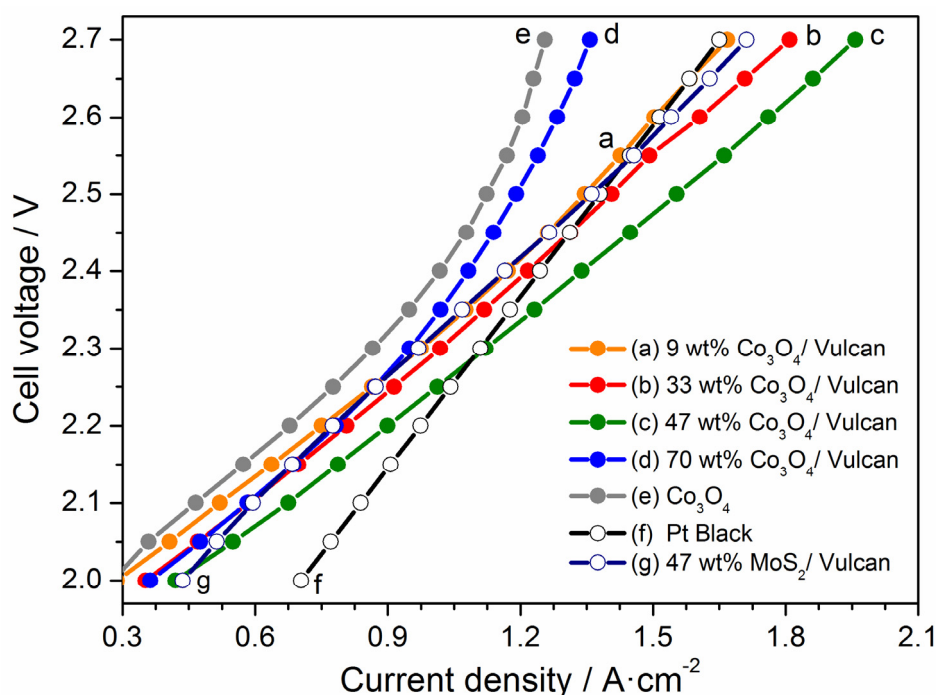


Figure 4.4. Polarization curves (potential sweep from 2.0 to 2.7 V, $\Delta V = 0.05$ V) in high potential region for PEM electrolysis using Co₃O₄/Vulcan as the cathode catalyst with same compositions as presented in Figure 4.3. As references, the performance of Pt black (f) and 47 wt% MoS₂/Vulcan (g) are also shown. Anode: IrO₂ 2 mg/cm², cathode: Vulcan (5 mg/cm²) mixed with specified amount of Co₃O₄ or bare Pt black 0.6 mg/cm².

Another notable observation was a loss of linearity between cell potential and current density of two materials with high Co₃O₄ loadings (70 and 100 wt%), starting at ca. 2.25 V (Figure 4.4). Apparently, the amount of carbon material in 70 wt% Co₃O₄/Vulcan was so low that the electronic behavior of the composite material followed that of bare Co₃O₄. Also, it should be pointed out that not only 47 wt% but also 33 wt% Co₃O₄/Vulcan overpass 47 wt% MoS₂/Vulcan (curve g) at ca. 2.2 V and Pt black (curve f) at ca. 2.5 V.

Following the trend observed in Figure 4.4, it can be concluded that the optimum amount of Co_3O_4 in $\text{Co}_3\text{O}_4/\text{Vulcan}$ is around 47 wt%. This is exactly the value verified for $\text{MoS}_2/\text{Vulcan}$ composites (Chapter 3) and the specific amount of Co_3O_4 in the $\text{Co}_3\text{O}_4/\text{Vulcan}$ composite is also beneficial when used for PEM electrolysis.

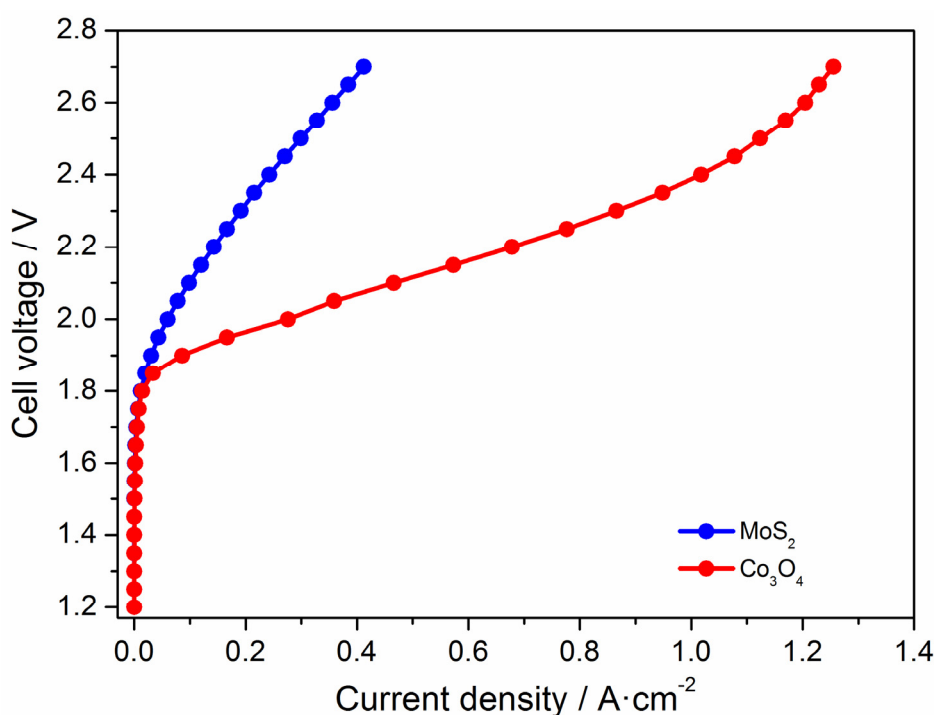


Figure 4.5. Polarization curves (I-V) of bare Co_3O_4 (red line) and bare MoS_2 (blue line). Potential steps (ΔV) of 0.05 V, from 1.2 to 2.7 V.

In order to clarify the difference of intrinsic HER activities of Co_3O_4 and MoS_2 , PEM performance of the two pure materials were investigated. Figure 4.5 shows the polarization curves of bare Co_3O_4 and MoS_2 in the full range investigated in this work (1.2 to 2.7 V). Performance of Co_3O_4 was much superior to that of MoS_2 in all the range where water splitting takes place at substantial rate (>1.8 V), next to the boundary in between low and high potential regions. At the highest cell

voltage studied (2.7 V), the current densities for Co₃O₄ and MoS₂ were ca. 1.25 and 0.40, respectively, showing nearly 3 times higher value for Co₃O₄. This comparison is consistent with what has been found above for composites with carbon; that is, Co₃O₄ is a promising candidate for high potential PEM electrolysis encouraging its utilisation in further studies.

4.5.2 Stability Tests

Short-term and long-term stability of electrolysers is of prime importance in practice, especially at a harsh condition such as at high cell voltage and consequently at higher current densities. This point has been investigated using the best Co₃O₄-based cathode catalyst found in this work for high potential region, 47 wt% Co₃O₄/Vulcan, at two cell voltages, 2.0 and 2.5 V. The same MEA was used for both tests.

We investigated long-term stability of the MEA prepared without hot-press, because we observed the negative effect of hot-press treatment on the overall performance for the MoS₂/Vulcan composites (Chapter 3) [18]. Figure 4.6 shows the variation of current density over 24 h of continuous PEM electrolysis of 47 wt% MoS₂/Vulcan at 2.0 (red line) and 2.5 V (blue line). This study was performed immediately after the continuous voltage ramp from 1.2 to 2.7 V (potential sweep, Figures 4.3 and 4.4).

Operating at 2 V, a stable and relatively high current density (ca. 0.42 A/cm²) was reached after 4 h. At 12 h indication of slight performance deterioration was observed. Such signal drift ($\Delta j / \Delta t$) was quantified and determined to be around 5 mA/cm²·h from 12h to 24h. This small signal drift may arise from the fact that

at 2.0 V the electrolysis performance lies within low-high current density transition region as shown in Figures 4.3 and 4.4. At higher potentials the Co_3O_4 -based material outperformed over other materials with a linear response against potential increase. Therefore, 2.0 V may be in the metastable range where the stability of the material in electrolysis is not well established. Furthermore, at the beginning of the test (first 4h) the performance slightly increased overtime, this is attributed to hydration effects to equilibrate the membrane for better proton and water transport through Nafion polymer [21].

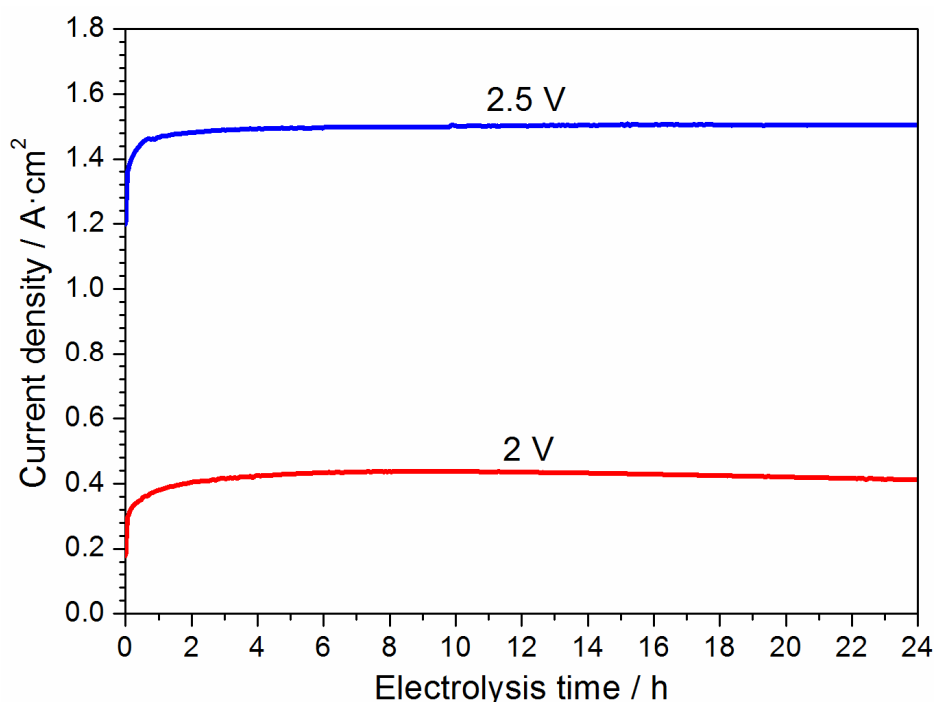


Figure 4.6. Stability tests of 47 wt% Co_3O_4 /Vulcan in PEM electrolysis. (i) Long term stability test at constant cell voltages of 2.5 V (blue line) and 2.0 V (red line).

Figure 4.6 (blue line) shows the long-term stability operating the electrolyser at 2.5 V. As in the previous case (2.0 V), at the beginning the performance slightly increased over time (1 h) because of the hydration effects. After this stabilization

period, the system was completely stable without noticeable performance deterioration in PEM electrolysis along the tested period of 24 h. The high current density value of ca. 1.50 A/cm² was stable. Based on these results, we can conclude that Co₃O₄/Vulcan is a very stable HER electrocatalyst in PEM electrolysis, especially operated at high potential regime (from 2.0 to 2.7 V) with outstanding long-term stability.

4.6 Conclusions

Co₃O₄ was found to be an efficient, inexpensive cathode catalyst for HER in PEM electrolysis. As in the previous study of MoS₂/Vulcan (Chapter 3), addition of carbon (Vulcan) to the HER active material (Co₃O₄) positively influenced the performance of the physically mixed Co₃O₄/Vulcan composites due to enhanced electrical conductivity and efficient use of active HER sites. The material showing the best performance among all the materials evaluated was 47 wt% Co₃O₄/Vulcan. The material enhanced its performance particularly at high potentials and notably it showed linear response of current density against cell voltage variations. Strikingly excellent long-term stability at 2.5 V up to 24 h of continuous PEM electrolysis was shown, elucidating robustness of Co₃O₄ based materials under harsh conditions.

Low cost and high abundance of Co₃O₄, excellent stability and high current density when used as cathode material in PEM electrolysis, and facile preparation of MEA are encouraging features to use Co₃O₄ for practical application, especially as a composite with carbon material to boost HER activity. Finally, it is important to mention about practical implications of the required high cell voltage

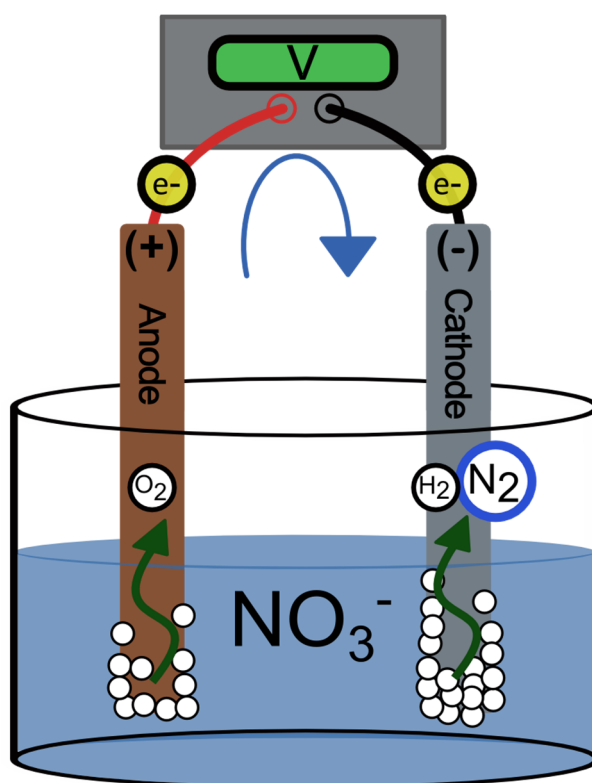
to achieve high current density which can exceed Pt-black cathode. Generally, lower cell voltages with high current density are the desired condition, but high cell voltage conditions are also of great value when the current density is very high. In reality, despite of the high cell voltages, smaller active catalyst area, i.e. smaller electrolyser, can achieve equivalent amount of H₂ production. Further studies on longer-term stability and heat loss due to higher voltage need to be performed. Nevertheless, the excellent performance of Co₃O₄-based materials shown by this work may pave a new way towards inexpensive, robust, high-performance electrolyser operated at high cell voltages.

BIBLIOGRAPHY

1. M. HAMDANI, R. SINGH, P. CHARTIER, *INT. J. ELECTROCHEM. SCI* **5**, 556, **2010**.
2. R. BOGGIO, A. CARUGATI, G. LODI, S. TRASATTI, *JOURNAL OF APPLIED ELECTROCHEMISTRY* **15**, 335, **1985**.
3. G. MARBÁN, I. LÓPEZ, T. VALDÉS-SOLÍS, A. B. FUERTES, *INTERNATIONAL JOURNAL OF HYDROGEN ENERGY* **33**, 6687, **2008**.
4. P. COX, D. PLETCHER, *JOURNAL OF APPLIED ELECTROCHEMISTRY* **20**, 549, **1990**.
5. F. JIAO, H. FREI, *ANGEWANDTE CHEMIE INTERNATIONAL EDITION* **48**, 1841, **2009**.
6. Y. MATSUMOTO, E. SATO, *MATERIALS CHEMISTRY AND PHYSICS* **14**, 397, **1986**.
7. S. TRASATTI, J. LIPKOWSKI, P. ROSS, *VCH, NEW YORK*, 207, **1994**.
8. V. SRINIVASAN, J. W. WEIDNER, *JOURNAL OF POWER SOURCES* **108**, 15, **2002**.
9. A. R. DE SOUZA, E. ARASHIRO, H. GOLVEIA, T. A. LASSALI, *ELECTROCHIMICA ACTA* **49**, 2015, **2004**.
10. F. HUANG, Z. YUAN, H. ZHAN, Y. ZHOU, J. SUN, *MATERIALS LETTERS* **57**, 3341, **2003**.
11. N. N. GREENWOOD, A. EARNSHAW, *CHEMISTRY OF THE ELEMENTS*, ELSEVIER, **1997**.
12. M. TARASEVICH, B. EFREMOV, S. TRASATTI, *ELECTRODES OF CONDUCTIVE METALLIC OXIDES, PART A*, ELSEVIER, USA, **1982**.
13. S. TRASATTI, G. LODI, *ELECTRODES OF CONDUCTIVE METALLIC OXIDES*, ELSEVIER AMSTERDAM, **1981**.
14. M. CARMO, D. L. FRITZ, J. MERGE, D. STOLTEN, *INTERNATIONAL JOURNAL OF HYDROGEN ENERGY* **38**, 4901, **2013**.
15. P. MILLET, N. MBEMBA, S. A. GRIGORIEV, V. N. FATEEV, A. AUKA LOO, C. ETIEVANT, *INTERNATIONAL JOURNAL OF HYDROGEN ENERGY* **36**, 4134, **2011**.
16. P. MILLET, R. NGAMENI, S. GRIGORIEV, N. MBEMBA, F. BRISSET, A. RANJBARI, C. ETIEVANT, *INTERNATIONAL JOURNAL OF HYDROGEN ENERGY* **35**, 5043, **2010**.
17. J. C. TOKASH, B. E. LOGAN, *INTERNATIONAL JOURNAL OF HYDROGEN ENERGY* **36**, 9439, **2011**.
18. T. CORRALES-SÁNCHEZ, J. AMPURDANÉS, A. URAKAWA, *INTERNATIONAL JOURNAL OF HYDROGEN ENERGY*.
19. W.-Y. LI, L.-N. XU, J. CHEN, *ADVANCED FUNCTIONAL MATERIALS* **15**, 851, **2005**.
20. X. WANG, L. YU, X.-L. WU, F. YUAN, Y.-G. GUO, Y. MA, J. YAO, *THE JOURNAL OF PHYSICAL CHEMISTRY C* **113**, 15553, **2009**.
21. M. CAPPADONIA, J. W. ERNING, S. M. S. NIAKI, U. STIMMING, *SOLID STATE IONICS* **77**, 65, **1995**.

CHAPTER 5

CONTINUOUS ELECTROLYSIS- ASSISTED NITRATE REDUCTION



5.1 Introduction

5.1.1 Catalytic and Electrocatalytic Nitrate Reduction

There are increasing concerns about contamination of drinking water with nitrogen containing ions such as nitrates, nitrites and ammonium (Chapter 1), especially nitrates because the other ions are typically derived from them. Among various physical and chemical methods for nitrates removal, catalytic hydrogenation (Figure 5.1a) has been considered as one of the most effective methods for nitrate reduction to nitrogen molecule [1]. In 1989, Vorlop and Tacke published a pioneering work describing how to successfully remove nitrates from water [2].

Nitrates hydrogenation is related to an electrochemical process since it involves the reduction of the nitrogen oxidation state through a stepwise mechanism leading to the formation of nitrites, ammonium ion/ammonia and N_2 . Supported metallic or bimetallic catalysts are known to show good activities for nitrates removal by catalytic hydrogenation [3-6]. Multiple combinations of noble metal-metal have been tested during the past decades aiming to find an optimal compromise between nitrate removal efficiency and selectivity towards nitrogen [2, 7]. PdCu bimetallic catalyst, with Cu as a promoter, is widely known [2, 8, 9] as one of the best catalysts for either catalytic [10] or electrocatalytic [11] nitrate hydrogenation. Pd performs in general better than Pt, both in nitrates conversion and selectivity [7, 8]. Cu is suggested to be indispensable for the first reaction step, i.e., from NO_3^- to NO_2^- [12]. Besides, the interaction between Cu and Pd is of major importance to maintain copper in the metallic state due to the high hydrogenation activity of Pd, facilitating Cu to be in the active, reduced state

(Figure 5.2). The major problem of the approach is the usage, storage, and infrastructure needed for hydrogen gas (H_2) that needs to be dissolved in the aqueous solution containing nitrate ion. Furthermore, poor N_2 selectivity is often reported, producing even more harmful NO_2^- and NH_4^+ by-products.

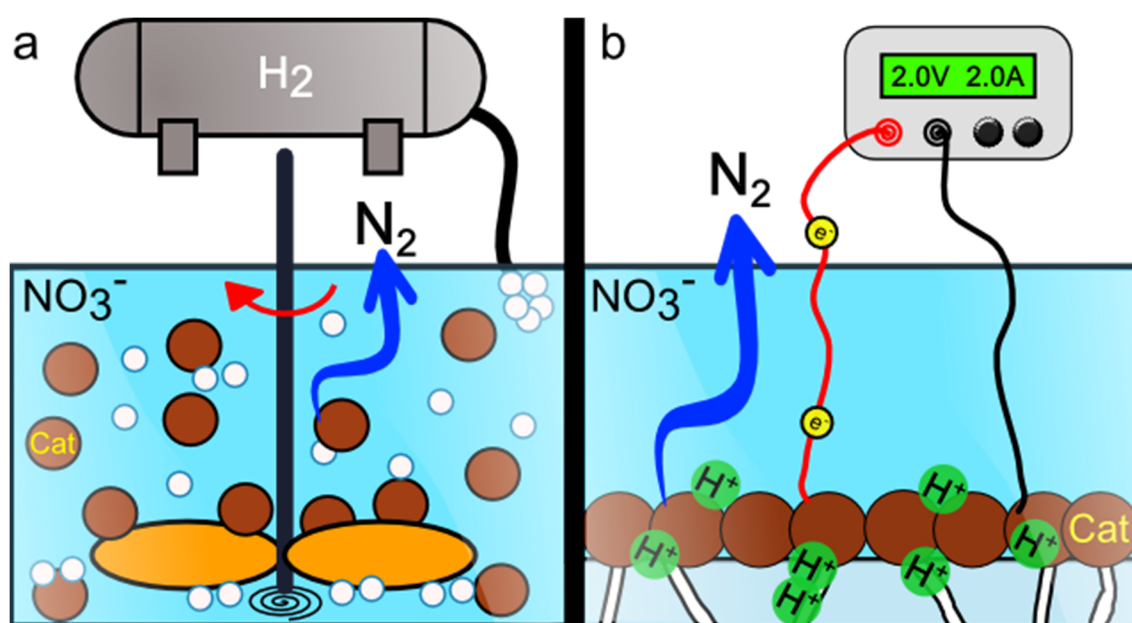


Figure 5.1. Catalytic versus electrocatalytic nitrate hydrogenation reaction strategies, schematic view of process. (a) Catalytic nitrate reduction and (b) electrocatalytic approach.

On the other hand, since past decades, electrocatalytic removal of nitrates (Figure 5.1b) embraces a big part of the nitrogen electrochemistry. In fact, the major reaction pathways for nitrate and nitrite reduction on noble-metal electrodes are properly described in literature [13]. In the light of these backgrounds, electrochemical and electrolysis-assisted nitrate reduction combination is a promising approach due to possible process simplicity and the generation of H_2 or H^+ , used for nitrate reduction, in situ by electrolysis of water. Recently, Machida and co-workers reported the possibility of selective

electrocatalytic hydrogenation of NO_3^- to N_2 using an electrochemical batch reactor [14, 15]. The use of a Nafion proton exchange membrane allowed the transport of in situ generated protons on the anode side to the surface of the catalyst deposited at the cathode, enabling nitrate reduction at cathode surface. However, its operation in batch mode restricts its industrial application since the amount of sample processed would be lower than those carried out in continuous mode, as well as, all the engineering drawbacks associated, like loading and emptying of reactor.

Currently, only a few studies working in electrocatalytic mode and in continuous conditions have been carried out [11]. However, the feasibility of this combined system for nitrate hydrogenation has been proven. Among others, some advantages of the electrochemical treatment include high system efficiency, almost ambient operating conditions, small equipment sizes, high purity oxygen production, no external hydrogen source and rapid start-up.

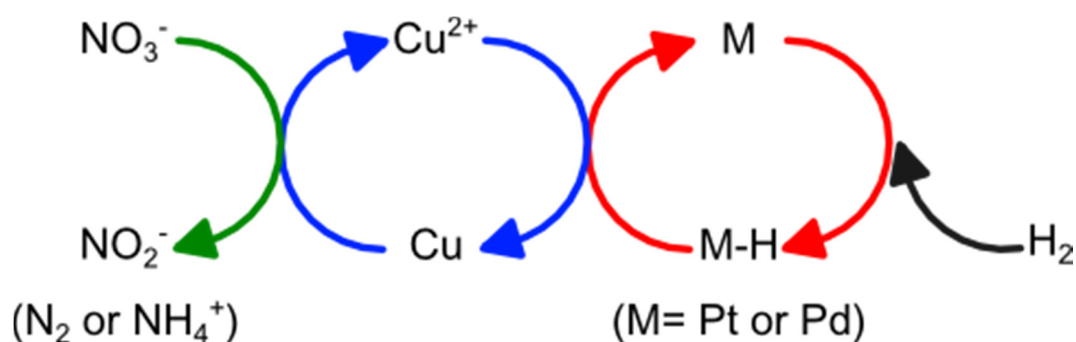


Figure 5.2. Generally accepted reaction mechanism for nitrate and nitrite catalytic reduction over bimetallic catalyst (Precious metal + Cu) postulated by Epron and co-workers [12].

5.1.2 Reaction Mechanism and Theoretical Basis

Electrochemical nitrate conversion uses cathodic reactions. At acidic pH, hydrogen adsorbed on the cathode surface inhibits the reduction of nitrate, whereas the reaction in alkaline solutions produces ammonia [16-18]. The reaction has been suggested to take place in a consecutive manner, NO_3^- to NO_2^- to (NO) and finally towards NH_4^+ or desired harmless N_2 in parallel reaction (Figure 5.3). Here we will focus on possible reactions involved during nitrate reduction towards nitrogen by means of either catalytic or electrocatalytic routes.

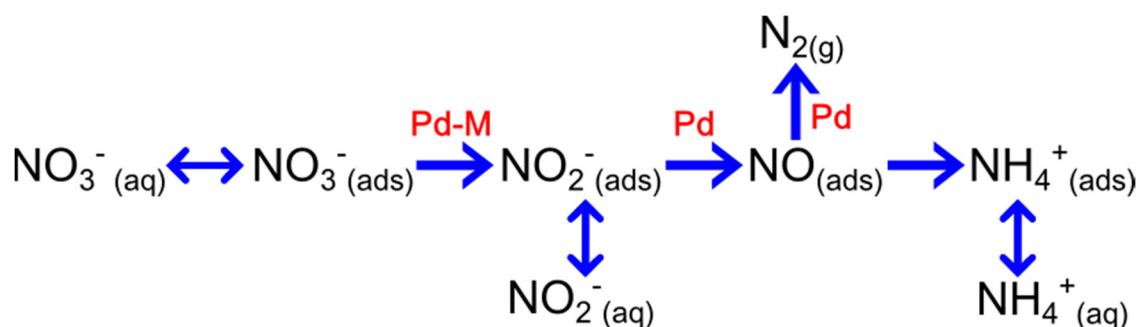


Figure 5.3. Scheme of the stepwise mechanism for the denitrification process involving bimetallic catalysts postulated by Warna and co-workers [20].

The most accepted reaction of catalytic nitrate reduction is eq. 5.1. In the ideal case, 1 mol of N_2 is formed for every 2 moles of NO_3^- hydrogenated. The change of pH during reaction is nearly equivalent to the amount of OH^- formed by eq. 5.1 [12, 19, 20].



The theoretical pH values, depending on initial concentration (C_0) and final conversion ($X_{\text{NO}_3^-}$) are summarized in Table 5.1 assuming that only the reaction (eq. 5.1) takes place.

Table 5.1. Theoretical pH values after catalytic nitrate reduction versus initial concentration (C_0) and conversion ($X_{\text{NO}_3^-}$) corresponding with eq. 5.1.

$C_0 /$ ppm NO_3^-	Conversion / $X_{\text{NO}_3^-}$					
	1%	10%	25%	50%	75%	100%
1	7.40	8.20	8.60	8.90	9.10	9.20
10	8.20	9.20	9.60	9.90	10.1	10.2
50	8.90	9.90	10.3	10.6	10.8	10.9
100	9.20	10.2	10.6	10.9	11.1	11.2
500	9.90	10.9	11.3	11.6	11.8	11.9
1000	10.2	11.2	11.6	11.9	12.1	12.2
3000	10.7	11.7	12.1	12.4	12.6	12.7

The maximum pH value assuming 100% conversion and 3000 ppm initial concentration would be ca. 12.7. pH values for C_0 100 and 1000 ppm are highlighted (red) since these were the two concentrations used in our study.

Eq. 5.2 [13, 15] describes electrocatalytic nitrate reduction to N_2 using protons. In this case, hydroxyl ions are not formed and therefore pH will not change during reaction. Protons (H^+) are evolved in situ by means of water splitting.



The third reaction proposed (eq. 5.3) [15] also includes pure electrocatalytic process since it involves electron transfer (5 mol of electrons per mol of NO₃⁻).

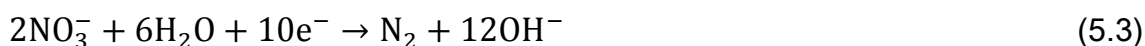


Table 5.2 summarizes theoretical pH values at different conversions of nitrates with various starting concentrations assuming that only the reaction (eq. 5.3) takes place. The C₀ values corresponding with 100 and 1000 ppm are highlighted (blue).

Table 5.2. After reaction theoretical pH values for electrocatalytic nitrate reduction versus initial concentration (C₀) and conversion (X_{NO₃⁻}) corresponding with eq. 5.3.

C ₀ / ppm NO ₃ ⁻	Conversion / X _{NO₃⁻}					
	1%	10%	25%	50%	75%	100%
1	8.00	9.00	9.40	9.70	9.70	10.0
10	9.00	10.0	10.4	10.7	10.9	11.0
50	9.70	10.7	11.1	11.4	11.6	11.7
100	10.0	11.0	11.4	11.7	11.9	12.0
500	10.7	11.7	12.1	12.4	12.6	12.7
1000	11.0	12.0	12.4	12.7	12.9	13.0
3000	11.5	12.5	12.9	13.2	13.3	13.4

Experimental pH values obtained in this work after nitrate reduction tests are compared with theoretical ones in order to judge whether the reaction is driven by catalytic or electrocatalytic path.

5.1.3 Aim of the Study

A novel approach in nitrate reduction is a process combining (i) electrochemical H_2/H^+ production by water electrolysis and (ii) utilisation of these as reactant to reduce nitrates over heterogeneous cathode catalysts in the same electrolyser cell. The obvious advantage is to produce hydrogen in situ, thus avoiding extra gaseous hydrogen sources, and also the reduction activity may be boosted due to the enhanced H_2/H^+ concentrations at the interface (cathode catalyst surface). The electrolysis-assisted approach has been reported recently by the group of Machida and co-workers using selected pure metals, e.g. tin, silver or other noble metals, as cathode catalyst typically using batch operation mode [21] [11]. The feasibility has been show proven, but it requires definitely deeper investigation and further development.

The target of this chapter was to evaluate electrolysis-assisted nitrate reduction process operated in continuous-flow mode using practical and highly stable, conducting metal oxide supported metal catalysts. Monometallic or bimetallic nanoparticles of Pt, Pd, Cu or PdCu were supported on high surface area tin oxide (SnO_2 , ca. $250\text{ m}^2/\text{g}$) as cathode catalyst. The optimum strategy for selective NO_3^- reduction to diatomic nitrogen was searched for by using several reactor configurations. The electrolysis-assisted approach takes a full advantage of our experience with PEM electrolysis and cell design we acquired previously (Chapters 3 and 4). The feasibility of the process and the contribution of monometallic (Pt, Pd, Cu) and bimetallic (PdCu) supported catalysts were evaluated based on nitrate conversion ($X_{NO_3^-}$) and product selectivity (S_i).

5.2 Experimental Section

5.2.1 Materials

Tin (IV) oxide was chosen as the support material for active metal components because of its good electric conductivity and good performance for PEM fuel cell technology [22]. Furthermore, we wished to avoid the utilisation of carbon-based supports in our electrocatalytic system due to possible contamination of liquid samples and generation of undesired side-reactions under high potential conditions despite of the higher electric conductivity of carbon materials than that of SnO₂.

In order to increase the active surface area of supported active metals, high surface area SnO₂ (ca. 250 m²/g similar to Vulcan) was synthesized according to the procedure described in [Chapter 2 \(section 2.1.1.1\)](#). The surface area is considerably high than that of a commercial SnO₂ (7.2 m²/g). [Figure 5.4](#) shows a TEM micrograph image (JEOL 1011 operated at 80 kV) of (a) synthesized high surface area SnO₂ and (b) commercial SnO₂. In case of the high surface area SnO₂, The particles size of high surface area SnO₂ was small, roughly 3 nm, whereas that of the commercial one was ca. 50 nm.

Iridium (IV) oxide (IrO₂, >99%, powder, same batch than that used for water electrolysis studies) was used as the anode catalyst in all MEAs prepared with a fixed loading of 2 mg/cm². Metallic nanoparticles were deposited over the high surface area SnO₂ support by means of the ultrasonic metal deposition method, i.e. reducing the metal precursor(s) by stepwise NaBH₄ (sodium borohydride >97%, 10-40 mesh granules, Alfa Aesar) addition in a liquid suspension of the SnO₂. After ultrasonic metal deposition, the powders were filtered, cleaned and

dried. Extended explanation about materials examined in this study can be found in Chapter 2 (section 2.1).

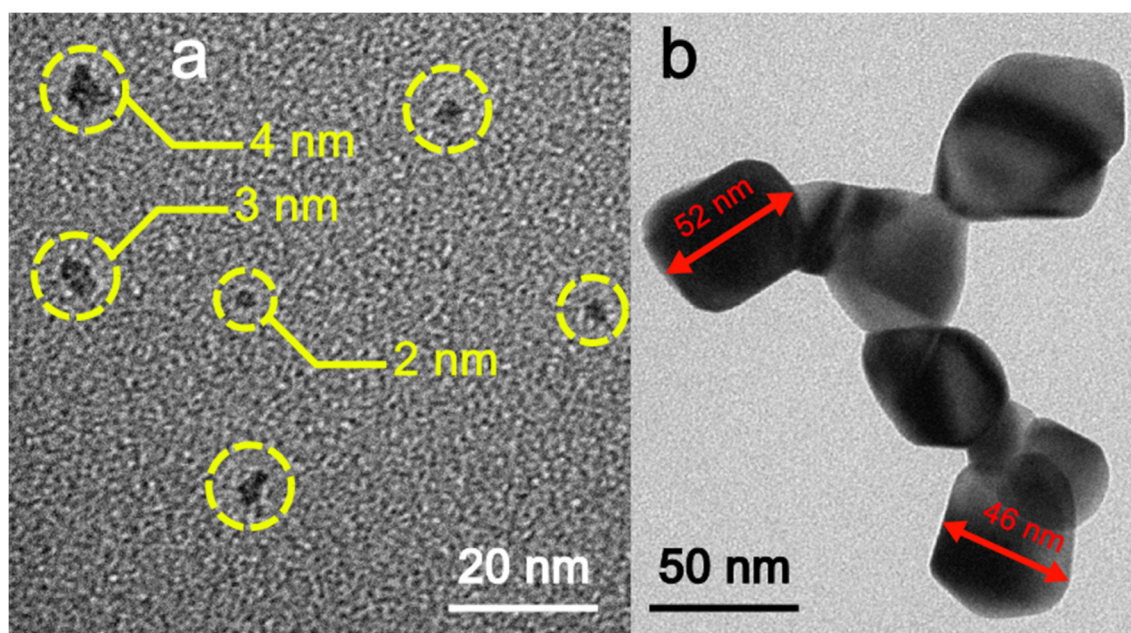


Figure 5.4. TEM micrograph images of (a) high surface area SnO_2 particles prepared by urea precipitation method and (b) commercial SnO_2 (*Alfa Aesar*) particles. Particle size is shown inside each the micrograph.

All the catalysts had same metal loading, adjusted to 40 wt% M/SnO_2 (where, $\text{M} = \text{Pt}, \text{Pd}, \text{Cu}$ and PdCu (4:1) [23]), in order to maximize the reaction rate. The metal types were chosen based on their high and contrasting nitrate reduction ability reported for catalytic reduction. Cathode catalyst loading over the Nafion membrane was fixed at 1 mg M/cm^2 corresponding to a total catalyst loading of 3.5 mg cat/cm^2 .

5.2.2 Reaction Setup

Detailed explanation of electrochemical reactor and reaction system can be found in [Chapter 2](#) ([Figures 2.7 and 2.10](#), [section 2.3.3](#)). Water and nitrate solution flow rates were 0.5 and 0.16 mL/min through anode and cathode compartments, respectively. Temperature was fixed at 80 °C. Five different MEAs, namely, IrO₂ | Nafion | 40 wt% M/SnO₂ (where M=Pt, Pd, Cu and PdCu) were examined (4x4cm² active area). Two different initial concentrations were tested (100 and 1000 ppm NO₃⁻) to study the concentration effects on the reduction performance.

Product analysis and quantification was performed by means of ion chromatography (883-IC Basic; Metrohm, Switzerland). Samples were injected directly or as a diluted form depending on the initial concentration of the nitrate stream. Nitrate/nitrite or other N-containing species were not detected in the effluent exiting from the anode compartment.

Electro-osmotic drag effect [24-26] ([Chapter 2](#)) was also taken in account in order to calculate the final concentration values properly. Therefore, correction was made depending on the drag impact, that is, the dilution effect by the transported water into the cathode compartment through the membrane. Assuming a value of 3 (H₂O/H⁺) as the drag coefficient (η_d), which corresponds with the case with highest water transported for a Nafion 117 membrane, the actual impact of η_d can be theoretically calculated depending on electrical current (directly correlated with H₂ production and therefore H⁺ transport) and solution flow rate through cathode compartment ([Table 5.3](#)).

Under our working conditions of 160 $\mu\text{L}/\text{min}$ nitrate solution, it can be emphasized that at low electrical current (e.g. 100 mA) electro-osmotic drag effect can be negligible since the dilution effect is ca. 1%. However, when the current rises typically as a consequence of increased cell potential, the dilution factor starts to be prominent i.e. 1 A about 10%. Obviously, there is a linear dependency among current and dilution effect.

Table 5.3. Electro-osmotic drag impact (dilution effect) on liquid solution flow rate (mL/min) in the cathode compartment versus electrical current (A) for a Nafion 117 membrane operating at 80 $^{\circ}\text{C}$, with the cathode flow rate of 160 $\mu\text{L}/\text{min}$ and assuming $\eta_d=3$.

Current / A	Dragged Water flow rate / $\mu\text{L}\cdot\text{min}^{-1}$	Dilution effect / %
0.00	0.00	0.00
0.10	1.72	1.10
0.50	8.60	5.10
1.00	17.2	9.70
5.00	86.0	35.0
10.0	172	51.8

As an example, Machida and co-workers used low current values in their electrolysis-assisted nitrate reduction studies using the PEM in batch (7 mL cathode reservoir) operation (100 mA and 16.7 mA/cm^2) [11, 14, 15, 27]. We suppose that they minimized the effect of electro-osmotic drag by the flow current and therefore continuous dilution of target solution, or their system was not fully optimized so that the electrical potential was too high to achieve higher current (used cell voltages were not disclosed).

5.3 System Flexibility

In this work several experimental arrangements were tested in terms of powering mode or flow conditions using an identical electrochemical reactor without making any modification to the MEAs. Figure 5.5 shows an illustrative scheme about the flexibility of our electrolysis-assisted nitrate reduction system.

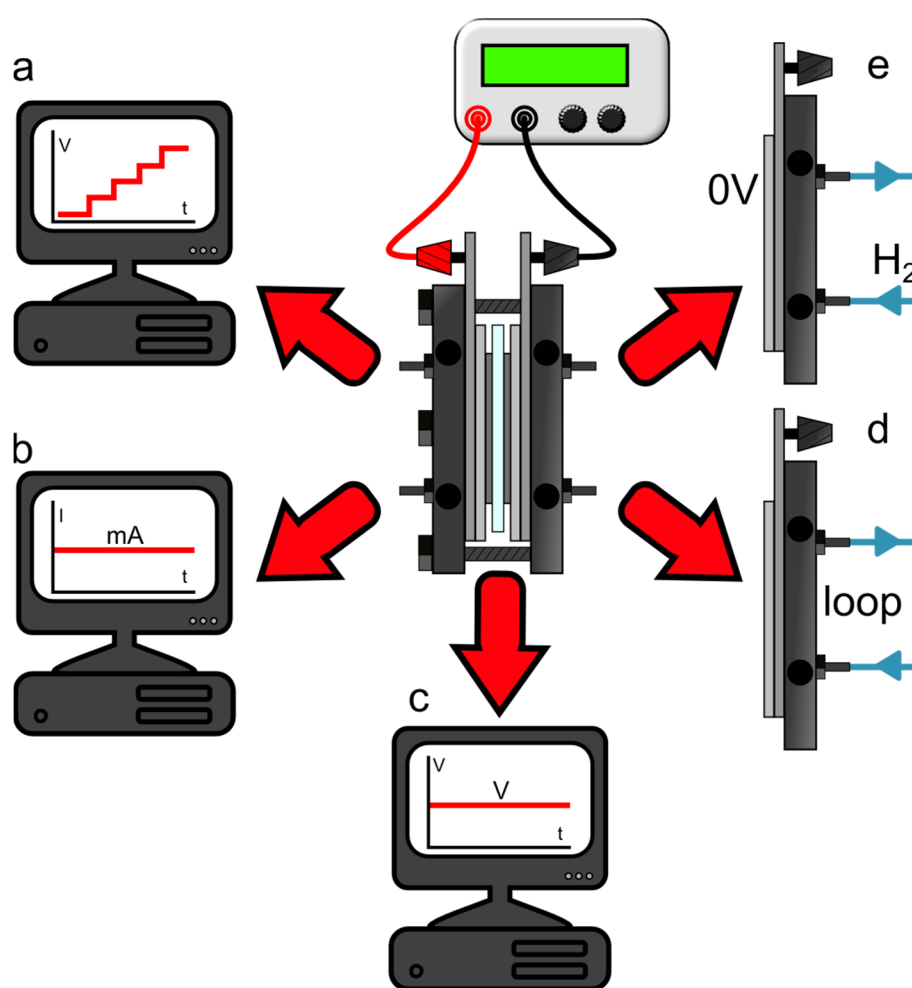


Figure 5.5. Various approaches for NO₃⁻ (electro)chemical reduction performed in this work: (a) potential sweep mode with step-wise cell voltage increase, (b) constant current mode, (c) constant potential mode, (d) recirculation mode at constant current of 100mA and (e) catalytic reduction at 0 V using hydrogen saturated solution.

Regarding the powering mode, our system allowed us to work in (i) potential sweep (potentiodynamic) conditions (Figure 5.5a), that is, gradually (step-wise) increasing cell voltage with time, (ii) continuous current mode (galvanostatic) (Figure 5.5b), or (iii) continuous voltage mode (Figure 5.5c). In all cases one-pass flow through condition was used. Related with flow conditions, we tested flow through condition in loop mode recirculating the solution through the cathode compartment (Figure 5.5d). Furthermore, hydrogen was directly bubbled at the inlet of cathode (saturated solution) without any cell voltage (Figure 5.5e) to examine the hydrogenation activity of the catalyst coated over the Nafion membrane instead of suspended in solution.

Among all working arrangements shown in Figure 5.5, the most efficient mode for catalyst screening was potential sweep mode, since it allowed screening several potential conditions and its effect on the reaction performance. Using this mode, selection of the most efficient catalyst for further tests as well as finding optimum working conditions were facilitated.

5.4 System Performance

5.4.1 Catalytic Nitrate Reduction

Prior to the investigation of electrolysis-assisted nitrate reduction, the activity of the prepared materials (40 wt% M/SnO₂) was evaluated in order to validate their activity and trends in selectivity as catalysts for NO₃⁻ reduction. The study was performed in a batch reactor (Figure 5.6). Catalyst was suspended in nitrate-containing solution by mechanical stirring under H₂ flow (bubbling through the solution at 30 mL/min). Initial concentration (C₀) of NO₃⁻ was 100 or 1000 ppm,

prepared from NaNO_3 as a precursor salt. A glass round bottom flask was used as the reactor and filled with 100 mL of starting solution kept at room temperature (RT). The catalyst amount was 50mg.

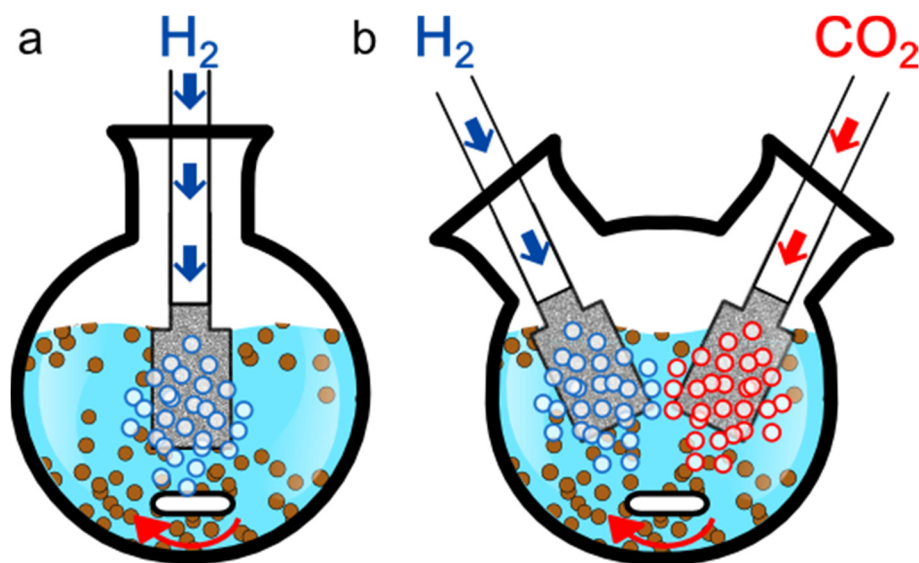


Figure 5.6. Catalytic NO_3^- hydrogenation. (a) H_2 bubbling (30 mL/min) without pH control and (b) pH buffering (constant pH achieved at ca. 5.5-7.5 depending on material and reaction) by means of CO_2 bubbled through the solution (20 mL/min). The reaction was performed under stirring condition at room temperature.

If catalytic nitrate reduction towards N_2 follows the general accepted reaction path (eq. 5.1), it generates OH^- as a side-product; therefore a final pH after the reaction is expected to be high (basic) as described previously. In literature, pH evolution during the reaction and its effects on final product distribution are described [19, 28]. Although it does not remarkably affect nitrate conversion, reaction selectivity can be greatly influenced, i.e. under basic conditions NH_4^+ as well as NO_2^- formations are known to be enhanced [28, 29]. Well accepted strategy for the mitigation of pH variation effect is pH buffering by bubbling CO_2 in the solution [28-31] since it dissolves in water and forms carbonic acid (H_2CO_3),

also dissociates into HCO_3^- and H^+ ($\text{pK}_a = 6.35$) (eq. 5.4) and thus allows keeping pH stable (buffering) during nitrate reduction.



Therefore, non-buffered (Figure 5.6a) and buffered (Figure 5.6b by 20 mL/min CO_2 bubbling) approaches were examined. The pH evolution during reaction was followed by a pH probe (Crison pH-meter model 5028 (probe $\varnothing = 3\text{mm}$)) immersed in solution and connected to a computer for continuous online monitoring.

5.4.1.1 Catalytic Activity with pH Buffering

First, catalytic nitrate reduction using pH buffered solution was tested to properly evaluate the catalytic activity because buffered conditions (pH range: 4-7) are known to show better nitrate reduction performance using the same catalyst in terms of conversion and selectivity. In this study, the four catalysts described in Section 5.2.1 (Pt, Pd, Cu and Pd supported over SnO_2) were evaluated. Figure 5.7 shows the profile of nitrate conversion ($X_{\text{NO}_3^-}$) using the catalysts and the nitrate solution with initial concentration of 100 ppm NO_3^- for a reaction time of 3 h.

Generally, Pd-containing catalysts showed significantly higher nitrate conversion rates, reaching nearly full conversion in 30 min for PdCu (black ■) and in 120 min for Pd (red ●). Excellent performance of PdCu and Pd catalysts in nitrate reduction is widely reported in literature [19, 32, 33] and it was confirmed here using SnO_2 supported catalysts. On the other hand, Pt (blue ▲) and Cu

(green ▼) catalysts reached about 60 and 25% conversion after 3 h, respectively. Cu is suitable metal for first reaction step of NO_3^- to NO_2^- [12]; however it is known to deactivate fast. This is likely the reason for the low reaction rate observed for the Cu catalyst. Pt is a valuable hydrogen activator and results in acceptable conversion for NO_3^- reduction, although its capability is not as high as that of Pd, as described in literature [28]. Catalytic activity using bare SnO_2 manifested no nitrate conversion without the presence of active metal component(s).

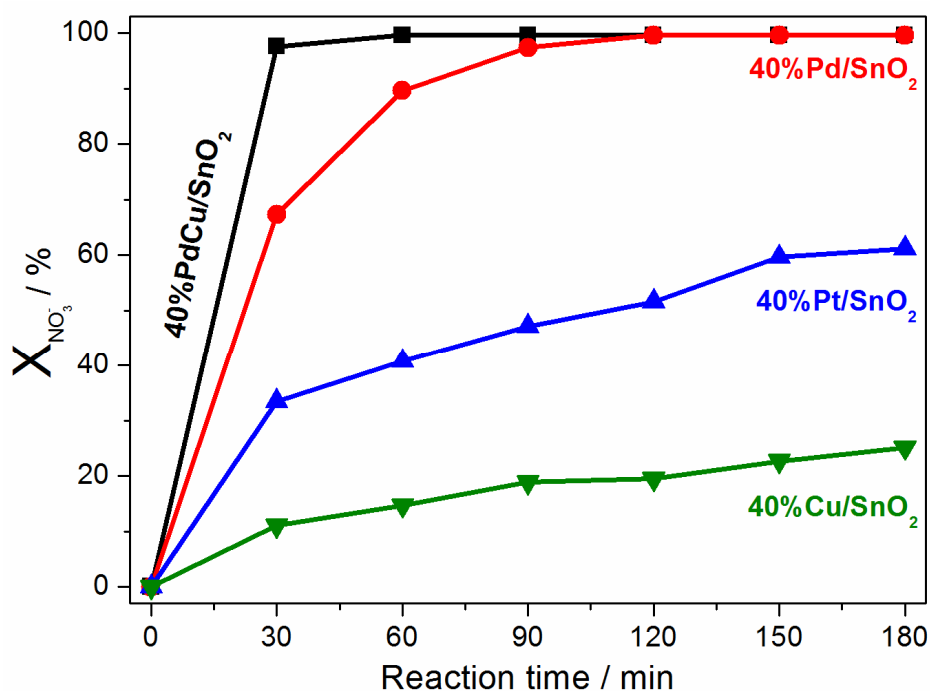


Figure 5.7. Nitrate conversion profile over 3 h during the batch reaction. Hydrogen flow of 30 mL/min and CO_2 flow of 20 mL/min. Four different metal catalysts supported on SnO_2 : Pt (blue ▲), Pd (red ●), Cu (green ▼) and PdCu (black ■). The initial nitrate concentration was 100 ppm.

Selectivity values (S_i) for NH_4^+ ($S_{\text{NH}_4^+}$) and NO_2^- ($S_{\text{NO}_2^-}$) as well as pH values after 3 h of the reaction are summarized on [Table 5.4](#).

Table 5.4. Selectivity ($S_{\text{NH}_4^+}$, $S_{\text{NO}_2^-}$) and pH after 3 h of catalytic nitrate reduction in a batch reactor. Hydrogen flow of 30 mL/min and CO_2 flow of 20 mL/min using four different catalysts: Pt, Pd, Cu and PdCu supported on SnO_2 .

Cathode Catalyst	pH	$S_{\text{NO}_2^-}$ / %	$S_{\text{NH}_4^+}$ / %
40 wt% Pt/ SnO_2	7.70	2.20	76.6
40 wt% Pd/ SnO_2	7.60	0.10	69.7
40 wt% Cu/ SnO_2	6.70	1.90	30.2
40 wt% PdCu/ SnO_2	5.50	0.30	21.3

Nitrite reduction towards N_2 and ammonia is self-inhibited by presence of hydroxide ions (OH^-) formed during reaction [32, 33]. However, as reported in literature, nitrite selectivity was well suppressed in all the cases by the use of CO_2 as a buffer agent for pH control (Table 5.4). This effect is attributed to a very efficient pH buffering, overtaking local diffusion problems, within the pores and over surface of catalyst [28, 29] allowing for OH^- removal from the active sites boundaries. For all catalysts $S_{\text{NO}_2^-}$ was lower than ca. 2.5%. On the other hand, selectivity towards ammonium was very high, even reaching values of ca. 77% for Pt catalyst and ca. 70% for Pd catalyst. Remarkable synergetic effect was confirmed for bimetallic PdCu, significantly lowering both $S_{\text{NO}_2^-}$ and $S_{\text{NH}_4^+}$, compared to Pd. Cu catalyst showed also lower $S_{\text{NH}_4^+}$, but considering the much higher reaction rate of PdCu catalyst over Cu catalyst, the benefits of the Pd-Cu synergetic effects are clear in catalytic nitrate reduction. Moreover, a clear trend between $S_{\text{NH}_4^+}$ and pH could be observed; the higher the $S_{\text{NH}_4^+}$ the higher pH.

5.4.1.2 Catalytic Activity of PdCu/SnO₂ without pH Buffering

Based on the much superior catalytic performance of PdCu catalyst, this catalyst was further investigated in nitrate reduction without pH buffering. Its conversion profile as well as pH evolution during the course of 3 h reaction are shown in Figure 5.8.

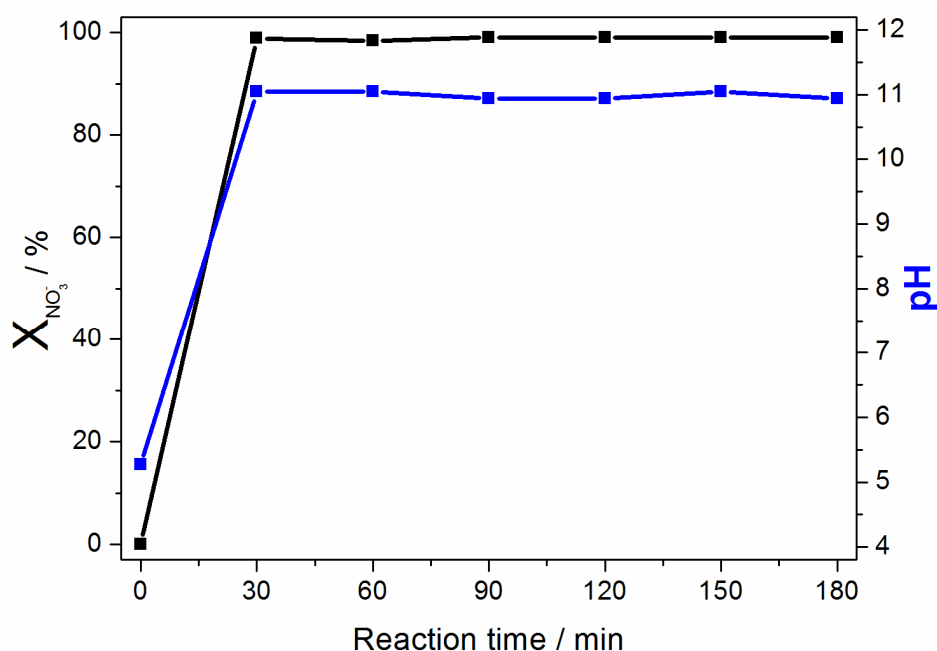


Figure 5.8. Nitrate conversion profile for 40 wt% PdCu/SnO₂ (black line, left y axis) over time after 3 h of continuous catalytic batch reaction. Hydrogen flow of 30 mL/min. Evolution of pH after 3 hours reaction (blue line, right y axis), 100 ppm nitrate solution.

Similar to previous study, after 30 min of reaction PdCu reached almost 100% conversion, showing its effectiveness even in the absence of a buffering agent. In terms of product selectivity, both selectivities to undesired products, $S_{\text{NO}_2^-}$ and $S_{\text{NH}_4^+}$, increased to 12.5 and 33%, which was expected due to the absence of CO₂. Consequently, pH was raised from 5.5 to 10.9 during the reaction. This final

pH indicates that almost 50% of nitrate in the solution was directly converted to N_2 (Table 5.1) starting from the 100 ppm initial concentration of nitrates.

As a final test, 1000 ppm nitrate solution was also subject to the catalytic reduction using PdCu catalyst with or without the presence of CO_2 . The most remarkable results are summarized in Table 5.5.

Table 5.5. Performance parameters (conversion and selectivity) of catalytic nitrate hydrogenation over 40 wt% PdCu catalyst. Initial nitrate concentration of 1000 ppm and 3 h of batch reaction. Hydrogen flow of 30 mL/min and CO_2 flow of 20 mL/min.

CO_2 buffering	pH	$X_{NO_3^-} / \%$	$S_{NO_2^-} / \%$	$S_{NH_4^+} / \%$
✗	12.2	76.2	20.9	13.2
✓	6.70	79.3	2.30	12.5

Resembling the case of 100 ppm initial nitrate concentration, CO_2 buffering did not affect $X_{NO_3^-}$ (76.2% without CO_2 vs. 79.3% with CO_2), although lower $X_{NO_3^-}$ values were found compared with the case 100 ppm nitrate solution was used (Figure 5.7). On the other hand, the selectivity to ammonium ion remained almost unaltered. The quantity affected greatly by CO_2 was nitrite concentration, differing roughly one order of magnitude (20 vs. 2%). The findings are in good agreement with literature [28, 29].

Finally, a long term reaction (24 h, $C_0 = 1000\text{ppm}$ of NO_3^-) under CO_2 flow was performed to clarify the reaction evolution over the long periods of time. Nearly 100% $X_{NO_3^-}$ was achieved (99.9%) with $S_{NO_2^-}$ and $S_{NH_4^+}$ values about 0.04 and 18.5%, respectively.

5.4.2 Continuous Flow Electrocatalytic Tests

5.4.2.1 Potential Sweep Study

After studying the catalytic behaviour of the SnO₂ supported catalysts, performance ($X_{\text{NO}_3^-}$ and S_i) of the catalysts in continuous electrolysis-assisted nitrate reduction was evaluated by potential sweep measurements, i.e. by gradually increasing PEM cell voltage step-wise (from 1.5 to 2.7 V, $\Delta V=0.2$ V, 60 min each step). Standard MEA composition, IrO₂ | Nafion | 40 wt% M/SnO₂ was employed to test four different catalysts and also bare support (SnO₂). Initially, aqueous solution containing 1000 ppm of nitrate ion was fed through the cathode compartment at a constant flow rate of 160 $\mu\text{L}/\text{min}$. Sampling was made as follows. 2 mL of solution were collected during the last 15 min of each potential step (60 min) after stabilized electrical current was confirmed.

Product quantification clarified that nitrate hydrogenation took place in all set of materials over the bare support (Figure 5.9). Generally, higher nitrate conversion was observed at higher cell voltage. This suggests that electrocatalytic promotion for nitrate reduction or enhanced hydrogenation activity due to higher surface hydrogen concentration at the cathode. Addition of metal to the SnO₂ support enhanced nitrate conversion. The conversion profiles of Pt (blue line ▲), Pd (red line ●) and PdCu (black line ■) catalysts were similar especially in a low potential range (from 1.5 to 1.9V). For these materials, a maximum $X_{\text{NO}_3^-}$ value was observed at the highest potential (2.7 V) with the value ranging from 58% (Pt) to 68% (Pd). Similar to the case of catalytic hydrogenation (Figure 5.7), Pd and PCu were giving good $X_{\text{NO}_3^-}$, but Pt yielded also as good results. Cu (green line, ▼) catalyst was the worst performing material, as in the

catalytic reduction, likely due to its low capability for H_2 activation. Still, at high potential region (from 1.9 to 2.7 V), the activity Cu catalyst was continuously improved, reaching about 50% $X_{NO_3^-}$.

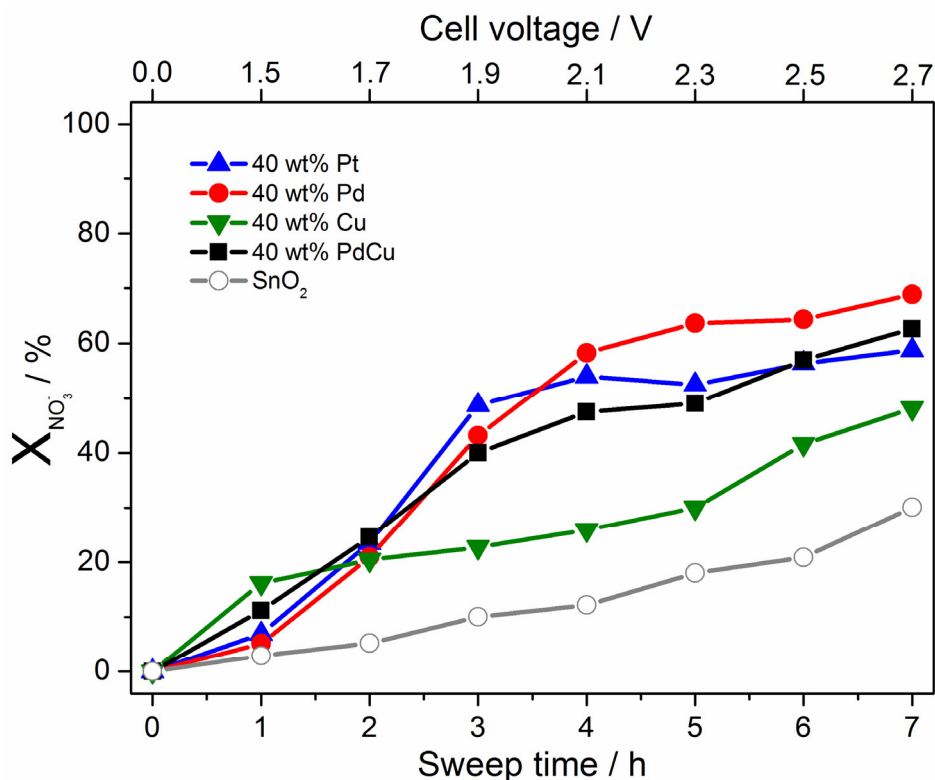


Figure 5.9. Nitrate conversion profiles over 7 h of potential sweep experiments (from 1.5 to 2.7 V, $\Delta V=0.2$ V, 60 min each step) of electrolysis-assisted nitrate reduction. Four different catalysts: Pt (blue \blacktriangle), Pd (red \bullet), Cu (green \blacktriangledown) and PdCu (black \blacksquare) and bare SnO₂ (grey \circ) were tested at 80°C with nitrate solution of 1000 ppm NO₃⁻ at 160 μ L/min. Electro-osmotic drag effect was corrected.

Change in pH of the effluent solution is a convenient way to verify that NO₃⁻ reduction is taking place. For all potential sweeps performed, a great increase in pH was observed (from 5.8 to ca. 12) due to the OH⁻ formation as more NO₃⁻ was converted to products (NO₂⁻, NH₄⁺/NH₃ or N₂) (Figure 5.10, only the profile of

representative PdCu catalyst is shown). Please note that hereafter we will refer to the $\text{NH}_4^+/\text{NH}_3$ pair as simply NH_4^+ .

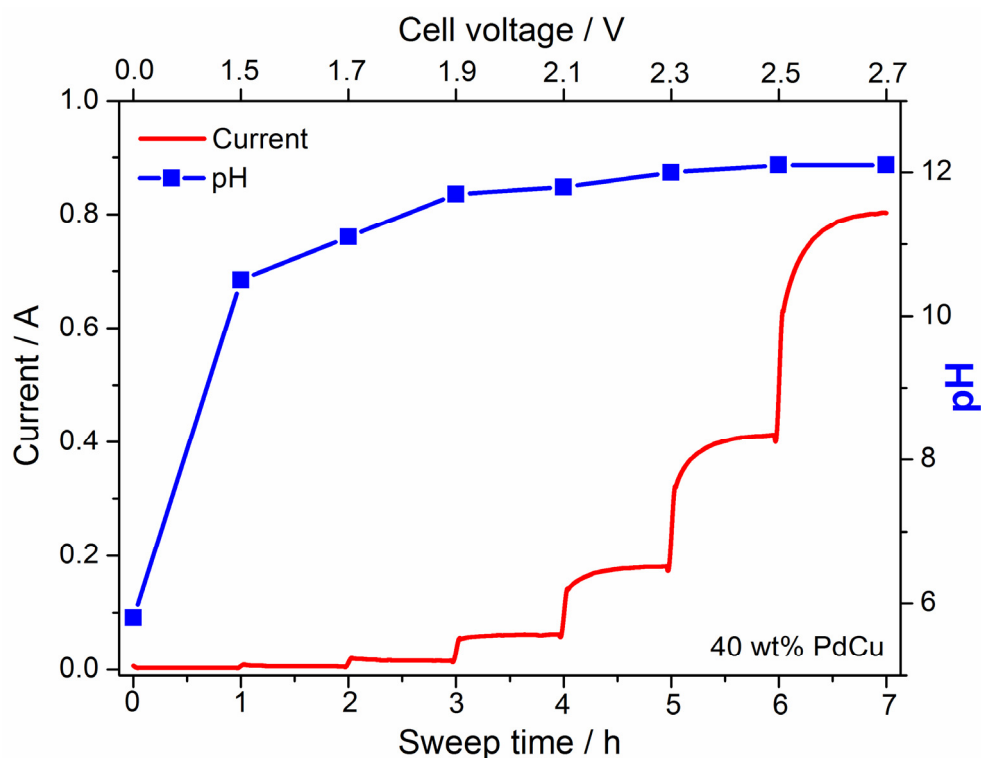


Figure 5.10. Current and pH profile during electrolysis-assisted nitrate reduction over 7 h of potential sweep experiment (from 1.5 to 2.7 V, $\Delta V=0.2$ V, 60 min each step) using 40 wt% PdCu/SnO₂ catalyst at 80°C, 1000 ppm NO₃⁻ at 160 $\mu\text{L}/\text{min}$. Electro-osmotic drag effect corrected.

The electrical current profile is also plotted together with pH evolution (Figure 5.10). From the electrical current profile, current reached a stable value after ca. 30 min at each potential step, allowing a reliable and representative sampling at the end of the step. Furthermore, final pH (ca. 12) together with $X_{\text{NO}_3^-}$ (ca. 62%) for PdCu indicates that the process is likely due to catalytic hydrogenation of NO₃⁻ by H₂ (Table 5.1), which is evolved electrochemically over the surface of the cathode catalyst. Theoretically, for a pure electrochemical process at such value of $X_{\text{NO}_3^-}$, final pH should be ca. 12.7-12.9.

Product distribution was also examined. Selectivity values at each potential point categorized by each material are summarized in [Table 5.6](#). For this and later calculation of product selectivity, we made an important assumption: Total selectivity (S_{Total}) only included $S_{\text{NO}_2^-}$, $S_{\text{NH}_4^+}$ and S_{N_2} since from MS analysis (Pfeiffer Vacuum, Omnistar GSD 320) we could not confirm the presence of any side-product (N_2O , NO , NH_3 or NH_2OH) even at high potentials where, for example, NH_2OH could be formed [18]. Therefore, S_{N_2} was estimated from the difference between total selectivity and the selectivity sum of nitrite and ammonium. Furthermore, for convenience and clarity we also defined selectivity towards undesired side-products (S_{Side}) as the sum of $S_{\text{NO}_2^-}$ and $S_{\text{NH}_4^+}$.

Interesting information about the performance of different catalysts in electrolysis-assisted reduction of nitrates can be extracted from [Table 5.6](#). First of all, at the lowest potential examined (1.5 V) $S_{\text{NH}_4^+}$ was higher than $S_{\text{NO}_2^-}$ for all materials except for Cu catalyst. This unique feature of Cu is most likely related to the efficiency of Cu for first step of nitrate reaction, i.e. NO_3^- to NO_2^- [12, 15]. In the low potential range (1.5-1.9 V) there is a clear trend of $S_{\text{NO}_2^-}$ increase, although at high potential range (2.1-2.7 V) $S_{\text{NO}_2^-}$ is lowered due to compensating increase of $S_{\text{NH}_4^+}$. As a general trend, the higher value of $S_{\text{NH}_4^+}$ was observed at higher cell voltage with exceptions of Cu and Pd catalysts for which their highest $S_{\text{NH}_4^+}$ was found at 1.5 V. This behaviour matches with conventional electrochemical nitrate reduction where the product distribution highly depends on the applied electrolysis potential, even in case of bare SnO_2 . At low cell voltages, selectivity to NO_2^- is high, whereas reduction at high cell voltages produces mainly NH_4^+ [15, 18].

Table 5.6. Selectivity towards nitrite and ammonium ions ($S_{\text{NO}_2^-}$ and $S_{\text{NH}_4^+}$ in %) using electrolysis-assisted nitrate reduction under potential sweep condition (from 1.5 to 2.7 V, $\Delta V = 0.2\text{V}$, 60 min each step) at 80 °C. Five different cathode materials: 40 wt% Pt, Pd, Cu and PdCu (4:1) catalyst and bare support (SnO_2). Initial nitrate initial concentration of 1000 ppm. Nitrate solution flow rate of 160 $\mu\text{L}/\text{min}$. $S_{\text{N}_2} = 1 - (S_{\text{NO}_2^-} + S_{\text{NH}_4^+})$.

Cell Voltage / V	40 wt% Pt		40 wt% Pd		40 wt% Cu		40 wt% PdCu		SnO ₂	
	SNO ₂ ⁻	SNH ₄ ⁺	SNO ₂ ⁻	SNH ₄ ⁺	SNO ₂ ⁻	SNH ₄ ⁺	SNO ₂ ⁻	SNH ₄ ⁺	SNO ₂ ⁻	SNH ₄ ⁺
1.50	20.9	30.3	22.2	66.6	32.2	24.6	15.2	23.2	6.10	39.9
1.70	35.8	12.7	20.9	74.1	45.5	30.6	17.8	32.9	4.40	8.80
1.90	44.0	25.2	33.4	35.9	28.8	37.6	32.2	47.3	7.70	1.50
2.10	41.3	42.2	44.6	27.9	14.5	22.8	30.6	47.2	6.60	0.30
2.30	29.1	46.3	34.8	28.6	7.70	19.9	23.3	44.0	3.70	0.20
2.50	16.7	51.5	22.7	39.1	4.60	18.6	12.5	46.7	2.70	15.6
2.70	8.90	55.9	11.4	39.6	3.00	20.4	6.50	45.8	2.30	46.3

In terms of total undesired products selectivity (S_{Side}), Pd catalyst exhibited the highest value ca. 90% at 1.5 V. At 2.7 V the maximum S_{Side} was observed for Pt catalyst (ca. 65%), followed by PdCu (ca. 52%) and Pd catalysts (ca. 51%), whereas the best catalyst in terms of S_{Side} was Cu (ca. 24%). At an intermediate potential (2.1 V), Pt was the catalyst with the highest selectivity towards undesired products (ca. 84%), followed by Pd catalyst family. Furthermore, Pt tend to yield high amount of NH_4^+ compared to other catalysts, which is in good agreement with electrochemical nitrate reduction using PEM [11, 27]. The relatively high NH_4^+ selectivity of PdCu and Pd catalyst are also in agreement with literature [14].

Performance of bare SnO_2 (grey line, \circ) is also interesting since $S_{\text{NO}_2^-}$ as well as $S_{\text{NH}_4^+}$ in the middle range of the cell potentials were lowest, thus showing the best selectivity towards N_2 . Although the conversion is markedly low over the cell potentials examined compared to the supported metal catalysts, the high selectivity of SnO_2 should be highlighted. The presence of metal components improves hydrogen activation, but at the same time it seems to facilitate over-reduction of nitrates and intermediate species to undesired nitrites and ammonium ions.

At high nitrate concentration examined here, mass transfer, active sites accessibility, and large pH change (in the absence of buffering agent) may be an issue since they can affect the reaction performance. For this reason we examined electrolysis-assisted nitrate reduction using the same catalysts using lower concentration nitrate solution (100 ppm). The results of potential sweep experiments using 100 ppm NO_3^- initial solution are summarized in [Figure 5.11](#) in same manner as the previous experiments.

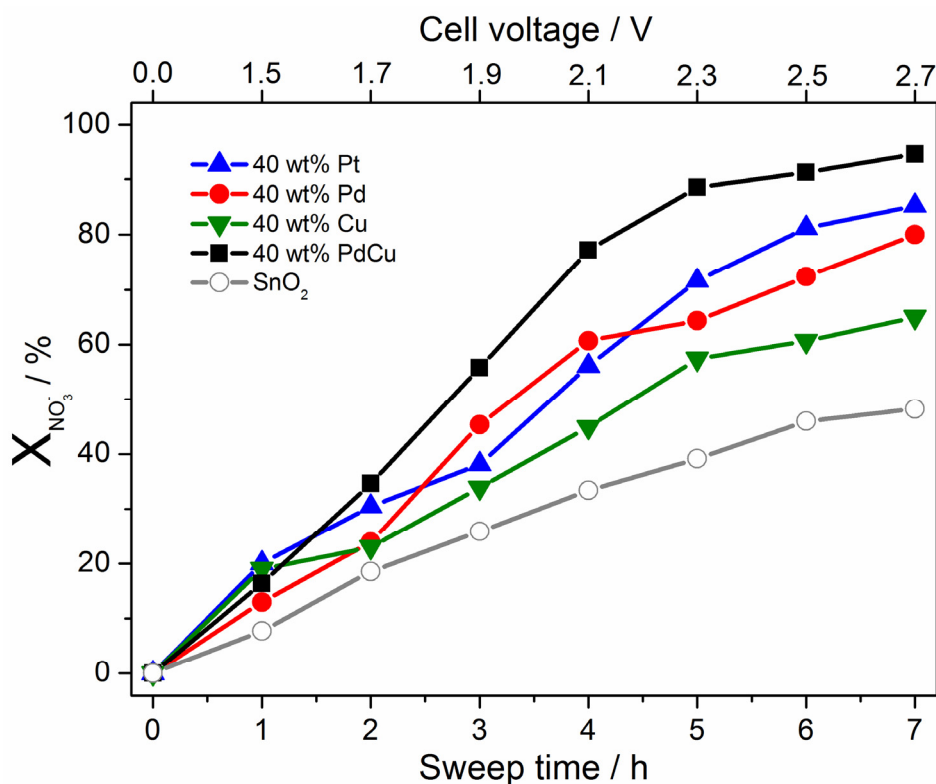


Figure 5.11. Nitrate conversion profiles over 7 h of potential sweep experiments (from 1.5 to 2.7 V, $\Delta V=0.2$ V, 60 min each step) of electrolysis-assisted nitrate reduction. Four different catalysts: Pt (blue \blacktriangle), Pd (red \bullet), Cu (green \blacktriangledown) and PdCu (black \blacksquare) and bare SnO₂ (grey \circ) were tested at 80°C with nitrate solution of 100 ppm NO₃⁻ at 160 μ L/min. Electro-osmotic drag effect was corrected.

As in case of 1000 ppm nitrate initial solution, $X_{\text{NO}_3^-}$ raised gradually with increase of cell voltage (Figure 5.11). Bare SnO₂ (grey line, \circ) consistently gave the lowest nitrate conversions among all the materials examined at all cell voltages, showing the important effects of metal components in nitrate reduction. With 100 ppm nitrate solution, PdCu catalyst (black line, \blacksquare) was clearly the best catalyst reaching almost full conversion, ca. 95% at 2.7 V, followed by Pt (ca. 85%) (blue line, \blacktriangle) and Pd catalysts (ca. 80%) (red line, \bullet). While the general

trend observed for 1000 ppm nitrate solution (Figure 5.9) holds for this study, the reaction performance was greatly enhanced for 100 ppm nitrate solution. Cu catalyst (green line, ▼) among the supported metal materials showed the poorest $X_{\text{NO}_3^-}$ (ca. 65%), although the activity was improving at higher cell potential without any sign of deactivation often reported for catalytic hydrogenation. It is also remarkable that for the best catalyst (PdCu), at an intermediate potential of 2.1 V, nitrate conversion value were already ca. 80%.

It is also important to point out that the current at each potential step was higher than in case of 1000 ppm nitrate solution with faster current stabilisation (Figure 5.12). The higher current level was attributed to the lower amount of cations in solution like Na^+ (originating from nitrate salt employed for nitrate solution preparation). The presence of such cations in contact with Nafion membrane is known to hinder and sometimes blocks the ionic channels for H^+ transport from anode to cathode. Na^+ has high affinity to the channels of Nafion according to literature [34-37]. In fact, such cations have a higher affinity than protons for the sulfonic acid group sites in the polymer electrolyte and can replace protons in the membrane by ion exchange processes.

From pH profile of 40 wt% PdCu/ SnO_2 shown in Figure 5.12 it can be observed that at the end of the potential sweep (2.7 V) the highest pH value reached is around 11, which is lower than the corresponding value using the 1000 ppm nitrate solution (ca. 12). The main explanation is due to the difference in the initial concentrations (C_0), yielding difference in the amount of produced OH^- . Again, this profile and obtained values are consistent with theoretically ones (Table 5.1) expected from catalytic nitrate reduction, although the reaction can be induced

by electrochemically triggered hydrogen production [15]. In case of pure electrochemical reaction pH should be around 12 (Table 5.2).

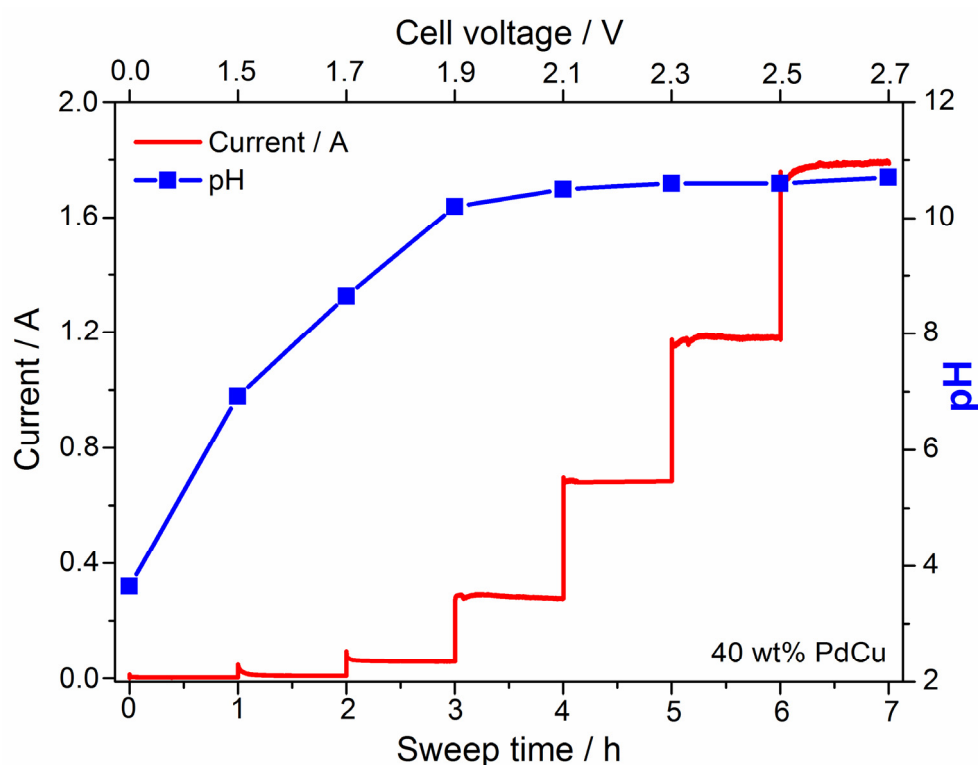


Figure 5.12. Current and pH profile during electrolysis-assisted nitrate reduction over 7 h of potential sweep experiment (from 1.5 to 2.7 V, $\Delta V=0.2$ V, 60 min each step) using 40 wt% PdCu/SnO₂ catalyst at 80°C, 100 ppm NO₃⁻ at 160 μ L/min. electro-osmotic drag effect corrected.

Furthermore, Table 5.7 summarises the product selectivity in terms of $S_{\text{NO}_2^-}$ and $S_{\text{NH}_4^+}$. Compared to the case of 1000 ppm nitrate solution, there was an evident decrease in S_{Side} for all materials tested. In fact, more than one order of magnitude decrease in S_{Side} was achieved.

Table 5.7. Selectivity towards nitrite and ammonium ions ($S_{\text{NO}_2^-}$ and $S_{\text{NH}_4^+}$ in %) using electrolysis-assisted nitrate reduction under potential sweep condition (from 1.5 to 2.7 V, $\Delta V = 0.2\text{V}$, 60 min each step) at 80 °C. Five different cathode materials: 40 wt% Pt, Pd, Cu and PdCu (4:1) catalyst and bare support (SnO_2). Initial nitrate initial concentration of 100 ppm. Nitrate solution flow rate of 160 $\mu\text{L}/\text{min}$. $S_{\text{N}_2} = 1 - (S_{\text{NO}_2^-} + S_{\text{NH}_4^+})$.

Cell Voltage / V	40 wt% Pt		40 wt% Pd		40 wt% Cu		40 wt% PdCu		SnO ₂	
	S _{NO₂⁻}	S _{NH₄⁺}	S _{NO₂⁻}	S _{NH₄⁺}	S _{NO₂⁻}	S _{NH₄⁺}	S _{NO₂⁻}	S _{NH₄⁺}	S _{NO₂⁻}	S _{NH₄⁺}
1.50	2.20	19.8	0.80	2.20	0.50	3.90	0.80	6.30	1.60	19.2
1.70	1.70	10.0	1.50	7.20	0.60	4.20	1.50	9.10	4.60	11.6
1.90	2.20	10.9	0.80	3.70	0.90	3.90	0.80	4.90	1.90	2.20
2.10	1.10	5.30	0.60	4.40	2.00	2.60	0.50	3.40	1.70	2.50
2.30	0.80	4.60	0.70	4.50	3.90	2.10	0.40	3.10	1.30	1.20
2.50	0.60	4.20	0.70	3.80	5.50	19.50	0.40	3.30	0.80	2.50
2.70	0.60	3.40	0.80	12.7	1.70	12.70	0.40	3.50	0.70	3.50

Generally, $S_{\text{NO}_2^-}$ was low at all cell voltages examined for all materials examined. Upon the potential rise, there was an increase in $S_{\text{NO}_2^-}$ at low potential region (1.5-2.1 V, it varies dependent on the material) then followed by noticeable decrease up to 2.7 V. Regarding $S_{\text{NH}_4^+}$, in case of Pd and Cu catalysts ammonium ion production was enhanced at higher cell voltages, whereas with PdCu, Pt and SnO_2 the tendency was opposite; $S_{\text{NH}_4^+}$ decreased at higher cell voltages. PdCu, which gave the highest conversion, also gave the best results in terms of S_{Side} (ca. 4% at 2.7 V) along all the potentials swept. Pt catalyst also presented similarly good results. In both cases this would mean about 96% of selectivity towards nitrogen (S_{N_2}) was achieved.

Evaluating both $X_{\text{NO}_3^-}$ and S_i values, it was obvious that the best performing material for electrolysis-assisted nitrate reduction at low nitrate concentration conditions was 40 wt% PdCu/ SnO_2 , giving almost full conversion of nitrates and high selectivity towards N_2 , although rather high cell potentials were required to achieve the excellent performance. We have selected this material as a reference cathode for further investigations.

5.4.2.2 System Flexibility Evaluation

Results obtained with 100 ppm nitrate solution in continuous mode are comparable with those reported by Machida and co-workers [11], with an important difference of the absence of pH buffering agent in this work. Encouraged by the results, we extended our study in order to minimize further the selectivity towards undesired products and improve performance. It has to be noticed that, although selectivity results ($S_{\text{NH}_4^+} + S_{\text{NO}_2^-}$) obtained working at 100

ppm of nitrates were promising (only 4% at 2.1 – 2.7 V) we have to keep in mind that milder conditions of cell voltage and also achieving 0% selectivity towards undesired products are of critical importance in practice because of possibly over-generated hydrogen at high potential conditions and the very stringent regulations for drinking water quality. Considering the actual regulation of NO_3^- (50 ppm), NO_2^- (0.1 ppm) and NH_4^+ (0.5 ppm) in drinking water (EEA 98/83/EC), $S_{\text{NH}_4^+} + S_{\text{NO}_2^-}$ should be lower than ca. 2.5%. To tackle this great challenge, different powering conditions as well as system configurations were tested as follows.

(a) The first operation mode we evaluated was a constant cell voltage condition (Figure 5.5c). In particular, electrolysis-assisted reduction under a high potential condition (2.5 V) was examined based on the excellent results given by PdCu catalyst under the high cell voltage conditions.

(b) The second operation mode was a constant-current condition (Figure 5.5b). The advantage of this operation is to avoid fluctuations in H^+ transport and therefore in hydrogen production rate over cathode catalyst (Chapter 3). The constant current was chosen to be low in order not to affect membrane stability. Other operation conditions remained unchanged (T, nitrate solution flow rate ($F_{\text{NO}_3^-}$) and cathode catalyst composition) from the previous measurements. A freshly prepared membrane was used and electrical current was fixed at 100 mA [11, 15] giving an average potential of 1.6 V, that is, in the low potential region.

(c) The third operation mode examined was a 'loop' (i.e. recirculation) mode (Figure 5.5d). The effluent solution was recirculated through nitrate solution/effluent solution reservoir (100 ppm, 20 mL) by means of the peristaltic pump. In this operation mode, improvement of the reaction performance was

aimed by increasing the contact time of nitrates and nitrites with the catalyst. According to the flow rate of solution and the volume of reservoir, roughly the solution passed through over the catalyst three times in 3 h. This mode was tested under constant current mode at 100 mA with an averaged cell potential of ca. 1.6 V.

(d) The fourth operation mode was catalytic nitrate hydrogenation over PdCu catalyst coated over the PEM membrane (Figure 5.5e). The reaction was performed at 80 °C by saturating nitrate solution with H₂ before passing into the reactor cell. Obviously, no cell voltage (0 V) was applied. Nitrate solution flow rate was kept the same as in the other modes (160 μL/min).

Figure 5.13 shows the $X_{\text{NO}_3^-}$ profiles over the reaction time of 3 h using the four different strategies described above. Continuous flow electrocatalytic reduction at constant cell voltage of 2.5 V (Figure 5.13a) showed the best results in terms of nitrate conversion (ca. 97%) after a short stabilization time of 30 min as previously observed (Figure 5.8). Also, it was remarkable to observe a stable performance at the high nitrate conversion, showing the stable continuous operation of the reaction under the high cell voltage condition. The second strategy of a constant current at 100 mA did not show a satisfactory performance with a slight decrease in activity (Figure 5.13b), although the nitrate conversion was stabilized at ca. 30% towards the end of the run. Employing the constant current, the recirculation strategy, by increasing the contact time of the reactants with the catalyst, can improve the reaction performance (Figure 5.13c). At 3 h reaction time NO₃⁻ conversion of ca. 68% was observed. Importantly, the conversion was linearly increasing with time and it is expected to be higher at higher reaction time. Indeed, after 4 h the conversion rose up to ca. 84%. This is

an important finding since this strategy clearly shows that the catalytic performance can be improved even under mild conditions (low cell voltages) by changing the operation modes and conditions. Furthermore, catalytic nitrate reduction (without applying cell voltage) using H₂ saturated 100 ppm NO₃⁻ solution exhibited the worst conversion (ca. 5% X_{NO₃⁻}) among all modes tested in this study (Figure 5.13d).

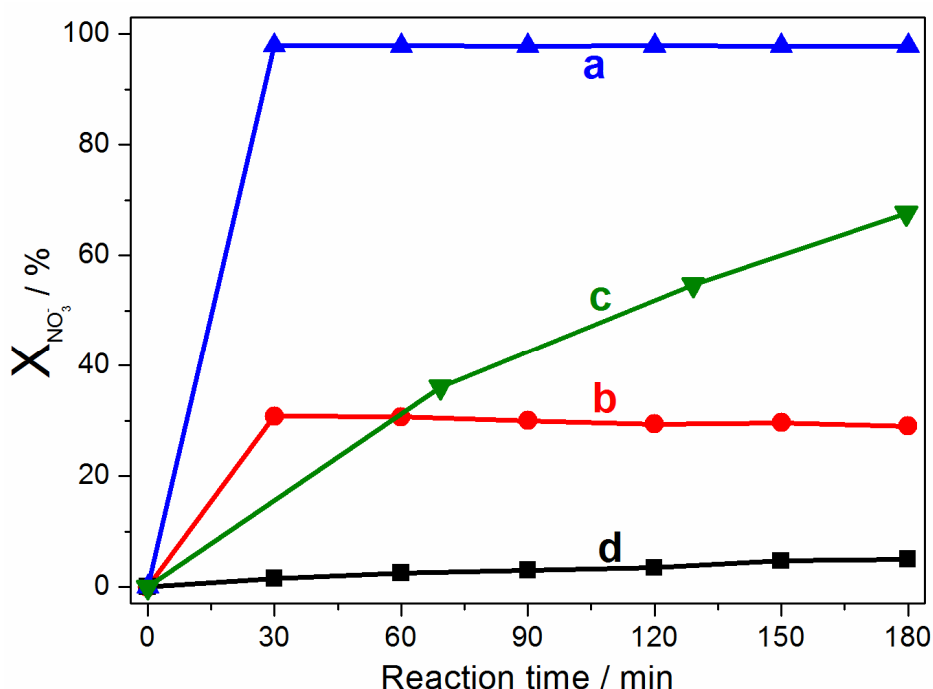


Figure 5.13. Evaluation of different operation modes in nitrate reduction using the PEM electrolysis cell using 40 wt% PdCu/SnO₂ as cathode catalyst at 80°C with 100 ppm nitrate solution for 3 h. Fresh membranes were employed for each measurement. (a) Constant cell voltage mode at 2.5V, (b) constant current mode at 100 mA, (c) recirculation mode at constant current of 100 mA and (d) catalytic nitrate hydrogenation over MEA without applying cell voltage. Nitrate flow rate was 160 μL/min.

Based on the findings above, it can be concluded that the electrochemically generated hydrogen/proton over the MEA is highly reactive compared to

molecular H_2 used in catalytic nitrate reduction. This enhancement may be originated from an electrochemical promotion effect known as NEMCA (Non-faradic electrochemical modification of catalytic activity) effect [38, 39] or electrochemical promotion of catalysis (EPOC) [40], although the origin of the activity enhancement has not been firmly identified in this work.

The reaction performance cannot be evaluated by only nitrate conversion. The reaction selectivity is graphically summarised in [Figure 5.14](#). Interestingly, a clear trend between product selectivity and conversion could be established; the higher the nitrate conversion, the lower the selectivity towards undesired products. The constant potential mode (a) showed the best overall selectivity to N_2 , while achieving the highest $X_{NO_3^-}$, ca. 97%. The second best strategy was recirculation mode at a constant current (100 mA) (c) with S_{Side} ca. 13.7% at $X_{NO_3^-}$ of 68%. The third one was constant current mode (100 mA) without recirculation (b), showing S_{Side} of 26% at $X_{NO_3^-}$ of 29%. Finally, the worst performing strategy in terms of reaction selectivity was the catalytic hydrogenation over MEA (d), showing S_{Side} ca. 32.5% at $X_{NO_3^-}$ of 5%. It is also worth mentioning that the high selectivity to both NO_2^- and NH_4^+ when the reaction was performed in catalytic hydrogenation mode (strategy d).

The detailed evaluation of system flexibility by studying different operation modes provided us very interesting and useful insights to operate the reaction for the best performance. Particularly, with a high constant cell voltage an excellent reaction performance was confirmed. In comparison to the reaction selectivities observed in the catalytic nitrate reduction in a conventional setup ([Tables 5.4 and 5.5](#)), the excellent catalytic performance in terms of high N_2 selectivity can be highlighted.

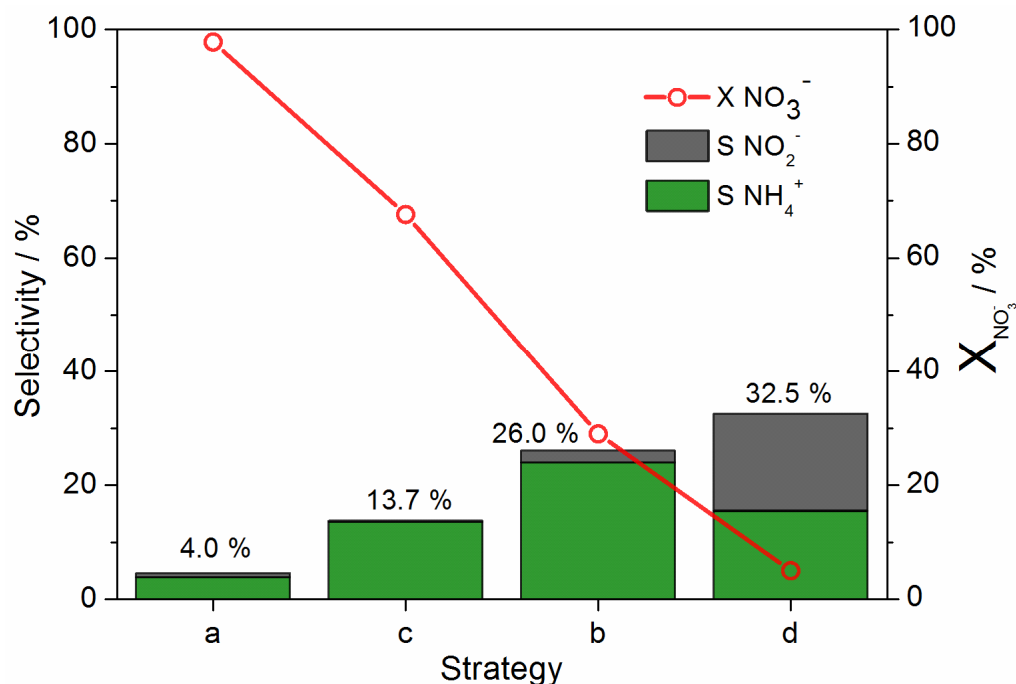


Figure 5.14. Nitrate conversion ($X_{NO_3^-}$) and product selectivity ($S_{NO_2^-}$ and $S_{NH_4^+}$) employing the four strategies (caption of Figure 5.13) shown above and using 40 wt% PdCu/SnO₂ at 80°C and 100 ppm nitrate solution after 3 h of reaction. Fresh membranes were employed for each individual measurement. The values shown on top of the bar are total selectivity to the undesired products ($S_{Side} = S_{NO_2^-}$ and $S_{NH_4^+}$).

5.5 Conclusions

The feasibility of PEM electrolysis-assisted concept for aqueous nitrates abatement under continuous operation was investigated in detail to maximize the nitrate conversion and N₂ selectivity. The results were compared with those of catalytic nitrate reduction using molecular H₂ saturated in aqueous nitrate solution.

Supported metal catalysts with 40 wt% loading of metal (Pt, Pd, Cu and PdCu (4:1)) over high surface area SnO₂ were synthesized and tested in catalytic hydrogenation as well as in electrolysis-assisted nitrate reduction. All the

catalysts prepared were active in the catalytic nitrate reduction showing high nitrate conversion, however, often with low N_2 selectivity. Among the catalysts tested, PdCu showed the best performance in terms of low nitrite and ammonium ion selectivity. In the electrolysis-assisted operation, the reaction performance using 1000 ppm nitrate solution did not show satisfactory reaction performance likely due to the high pH of the solution (no pH-buffering CO_2 was added in this work), which resulted in low N_2 selectivity, as well as due to deteriorating performance in PEM electrolysis by blockage of the H^+ transport channels of Nafion membrane by the metal cations (Na^+). Nevertheless, using a more realistic concentration for drinking water, i.e. the nitrate solution of 100 ppm, excellent results have been gained using the electrolysis-assisted approach. 40 wt% PdCu was found as the best performing material among those tested. Excellent $X_{NO_3^-}$ and S_{Side} of ca. 97% and 4%, respectively, could be achieved. Using different modes of operation based on constant cell voltage, constant current with/without recirculation, and catalytic hydrogenation; the flexibility of operation strategy was shown and the best mode of operation, approaches towards more effective nitrate abatement, were suggested.

According to the pH profiles during the reaction, we concluded that nitrate reduction in the electrolysis-assisted mode occurs via catalytic hydrogenation of NO_3^- by H_2 , the latter being evolved electrochemically on the surface of the cathode electrode. Moreover, the synergetic effects of PdCu catalyst, well documented in catalytic hydrogenation, hold for the electrolysis-assisted nitrate reduction. Using 100 ppm nitrate solution, the electrolysis-assisted operation performed considerably better than classical catalytic reduction in terms of N_2 selectivity.

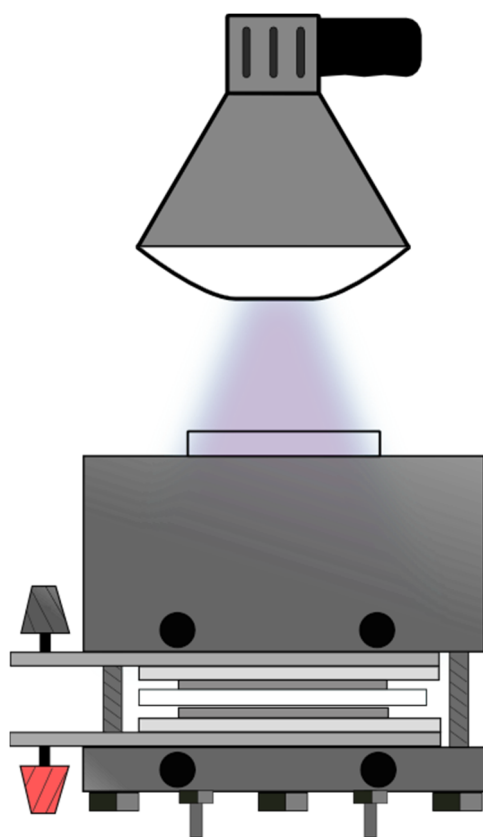
BIBLIOGRAPHY

1. M. D'Arino, F. Pinna, G. Strukul, *Applied Catalysis B-Environmental* **53**, 161, **2004**.
2. K. D. Vorlop, T. Tacke, *Chemie Ingenieur Technik* **61**, 836, **1989**.
3. H. Berndt, I. Mönlich, B. Lücke, M. Menzel, *Applied Catalysis B: Environmental* **30**, 111, **2001**.
4. A. Palomares, J. Prato, F. Rey, A. Corma, *Journal of Catalysis* **221**, 62, **2004**.
5. G. Strukul, F. Pinna, M. Marella, L. Meregalli, M. Tomaselli, *Catalysis Today* **27**, 209, **1996**.
6. K. D. Vorlop, T. Tacke, *Chemie Ingenieur Technik* **61**, 836, **1989**.
7. F. A. Marchesini, S. Irusta, C. Querini, E. Miro, *Applied Catalysis a-General* **348**, 60, **2008**.
8. N. Barrabes, J. Sa, *Applied Catalysis B-Environmental* **104**, 1, **2011**.
9. S. Horold, K. D. Vorlop, T. Tacke, M. Sell, *Catalysis Today* **17**, 21, **1993**.
10. F. Gauthard, F. Epron, J. Barbier, *Journal of Catalysis* **220**, 182, **2003**.
11. M. A. Hasnat, I. Ishibashi, K. Sato, R. Agui, T. Yamaguchi, K. Ikeue, M. Machida, *Bulletin of the Chemical Society of Japan* **81**, 1675, **2008**.
12. F. Epron, F. Gauthard, C. Pineda, J. Barbier, *Journal of Catalysis* **198**, 309, **2001**.
13. M. Duca, M. T. Koper, *Energy & Environmental Science* **5**, 9726, **2012**.
14. M. Hasnat, M. Karim, M. Machida, *Catalysis Communications* **10**, 1975, **2009**.
15. M. Machida, K. Sato, I. Ishibashi, M. A. Hasnat, K. Ikeue, *Chemical communications*, 732, **2006**.
16. J. Genders, D. Hartsough, D. Hobbs, *Journal of applied electrochemistry* **26**, 1, **1996**.
17. K. Bouzek, M. Paidar, A. Sadilkova, H. Bergmann, *Journal of applied electrochemistry* **31**, 1185, **2001**.
18. N. Chebotareva, T. Nyokong, *Journal of applied electrochemistry* **27**, 975, **1997**.
19. N. Barrabés, J. Sá, *Applied Catalysis B: Environmental* **104**, 1, **2011**.
20. J. Warna, I. Turunen, T. Salmi, T. Maunula, *Chemical Engineering Science* **49**, 5763, **1994**.
21. M. A. Hasnat, M. S. Alam, M. H. Mahbub-ul Karim, M. A. Rashed, M. Machida, *Applied Catalysis B-Environmental* **107**, 294, **2011**.
22. K. Sasaki, F. Takasaki, Z. Noda, S. Hayashi, Y. Shiratori, K. Ito, *Ecs Transactions* **33**, 473, **2010**.
23. U. Prüße, N. Thielecke, K. D. Vorlop, *Handbook of Heterogeneous Catalysis*, **2008**.
24. X. M. Ren, S. Gottesfeld, *Journal of The Electrochemical Society* **148**, A87, **2001**.
25. T. A. Zawodzinski, J. Davey, J. Valerio, S. Gottesfeld, *Electrochimica Acta* **40**, 297, **1995**.

26. T. A. Zawodzinski, C. Derouin, S. Radzinski, R. J. Sherman, V. T. Smith, T. E. Springer, S. Gottesfeld, *Journal of The Electrochemical Society* **140**, 1041, **1993**.
27. M. Hasnat, R. Agui, S. Hinokuma, T. Yamaguchi, M. Machida, *Catalysis Communications* **10**, 1132, **2009**.
28. M. D'Arino, F. Pinna, G. Strukul, *Applied Catalysis B: Environmental* **53**, 161, **2004**.
29. R. Gavagnin, L. Biasetto, F. Pinna, G. Strukul, *Applied Catalysis B: Environmental* **38**, 91, **2002**.
30. A. Pintar, G. Berčić, J. Levec, *AIChE Journal* **44**, 2280, **1998**.
31. A. Pintar, M. Setinc, J. Levec, *Journal of Catalysis* **174**, 72, **1998**.
32. U. Prüsse, M. Hähnlein, J. Daum, K.-D. Vorlop, *Catalysis Today* **55**, 79, **2000**.
33. U. Prüsse, S. Hörold, K. D. Vorlop, *Chemie Ingenieur Technik* **69**, 93, **1997**.
34. T. Okada, S. Møller-Holst, O. Gorseth, S. Kjelstrup, *Journal of Electroanalytical Chemistry* **442**, 137, **1998**.
35. T. Okada, *Journal of Electroanalytical Chemistry* **465**, 1, **1999**.
36. T. Okada, *Journal of New Materials for Electrochemical Systems* **4**, 209, **2001**.
37. T. Okada, H. Satou, M. Okuno, M. Yuasa, *The Journal of Physical Chemistry B* **106**, 1267, **2002**.
38. C. Vayenas, S. Brosda, C. Pliangos, *Journal of Catalysis* **203**, 329, **2001**.
39. C. G. Vayenas, S. Bebelis, S. Neophytides, *Journal of Physical Chemistry* **92**, 5083, **1988**.
40. A. Katsaounis, *Journal of applied electrochemistry* **40**, 885, **2010**.

CHAPTER 6

ADVANCING NITRATE MITIGATION STRATEGIES



6.1 Introduction

The effectiveness of electrolysis-assisted nitrate reduction using supported catalysts and hydrogen generated in situ has been proven in [Chapter 5](#). Despite of the excellent results obtained, there are two aspects which could be and need to be improved further, related to (i) lowering cell voltage and (ii) lowering ammonium ion concentration to meet with the stringent regulations for drinkable water. This chapter describes our attempts to tackle the two issues by making modifications to the electrolyser cell and by examining new reaction system configurations.

As described in [Chapter 5](#), almost full conversion (ca. 97%) of nitrates was achieved using PdCu catalyst in electrolysis-assisted nitrate reduction with a low selectivity towards undesired side products of ca. 4% at 2.5-2.7 V. Although the performance was very good, lowering the working cell voltage (thus electrical current) would be beneficial in (i) overall system long-term stability, (ii) decrease in electro-osmotic drag effects, and (iii) lowering electrical energy for operation. Our study ([Chapter 5](#)) already showed that increase of residence time of solution in the cathode compartment can proportionally enhance the nitrate conversion. The next step was to examine operations with a long residence time and thus a batch operation in electrolysis-assisted mode was investigated. Feasibility of such operation mode has been reported by Machida and co-workers [1-4] at 100 mA constant current using unsupported metal catalysts.

Another very important point for further investigation is the mitigation of NH_4^+ as evidenced from the major constituent of undesired side-products (ca. 85% of NH_4^+ out of 4% of S_{Side} observed in the constant cell voltage mode). Careful

literature survey indicated that NH_4^+ conversion to N_2 can be carried out by means of oxidation or decomposition reactions. Several of these reaction are known such as catalytic oxidation [5, 6], electrocatalytic oxidation [7-9] and photocatalytic oxidation [10-12]. We examined these paths to manage and mitigate the produced NH_4^+ (instead of suppressing its formation) upon nitrate reduction to the tolerated level, which is very difficult in reality.

6.2 Low-Potential Electrolysis-Assisted Batch Operation

Decreasing both ammonium selectivity and cell voltage while keeping high catalytic activity ($X_{\text{NO}_3^-}$) is a great challenge we wish to tackle and for this reason we have investigated batch operation mode. For this purpose we modified our PEM electrolysis cell. The flow through cathode compartment was replaced by batch cell compartment made of aluminium, with 20 mL solution reservoir. Herein, we will refer to this new approach as electro-batch configuration. The main features and design of electro-batch cell are shown in [Figure 6.1](#).

In the electrochemical cell the solution was in contact with the cathode catalyst ([Figure 6a](#)). This reactor was placed in a horizontal-MEA position ([Figure 6a](#)) since the batch cell had a small hole at upper part for gas (mainly H_2) release ([Figure 6.1b](#)). MEA composition (PdCu catalyst) was same as in [Chapter 5](#). Fresh MEA was tested for 3 h at 100 mA. The mode of operation slightly influenced and increased the cell voltage at the constant current and the average cell voltage was ca. 1.8 V (ca. 1.6 V in case of flow-through operation). Water flow rate in the anode compartment was kept at the same level as in the previous studies (0.5 mL/min). The solution in the cathode compartment was stirred in order to

enhance mass transfer and solution homogeneity. Operation at 100 mA has the benefit of low electro-osmotic drag and the amount of dragged water (continuously accumulating at the cathode compartment) is ca. 2 $\mu\text{L}/\text{min}$, so its impact on the concentration after 3 h of batch operation would be less than 1.5% (0.3 mL over 20 mL initial solution).

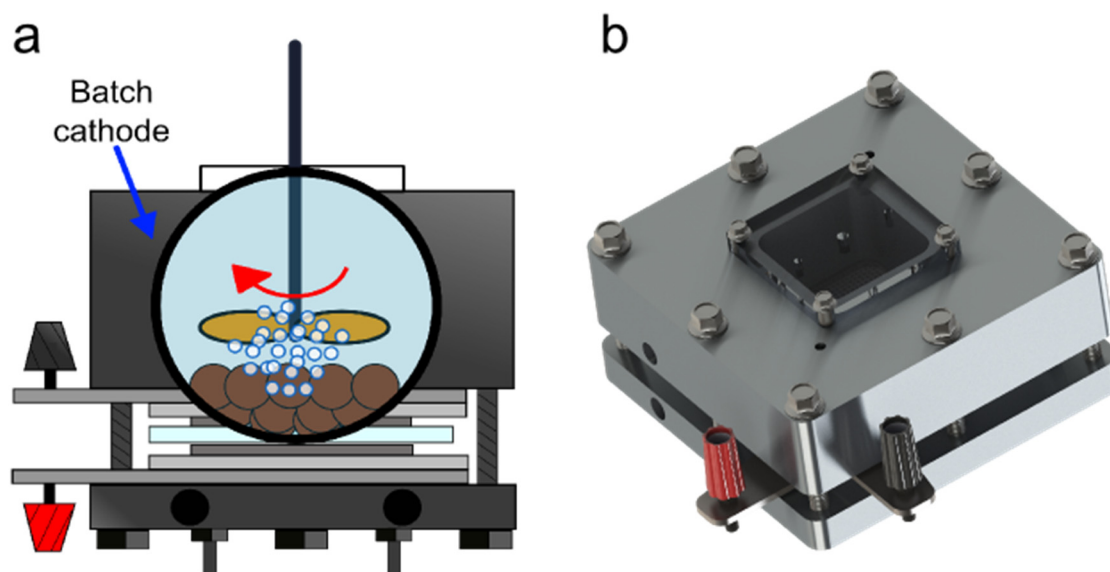


Figure 6.1. Home-made PEM electrolysis cell for electrocatalytic tests in batch configuration. 20mL cathode reservoir and 80°C, operation in horizontal position. (a) Schematic side view of the electrolysis-assisted batch cell and (b) the assembled cell ready for operation, top part was closed with a plastic window.

Electro-batch conditions were also tested under flow of CO_2 (20 mL/min) as a pH buffer so that comparisons of product distribution could be made. Nitrate conversion profile using this operation mode with/without CO_2 is shown in [Figures 6.2 and 6.3](#).

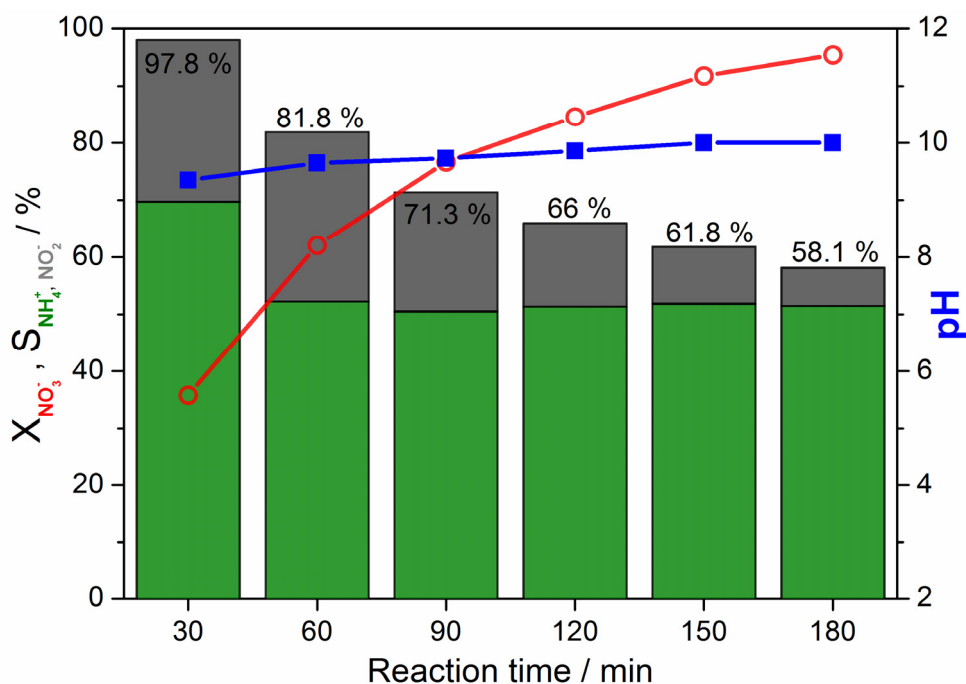


Figure 6.2. Nitrate conversion ($X_{NO_3^-}$, red line), product selectivity ($S_{NO_2^-}$ (grey bar) and $S_{NH_4^+}$ (green bar)), and pH change (blue line) using the electro-batch operation over 3 h using 40 wt% PdCu/SnO₂ at 80°C and with 20 mL of 100 ppm nitrate solution. The values shown on top of the bar is total selectivity to the undesired products ($S_{side} = S_{NO_2^-}$ and $S_{NH_4^+}$).

After 3 hours of batch operation starting from 100 ppm NO₃⁻ without CO₂ flow (Figure 6.2), $X_{NO_3^-}$ reached ca. 95%, showing very similar high catalytic activity as in case of flow system at high potential (Chapter 5). PdCu catalyst demonstrated its ability for nitrate conversion in batch mode as in the continuous flow mode. Conversion increased proportionally with time, but the very high S_{side} was observed, decreasing from almost 100% to 58% (Figure 6.2). Such selectivity values were more than one magnitude order higher than those observed under flow conditions (ca 4%, 2.5 V and continuous flow). Main contributor for this high S_{side} was due to the formation of ammonium ion, reaching a constant value of ca. 50% with time. On the other hand, NO₂⁻ selectivity

continuously decreased with time up to the end of the test due to further reduction to N_2 and NH_4^+ over time. Besides, the evolution of the solution pH showed its maximum value at ca. 10 at 3 h. This value matches again with the previous interpretation regarding the origin of reduction activity; it is an electrochemically promoted catalytic process.

Due to the high selectivity towards NH_4^+ under the non-buffered condition, a further test was performed using CO_2 -buffered nitrate solution.

Figure 6.3 shows that CO_2 buffering has great beneficial impacts particularly on suppressing nitrite formation. This observation was previously discussed (Chapter 5) and also described in literature [13, 14]. From 0 to 90 min, $S_{NO_2^-}$ was stepwise decreasing (from 15 to 2.5% approximately) and later the amount of nitrite was very low (ca. 0.5%). On the other hand, $S_{NH_4^+}$ was not positively affected by CO_2 buffering. The value was almost constant throughout the reaction (ca. 60%). It was also interesting to observe that under pH-buffered conditions (pH of ca. 8) the amount of ammonium ion produced was higher than in the case of non-buffered condition (ca. 60% vs 50%, respectively) (Figure 6.2 and 6.3). Nitrate conversion rate was higher with pH buffering and the conversion value was almost full (ca. 99%) after 120 min of reaction. All the observations resulted from the CO_2 addition, namely, nitrite suppression and enhanced ammonium ion formation, agree with the trend observed in literature [1, 4].

Therefore, it could be concluded that the electro-batch strategy operating at mild conditions allowed us to reach the maximum level of nitrate conversion having as a drawback its poor selectivity towards nitrogen ($S_{N_2} < 50\%$) with high level of ammonium ion formation. Therefore, the strategy as it is cannot be used for water purification for drinking water. However, such approach could be used

for the production of concentrated ammonium ion solution such as the one used in selective catalytic reduction (SCR) in automotive industry or for the production of gaseous ammonia.

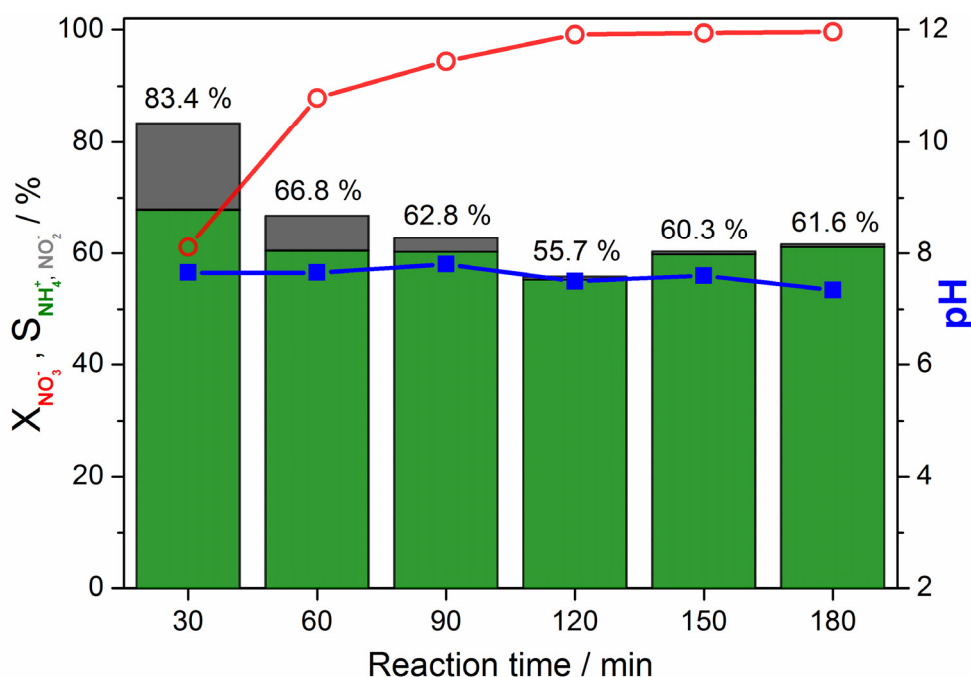


Figure 6.3. Nitrate conversion ($X_{NO_3^-}$, red line), product selectivity ($S_{NO_2^-}$ (grey bar) and $S_{NH_4^+}$ (green bar)), and pH change (blue line) using the electro-batch operation over 3 h using 40 wt% PdCu/SnO₂ at 80°C and with 20 mL of 100 ppm nitrate solution buffered with CO₂ (bubbling at 20 mL/min). The values shown on top of the bar is total selectivity to the undesired products ($S_{Side} = S_{NO_2^-}$ and $S_{NH_4^+}$).

Since ammonium ion formation was recognized as the bottleneck of the electrolysis-assisted process (also in catalytic reduction), our research was directed towards ammonium ion mitigation instead of preventing its formation; its conversion towards N₂ was targeted. Such strategies are described in the next sections.

6.3 NH₄⁺ Abatement Strategies

Throughout our research on nitrate reduction, we noticed that reduction of ammonium ion concentration below the maximum limits allowed for drinking water (i.e. NH₄⁺ < 0.5ppm) is very challenging regardless of mitigation strategies (catalytic or electrolysis-assisted one) employed. Therefore, we investigated two different approaches for NH₄⁺ oxidation towards N₂: (i) oxidation of ammonium ion in the anode compartment where oxygen is generated by directly feeding the cathodic effluent stream containing ammonium ions, leading to sequential Red-Ox strategy (Figure 6.4) and (ii) photocatalytic NH₄⁺ oxidation [10-12] (Figure 6.5).

6.3.1 Electrolysis-Assisted Ammonium Oxidation

Electrolysis-assisted ammonium oxidation strategy was examined in flow configuration passing NH₄⁺-containing effluent stream to the anode compartment of either the same reaction cell (Figure 6.4a) or the separate cell (Figure 6.4b). The electrolyser cell(s) was (were) maintained at 80 °C. NH₄⁺-containing effluent stream was fed to a selected anode compartment at constant flow rate of 160 μL/min. For tests performed using the same cell for both NO₃⁻ reduction and NH₄⁺ oxidation (Figure 6.4a), MEA configuration was IrO₂ | Nafion | 40 wt% PdCu/SnO₂. Pt either in the supported or unsupported form is widely used as catalyst for electro-oxidation of NH₄⁺ using batch reactors [7]. Therefore, when the reactions were performed in separate cells (Figure 6.4b), the MEA composition of NH₄⁺ oxidation cell was Pt black | Nafion | Pt black. Cell voltage for both primary and auxiliary were fixed at 2.5 V (in flow conditions suitable potential for X_{NO₃⁻} > 90%), as well as, nitrate C₀ was fixed at 100 ppm.

In the electrolysis-assisted NH_4^+ oxidation mode (Figure 6.4a), we observed a considerable decrease in the concentration of NH_4^+ in the final effluent stream. The final NH_4^+ concentration was ca. 2 ppm, giving us a hint on how to lower NH_4^+ concentration below the maximum allowed for drinking water. However, optimizing the reaction conditions did not show further improvement. The reasons for this could not be found out at that time, but we suspected about anode catalyst used in this mode, IrO_2 , since it may not be efficient enough for ammonium oxidation.

On the other hand, using the separate cell strategy (Figure 6.4b), NH_4^+ concentrations below 0.5 ppm were systematically observed. However, there was one major issue associated with the approach. Unfortunately after detailed investigations of all effluent streams from the two electrolyser cells, we realized that ammonium ion was diffusing from anode to cathode compartments through Nafion membrane continuously. Therefore, we obtained a highly concentrated ammonium solution in the cathode effluent stream from the NH_4^+ oxidation cell. Actually, the same phenomena, i.e. transport of NH_4^+ through the membrane, was also suspected to occur in the first one-cell approach (Figure 6.4a). In fact, the high affinity of NH_4^+ to Nafion and its transport through its channelled structure is known [15], surprisingly with higher transport rate than that of H^+ . Besides, incorporation of ammonium ion (and other ions like alkali and alkali earth metal ions in reality) in the membrane can decrease system performance (current and stability drop).

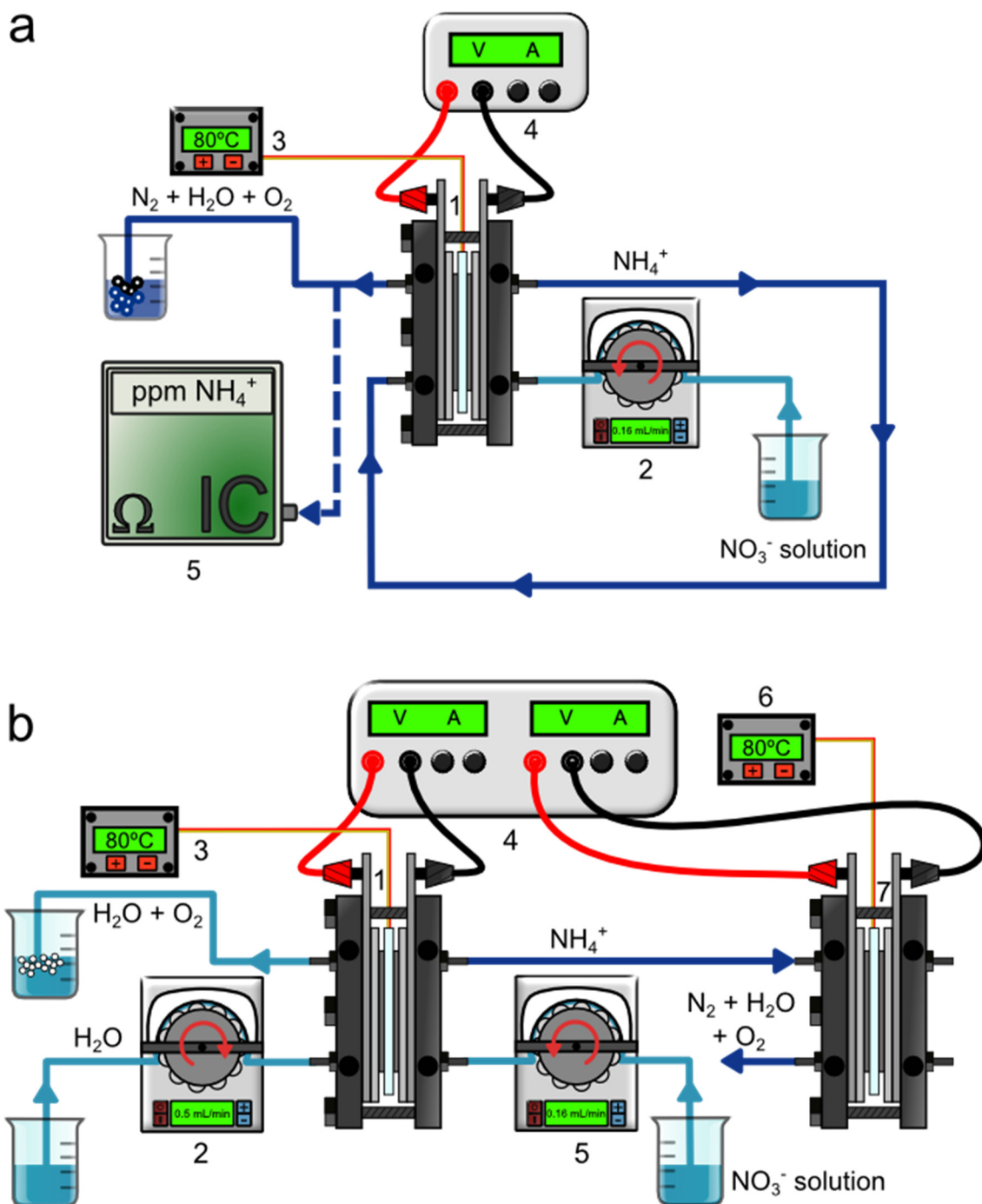


Figure 6.4. Electrolysis-assisted ammonia oxidation. (a) One-cell mode; nitrate reduction and ammonia oxidation in the same PEM electrolysis cell and (b) Two-cells mode, nitrate reduction cell (1) and ammonia oxidation (7) in separate cells under continuous flow of nitrate solution (100 ppm, 160 μ L/min).

Not being able to achieve effective NH_4^+ oxidation we focused our interest towards ammonium photo-catalytic oxidation.

6.3.2 Photocatalytic Ammonium Oxidation

Photocatalytic ammonium oxidation is an environmentally friendly technique for ammonium oxidation, since only UV light and a suitable catalyst are required. Taking advantage of the knowledge in our laboratory about photocatalytic reactions and the availability of all equipment required, we have examined this strategy in depth. Commercial, and non-toxic, P25 Titania (TiO_2 , Degussa) prepared by flame pyrolysis was chosen as the catalyst for ammonium photooxidation. Capability of the material for such photo-oxidative reactions has been reported during the last 15 years by the scientific community [12, 16]. Besides this standard well-known P25 photocatalyst, other catalysts were also tested, namely NH_3 -treated P25, commercial Ta_2O_5 (tantalum (V) oxide, 99.993%; Alfa Aesar) and photo-deposited 0.5 wt% Pt/P25. Among them, only P25-based catalysts showed good activity and these results are described below.

Round bottom flask equipped with cooling jacket for temperature control (built in our glass blowing workshop) was used as batch photo-reactor (Figure 6.5) with catalyst concentration of 3 g/L under vigorous stirring. The light source was a UV-curing 100 W high-pressure Hg lamp (Handy Cure HLR400T-1, Senlight Corp. with a nominal UV-light intensity of 170 mW/cm^2 , specified by the supplier). Round UVFC window was placed on top (EK SMA OPTICS, 1 cm thick) to avoid evaporation of the solution (Figure 6.5).

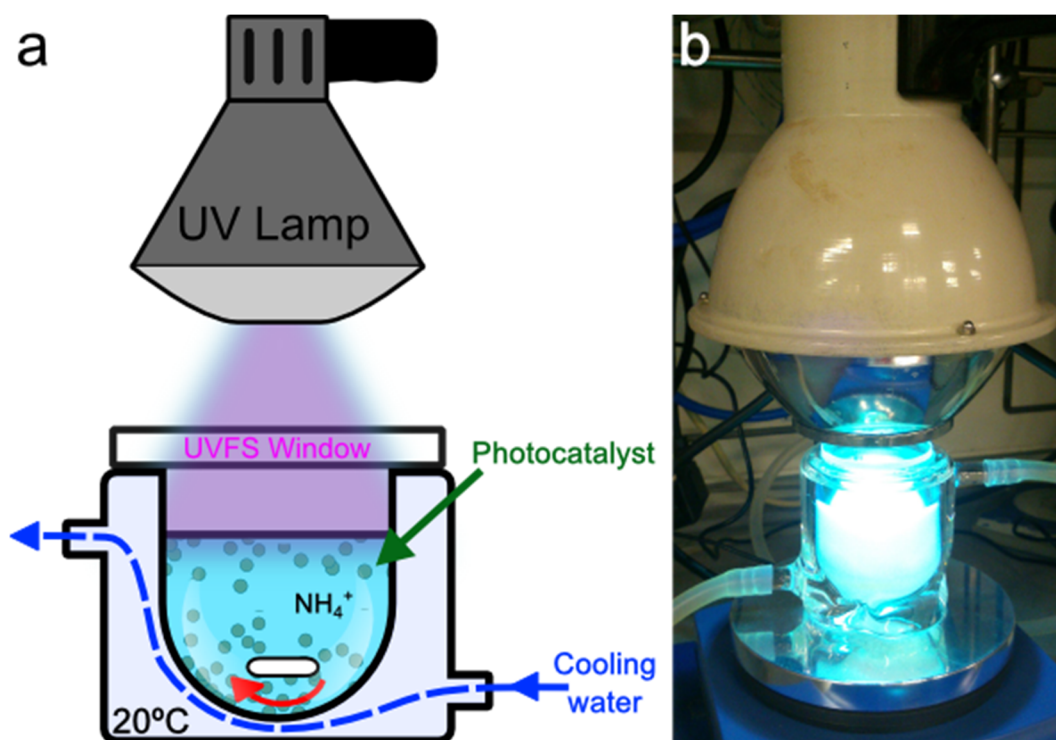


Figure 6.5. Batch reactor used for photocatalytic ammonium oxidation. (a) Schematic representation and (b) lab system equipped with cooling water.

Selectivity towards N_2 was the key factor in order to evaluate the feasibility of photo-oxidation approach. Metal doped P25 is known to enhance NH_4^+ conversion into N_2 [10]. In this work, photo-deposited Pt/P25 is used because it has been reported as one of the most promising photocatalysts to convert NH_4^+ into H_2 and N_2 as main products [11]. Bare P25 is also well known for its capabilities to convert NH_4^+ to NO_3^- and NO_2^- . [10, 12]. Figure 6.6 shows a comparison between P25 and Pt/P25 in terms of $X_{NO_3^-}$ and S_{N_2} during 6 h of photo-oxidation of 1000 ppm NH_4^+ (pH ca. 11) at room temperature (ca. 20 °C).

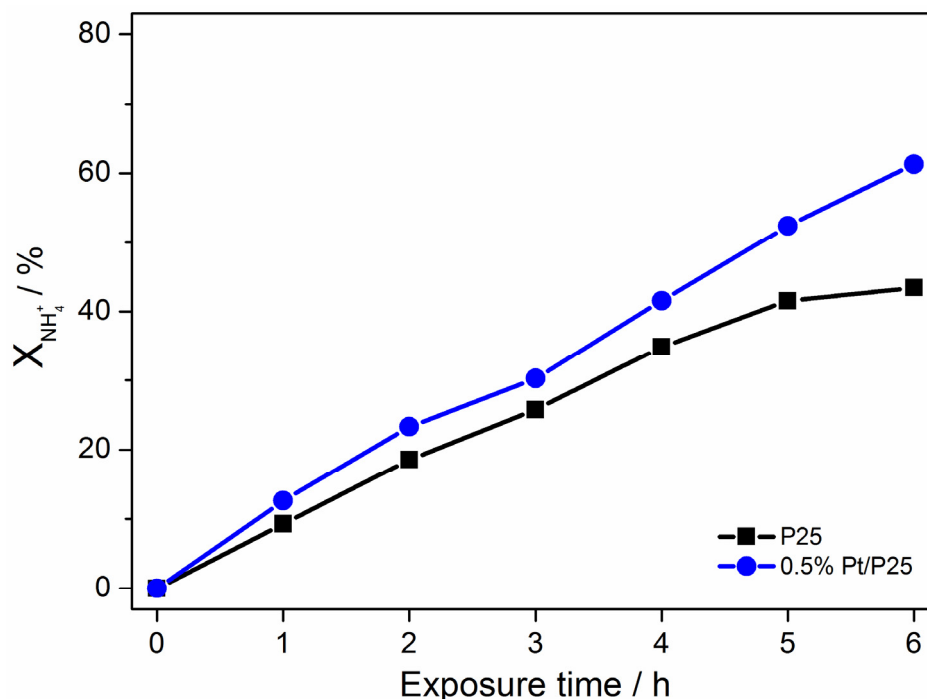


Figure 6.6. Conversion NH_4^+ versus UV-light exposure time at 20 °C using 3 g/L of (blue ●) 0.5 wt% Pt/P25 and (black ■) P25. Initial concentration of ammonium ion was 1000 ppm.

NH_4^+ conversion profile (Figure 6.6) elucidated that photocatalytic reaction took place over both materials. As expected, Pt/P25 showed better photocatalytic activity for ammonium transformation (ca. 60%) than raw P25 (ca. 40%) after 6 h of continuous exposure to UV radiation. Furthermore, for all reaction sampling points Pt/P25 catalyst gave consistently better performance.

From the results of reaction selectivity shown in Table 6.1, after first hour of exposure to UV-light both materials achieved similar total selectivity towards nitrate and nitrite ($S_{\text{NO}_x^-} = S_{\text{NO}_2^-} + S_{\text{NO}_3^-}$). Thus, assuming nitrogen selectivity (S_{N_2}) as the difference in between S_{Total} (100%) and $S_{\text{NO}_x^-}$, maximum value achieved of S_{N_2} was ca. 70% for both materials after 6 h. The concentration of nitrates is rather high after this process, but this scenario is better than higher concentrations of nitrites and ammonium ion because of more stringent

regulations of the latter ions. Evidently, 0.5 wt% Pt/P25 nitrate formation was enhanced compared with that of P25 (Table 6.1). From the concentration evolutions of nitrites and nitrates, it is evidenced that the presence of Pt on P25 enhances the secondary oxidation of nitrites to nitrates.

Table 6.1. Product distribution versus exposure time for 0.5 wt% Pt/P25 and P25. Ammonium onset concentration of 1000 ppm. Working temperature 20°C. S_i in (%), where $S_{NO_x^-} = S_{NO_2^-} + S_{NO_3^-}$.

Exposure time / h	P25			0.5 wt% Pt/P25		
	$S_{NO_2^-}$	$S_{NO_3^-}$	$S_{NO_x^-}$	$S_{NO_2^-}$	$S_{NO_3^-}$	$S_{NO_x^-}$
1	21.1	3.90	25.0	25.1	10.3	35.4
2	24.8	4.20	29.0	16.3	10.9	27.2
3	26.0	4.00	30.0	11.8	18.1	29.9
4	23.8	4.40	28.2	6.90	24.0	30.9
5	24.5	4.40	28.9	3.00	28.0	31.0
6	24.7	4.20	28.9	1.00	29.0	30.0

After confirming catalytic activity, photocatalytic ammonium oxidation and its product selectivity, next step was the evaluation of the approach using the effluent stream after electrolysis-assisted nitrate reduction. Only 0.5 wt% Pt/P25 was tested since its better performance (Figure 6.6 and Table 6.1) compared to P25. The typical effluent solution containing ca. 8 ppm NH_4^+ (pH ca. 9) was tested under the same condition (6 h, 20 °C, stirring, 100W UV lamp) for its oxidation. Unfortunately, at 20 °C almost no conversion of NH_4^+ was observed (ca. <4%). For this reason higher reaction temperature was tested. Operation at 50 °C for 6 h enhanced the reaction performance to some extent, reaching roughly ca. 30%

NH_4^+ conversion. Thus, we concluded that probably the strategy is not as effective when the concentration of ammonium ion is low and prevents bringing down ammonium ion concentration up to the desired value (<0.5 ppm).

6.4 Reduction-Oxidation Cycle

After reaching the limit of the approaches tested above, we further evaluated possible ideas on how to deal with nitrates, nitrites and most importantly ammonium ions. As the result, a combined Red-Ox cycle is proposed here (Figure 6.7), stimulated by the concept given by Al Sawah and co-workers [10]. This new model graphically shown in Figure 6.7 combines two processes in one; where waste and process water (for H^+/H_2 production) would be required as feedstock and the main products would be clean water and nitrogen. Once formed nitrate and ammonium would be continuously recycled (reduction and re-oxidation in loop) until the desired quality of water is reached.

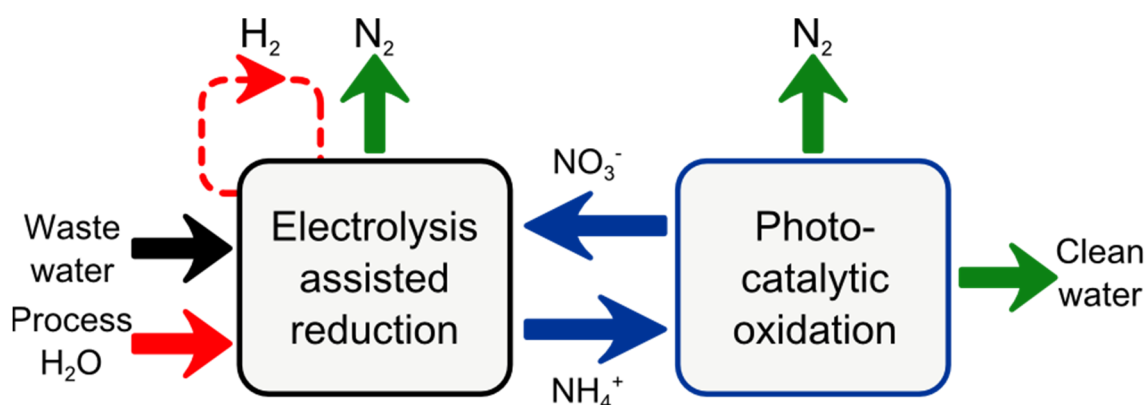


Figure 6.7. All in one reduction-oxidation cycle proposed for water denitrification. Idea taken from literature [10].

An electrolysis-assisted-photocatalytic system was developed taking advantage of positive effects resulting from electrolysis-assisted nitrate reduction process either in continuous or batch mode (high nitrate conversion, > 90% and low $S_{NO_2^-}$) and the possibility of ammonium oxidation via photocatalytic route, (Figure 6.8). Among all strategies and modifications examined for electrolysis-assisted reduction system, the most convenient one to couple with photo-reaction system was electro-batch configuration (Figure 6.1) giving $X_{NO_3^-} > 90\%$, $S_{NO_2^-}$ ca. 8% and $S_{NH_4^+}$ ca. 50%. This combination was possible by covering the cell with a UV-light transparent window instead of a plastic one used previously. (Figure 6.8).

Square UVFS window (1 cm thick) was placed on top of cathode reservoir to irradiate the desired spectrum of the UV-light. Standard MEA composition was employed, using 40 wt% PdCu/SnO₂ as cathode material. Photocatalysts (0.5 wt% Pt/P25) was suspended in solution by means of vigorous stirring inside cathode compartment (Figure 6.8a). Real appearance of the lab-scale cell is shown in Figure 6.8b.

As an example, results obtained after 8 h of continuous batch operation (100 ppm synthetic nitrate solution) under photoelectro-conditions were: $X_{NO_3^-} > 97\%$, $S_{NO_2^-}$ ca. 0.6% and $S_{NH_4^+}$ ca. 2.0%, with final concentrations for NO₃⁻, NO₂⁻ and NH₄⁺ being ca. 2.4, 0.6 and 0.5 ppm, respectively. These values were very close to the final aim of this research (maximum limit for drinking water: 50, 0.1 and 0.5 ppm for NO₃⁻, NO₂⁻ and NH₄⁺, respectively). Notably, the high concentration of NH₄⁺ observed in our electro-batch approach was greatly solved.

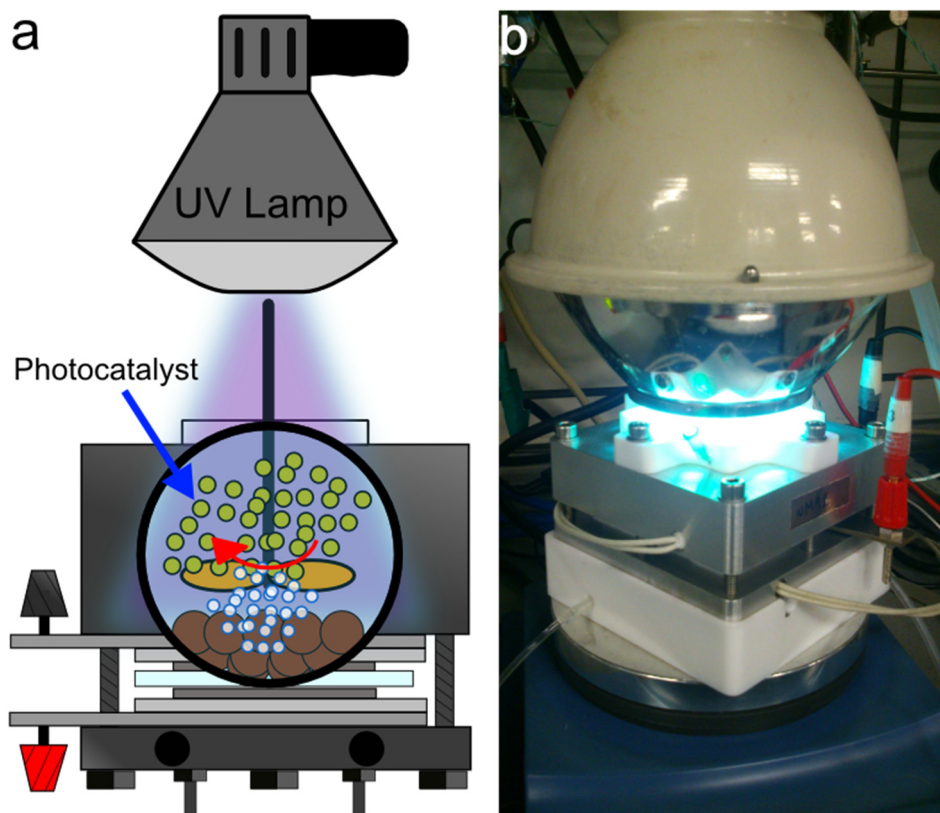


Figure 6.8. Reduction-oxidation in one step for water denitrification combining electro-batch reduction conditions with UV lamp irradiation (photoelectro-batch cathode). (a) Schematic representation and (b) lab system. Operation at 80 °C under stirring condition and 100 W UV light.

Only few tests could be performed using this new Red-Ox cycle system, since several issues such as cathode reservoir temperature and stirring efficiency to enable suitable photocatalyst dispersion had to be overcome. Therefore, further systematic measurements and optimization have to be performed to confirm the results and verify the power of such combinations to abate all nitrogen containing contaminants in water.

6.5 Conclusions

In this chapter, several system configurations, modifications and couplings for electrolysis-assisted nitrate reduction and ammonium ion oxidation were presented. The main aim was to develop a feasible and reliable strategy for (i) performance enhancement at low cell voltages and (ii) mitigation of by-products by adding secondary reaction step using one or two reactors.

Related with the enhancement of reaction performance under mild conditions, electro-batch configuration system was developed and tested in detail. Low current/potential operation (100 mA, average cell voltage of 1.8 V) was feasible with this configuration, achieving almost full conversion of nitrate and minimizing nitrite selectivity, although large ammonium ion production appeared as the main drawback of the process.

Different approaches were evaluated aiming for ammonia mitigation. Electrolysis-assisted ammonium ion oxidation strategy showed good performance; however, ammonia oxidation did not seem to occur since the ammonium ions accumulated at cathode by its transport through Nafion membrane.

A different photocatalytic oxidation approach was examined. Titania-based catalyst, P25 or Pt/P25, showed good conversion of ammonium (ca. 60%) and selectivity towards nitrogen (ca. 70%) when synthetic test solutions were employed, but the activity was not satisfactory with the real solution with low concentration of contaminants.

Finally as the last approach examined here, electrolysis-assisted nitrate reduction and photocatalytic ammonium oxidation were combined in one single

batch cell. Preliminary results were encouraging; reaching nearly the target concentration of the contaminants starting from 100 ppm of nitrates, although further experiments are required to guarantee both reliability and feasibility of this hybrid approach.

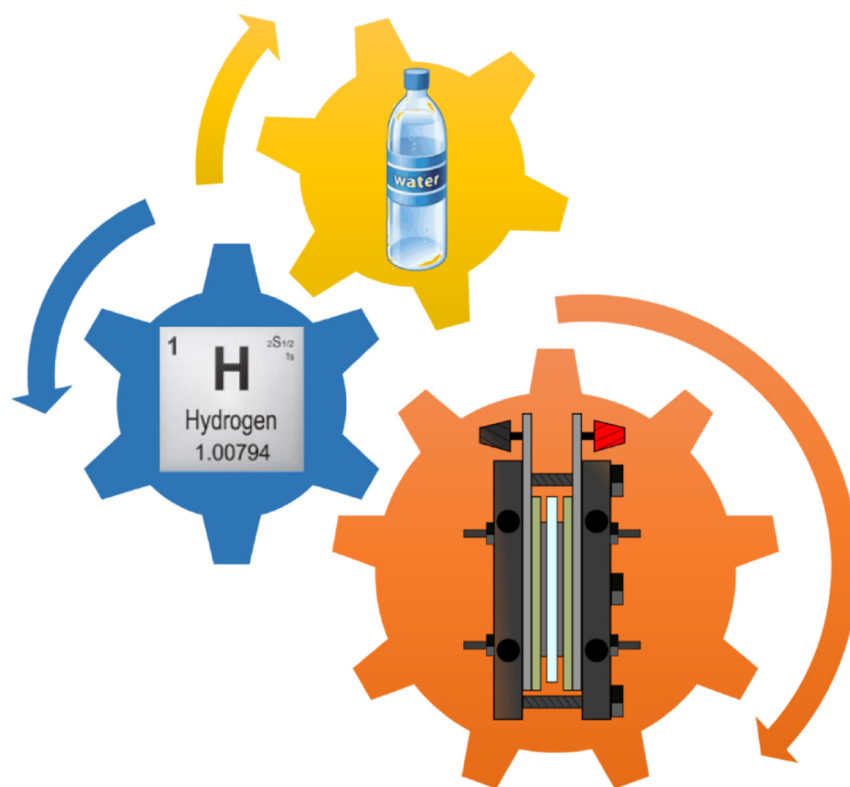
More importantly, the work presented in this chapter shows new directions and approaches for water denitrification and ammonium ion abatement. The electrolysis-assisted and combined approaches have been shown to be extremely powerful because of the great difficulty in achieving full selectivity to N_2 by nitrate reduction and consequent formation of NH_4^+ in reality. Thus, incorporation of an effective NH_4^+ mitigation method in nitrate reduction system seems to be promising.

BIBLIOGRAPHY

1. M. MACHIDA, K. SATO, I. ISHIBASHI, M. A. HASNAT, K. IKEUE, *CHEMICAL COMMUNICATIONS*, **732**, **2006**.
2. M. HASNAT, R. AGUI, S. HINOKUMA, T. YAMAGUCHI, M. MACHIDA, *CATALYSIS COMMUNICATIONS* **10**, 1132, **2009**.
3. M. HASNAT, M. KARIM, M. MACHIDA, *CATALYSIS COMMUNICATIONS* **10**, 1975, **2009**.
4. M. A. HASNAT, I. ISHIBASHI, K. SATO, R. AGUI, T. YAMAGUCHI, K. IKEUE, M. MACHIDA, *BULLETIN OF THE CHEMICAL SOCIETY OF JAPAN* **81**, 1675, **2008**.
5. M. BAERNS, R. IMBIHL, V. KONDRATENKO, R. KRAEHNERT, W. OFFERMANS, R. VAN SANTEN, A. SCHEIBE, *JOURNAL OF CATALYSIS* **232**, 226, **2005**.
6. R. IMBIHL, A. SCHEIBE, Y. ZENG, S. GÜNTHER, R. KRAEHNERT, V. KONDRATENKO, M. BAERNS, W. OFFERMANS, A. JANSEN, R. VAN SANTEN, *PHYSICAL CHEMISTRY CHEMICAL PHYSICS* **9**, 3522, **2007**.
7. N. J. BUNCE, D. BEJAN, *ELECTROCHIMICA ACTA* **56**, 8085, **2011**.
8. L. CANDIDO, J. A. C. PONCIANO GOMES, *MATERIALS CHEMISTRY AND PHYSICS* **129**, 1146, **2011**.
9. L. LI, Y. LIU, *JOURNAL OF HAZARDOUS MATERIALS* **161**, 1010, **2009**.
10. M. A. AL SAWAH, D. RICHARD, C. DE BELLEFON, J.-M. CHOVELON, C. FERRONATO, *COMPTES RENDUS CHIMIE* **13**, 502, **2010**.
11. J. NEMOTO, N. GOKAN, H. UENO, M. KANEKO, *JOURNAL OF PHOTOCHEMISTRY AND PHOTOBIOLOGY A-CHEMISTRY* **185**, 295, **2007**.
12. X. D. ZHU, S. R. CASTLEBERRY, M. A. NANNY, E. C. BUTLER, *ENVIRONMENTAL SCIENCE & TECHNOLOGY* **39**, 3784, **2005**.
13. M. D'ARINO, F. PINNA, G. STRUKUL, *APPLIED CATALYSIS B: ENVIRONMENTAL* **53**, 161, **2004**.
14. R. GAVAGNIN, L. BIASETTO, F. PINNA, G. STRUKUL, *APPLIED CATALYSIS B: ENVIRONMENTAL* **38**, 91, **2002**.
15. T. OKADA, H. SATOU, M. OKUNO, M. YUASA, *THE JOURNAL OF PHYSICAL CHEMISTRY B* **106**, 1267, **2002**.
16. E. M. BONSEN, S. SCHROETER, H. JACOBS, J. A. C. BROEKAERT, *CHEMOSPHERE* **35**, 1431, **1997**.

CHAPTER 7

SUMMARY AND OUTLOOK



7.1 Summary

Multipurpose polymer electrolyte membrane (PEM) electrocatalytic reactors operated at 80 °C and integrated in a continuous flow-through system for (i) hydrogen production and (ii) nitrate reduction; were successfully designed, constructed and evaluated for the target reactions, accomplishing the major tasks of this thesis. However, other related tasks such as materials synthesis, characterization, catalyst coating strategy optimisation, flow system design and reaction products analysis, were successfully accomplished too.

Utilisation and application of PEM technology has become hot topic in the last few decades [1-4], since it offers efficient alternatives for industrial-scale pure hydrogen production and electrochemical reactions. Despite of the knowledge reported in literature, the development of this project, initiated about 4 years ago, was very challenging.

Membrane electrode assembly (MEA) is the engine of the PEM system since catalyst layers as well as Nafion membrane are its main constituents. In fact, Red-Ox reactions take place over the electrode catalyst surface. Thus, successfully optimised processes related with MEA preparation include (i) catalyst synthesis, (ii) catalyst ink preparation and (iii) catalyst ink deposition over PEM. A standard MEA formulation was established for majority of the tests performed namely, IrO₂ | Nafion | CC, where CC refers to the cathode catalysts employed. Several anode catalysts were examined, and we finally selected iridium oxide (IrO₂) with 2 mg/cm² loading because of its stability and greater performance in water oxidation. Also, depending on purpose (i.e. target reaction) cathode catalyst material and composition were modified.

Efficient hydrogen production from water by PEM electrolysis using novel materials was the first goal to be achieved. For hydrogen evolution reaction (HER) commonly platinum or platinum supported catalyst (usually conducting support like carbon) are employed. These catalysts show excellent efficiency and low overpotentials, but their high price and low abundance will restrict their use in near future. Therefore, our attention was given to find promising alternative catalysts with high performance and - elemental abundance. On our quest for non-noble metal based catalyst, MoS₂ appeared as promising candidate, since it had been already tested for HER [5-7] with significant performance, although it had never been tested in PEM electrolysis. Systematic studies were performed in order to elucidate its feasibility. MoS₂ was found to be an efficient, inexpensive cathode catalyst for PEM electrolysis, especially when electrical conductivity of the catalyst material was enhanced by simple physical mixing of MoS₂ with highly conducting carbon materials (Vulcan) or by finely dispersing MoS₂ over reduced graphene oxide (RGO) [8]. The best performance (ca. 0.30 A/cm² at 1.9 V) among all the materials evaluated in this study was achieved with 47 wt% MoS₂/Vulcan. This material also showed high long-term stability up to 18 h of continuous operation in PEM electrolysis. This material's stability, facile preparation and improved performance when compared to pristine MoS₂ were encouraging features for practical application.

After this remarkable success, other common materials were tested in order to achieve a similar or better performance than that of MoS₂-based materials for HER. Following with the quest for novel materials, Co₃O₄ was found to be a promising candidate too. The material's capabilities, stability and robustness for both oxygen evolution reaction (OER) and oxygen reduction reaction (ORR)

have been already reported [9]. However, its performance for HER had never been tested before. Therefore, a similar study to that of MoS_2 was systematically performed by physically mixing with carbon black to increase the conductivity. In conclusion, Co_3O_4 was found to be very efficient and inexpensive cathode material for HER in PEM electrolysis at high potential range (2.0 to 2.7 V) when its electrical conductivity is enhanced by simple physical mixing with Vulcan. The best performance among all the materials tested was obtained with 47wt% Co_3O_4 /Vulcan (ca. 1.95 A/cm^2 at 2.7 V). Strikingly good long-term stability up to 24 h of continuous operation in PEM electrolysis was achieved at 2.5 V (ca. 1.5 A/cm^2), elucidating a high robustness of Co_3O_4 based materials for HER in electrolysis at high cell voltages.

After confirming the functionality of our electrochemical system as electrolyser, the idea of using this electrochemically evolved hydrogen to perform hydrogenation reaction came out. As the target reaction, we chose nitrate abatement by means of nitrate reduction from waste or ground water. Our major aim was to operate the reaction under continuous flow using supported catalysts. Specific cathode catalyst materials were synthesized and deposited over the PEM. In situ H_2 produced was directly used with no-requirement of an external source, like in case of classical catalytic reduction [10]. This approach was named in this work as electrolysis-assisted nitrate reduction. The feasibility of this concept was investigated, targeting at nearly full conversion of nitrate to N_2 . 40 wt% Pt, Pd, Cu and PdCu (4:1) catalysts supported over SnO_2 were synthesized and further tested in MEA format (IrO₂ | Nafion | 40 wt% M/ SnO_2 , M: Pt, Pd, Cu, PdCu). Product distribution was determined by ion chromatography (IC).

After verifying the suitability of 40 wt% M/SnO₂ catalysts for nitrate reduction (standard catalytic hydrogenation), these catalysts were tested for electrolysis-assisted nitrate reduction. Based on the potential sweep experiments, 40 wt% PdCu was found to be the best performing material with nitrate conversion ($X_{\text{NO}_3^-}$) and total selectivity to undesired side products (S_{Side} ; sum of nitrite and ammonium ion selectivity) of ca. 97% and 4.0%, respectively. Such promising results are comparable with those already reported in literature [11] but with the added value of working with supported catalysts instead of pure metals and without pH buffering.

Taking into account pH evolution during reaction, nitrate reduction takes place via catalytic hydrogenation of NO₃⁻ by H₂, which was evolved electrochemically on the surface of the cathode. This mechanism, implies that the reduction of nitrate could be promoted significantly by applying a cathodic potential due to higher concentration of hydrogen/proton at the catalyst surface.

Furthermore, versatility of electrolysis-assisted systems was examined to enhance overall performance of the reaction and at same time exploring new ways of performing nitrate reduction reaction without modifying reaction cell design. Among all modifications explored, constant potential approach yielded the best overall results. Along the same direction, several system configurations involving cell modifications from continuous to batch, and various couplings of electrolysis-assisted and photocatalytic reactions were evaluated (Chapter 6). The main aim was to develop a feasible and reliable strategy to enhance the reaction performance at mild conditions (low cell voltage) and to minimise undesired by-products, nitrites and ammonium ion, by means of additional secondary step.

Electrolysis-assisted reduction in batch reactor (electro-batch) configuration was developed to perform the reaction at low cell voltage and electrical current. Low current/potential operation (100 mA, average cell voltage of 1.8 V) was feasible with this configuration, achieving almost full conversion of nitrate and minimizing nitrite selectivity. However, a great amount of ammonium ion production appeared as the main issue of the process.

To deal with that ammonium ion production, secondary treatment methodologies were evaluated, namely (i) electrolysis-assisted ammonium oxidation and (ii) photocatalytic oxidation. Oxidation of ammonium ion did not work as we expected using the electrolysis-assisted approach because ammonium ion could diffuse to the cathode compartment via Nafion membrane. It could be used as a potential removal strategy of ammonium ion but it was not an effective approach for its oxidation. For this reason, we tested a different approach, photocatalytic oxidation using titania-based catalysts. The results showed good conversion of ammonium (ca. 60%) and selectivity towards nitrogen (ca. 70%) when synthetic test solutions were employed. However, the method was not effective for actual effluent stream containing low concentration NH_4^+ .

Finally, electrolysis-assisted nitrate reduction was combined with photocatalytic ammonium oxidation in a batch reactor (photoelectro-batch system). The results were preliminary but excellent, showing feasibility of simultaneous abatement of nitrates, nitrites, and ammonium ion. This work shows a promising new strategy for deep nitrate reduction to N_2 .

7.2 Outlook

This thesis dealt with hydrogen production by PEM electrolysis and secondly electrolysis-assisted nitrate reduction. There are many ways to improve both reactions such as by improving cell design, material characteristics, and operation mode. Regarding the second part, i.e. electrolysis-assisted reduction, there are new open challenges in terms of new applications as a novel method for hydrogenation reaction. Among them, CO₂ electrochemical hydrogenation in gas phase by using PEM system attracted our attention. In the next sections, an overview about carbon dioxide transformation as well as strategy for electrolysis-assisted CO₂ hydrogenation will be presented.

7.2.1 Background on CO₂ Conversion

Converting captured CO₂ into products such as valuable chemicals, fuels, building materials, and other commodities could form an important part of a solution to reduce CO₂ emissions in an economic, ecological, thus sustainable way. Heterogeneous catalytic hydrogenation of CO₂ bears a strong potential to treat large amount of CO₂ in a short time, rendering it an important mean for CO₂ mitigation. In the past few decades conversion of CO₂ by means of catalytic hydrogenation has attracted considerable attention as one of the key processes for CO₂ fixation and as recycling of elemental carbon emitted as CO₂ [12]. Numerous research works have been reported on converting CO₂ into fundamental chemicals such as methanol [13], hydrocarbons, esters, and ethers by means of CO₂ hydrogenation.

Appropriate choice of catalysts allows conversion of CO₂ to useful chemicals by hydrogenation reaction [13, 14]. Bearing in mind the continuous decrease of fossil fuels resources, the needs to develop feasible, new and safe ways to store and distribute the energy as well as to produce efficiently manmade hydrocarbons out of CO₂ are urged due to its increasing abundance.

Heterogeneous catalytic processes facilitate convenient, continuous production of desired products. Three main different routes, namely thermo [12-14], photo [15-18] and electrocatalytic [19-22] routes, can be employed in order to hydrogenate CO₂ towards added value fuels and chemicals like methane and methanol. In each route, the driving force to carry out the reaction is different. In the case of thermocatalytic route pressure and temperature (P and T) are the key parameters (Figure 7.1a), while in photocatalytic pathway the driving force is commonly visible and/or UV light (Figure 7.1b). Finally, electrocatalytic strategy is driven by electrical potential and flow of electrons (Figure 7.1c).

All of the strategies shown in Figure 7.1 can be flexibly tuned and the reaction can operate under either batch or continuous flow conditions. Application of such strategies may give light to the current global concern about climate change due to CO₂ accumulation on the atmosphere. As previously mentioned, electrochemical route was chosen as outlook of this thesis for CO₂ reduction, since it is closely related to the topic presented in this thesis and we have already initiated the investigation. An overview of the current status of our research on electrochemical CO₂ reduction and future challenges will be described in the following section.

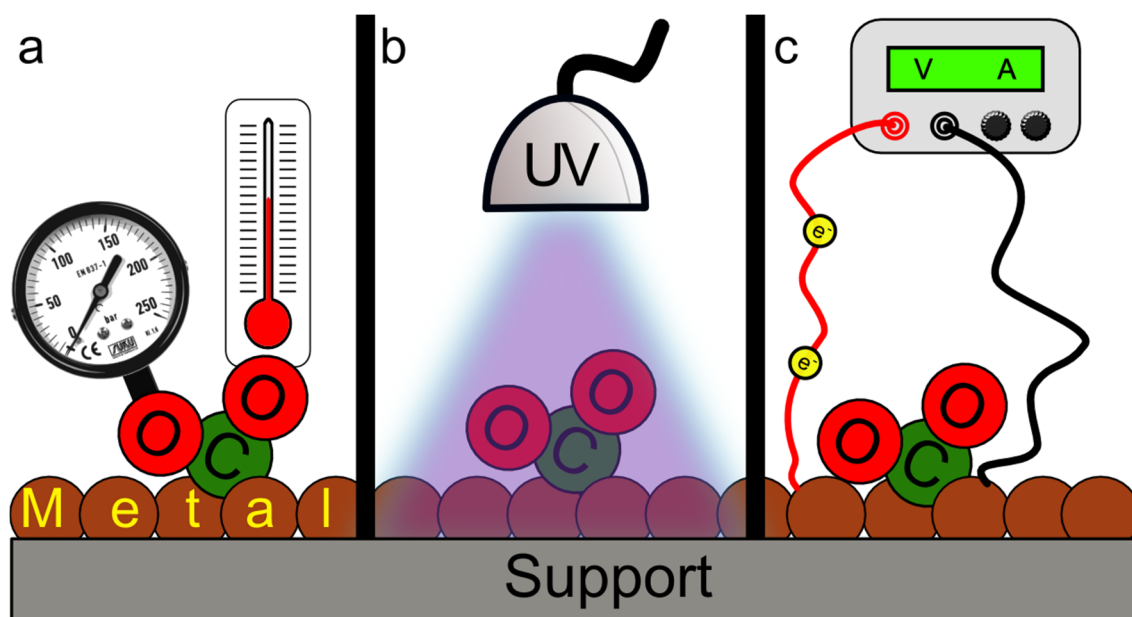


Figure 7.1. Common CO₂ mitigation strategies: (a) thermocatalytic, (b) photocatalytic and (c) electrocatalytic methods using heterogeneous catalysts.

7.2.2 Electrolysis-Assisted CO₂ Reduction

Making analogy with the nitrate reduction study, this approach is called electrolysis-assisted CO₂ reduction, since the goal is to (electro)catalytically reduce carbon dioxide by using in situ evolved hydrogen in an electrolyser cell. Based on the previous experience, (Chapters 5 and 6), a flow through system for gas phase CO₂ electrochemical reaction was designed (Figure 7.2). The PEM reactor is essentially the same as that described in Chapters 2 and 5, with some modifications to adapt the cell for gas phase reactions.

CO₂ is fed to the cathode compartment from a gas cylinder by means of an MFC. We expect that working temperature is an important parameter and it was raised to 120-200 °C, since the typical temperature used for electrolysis (80 °C) is likely too low for common CO₂ hydrogenation reactions. Moreover, operation

at higher temperature should be beneficial for the electrocatalytic process in terms of reaction kinetics.

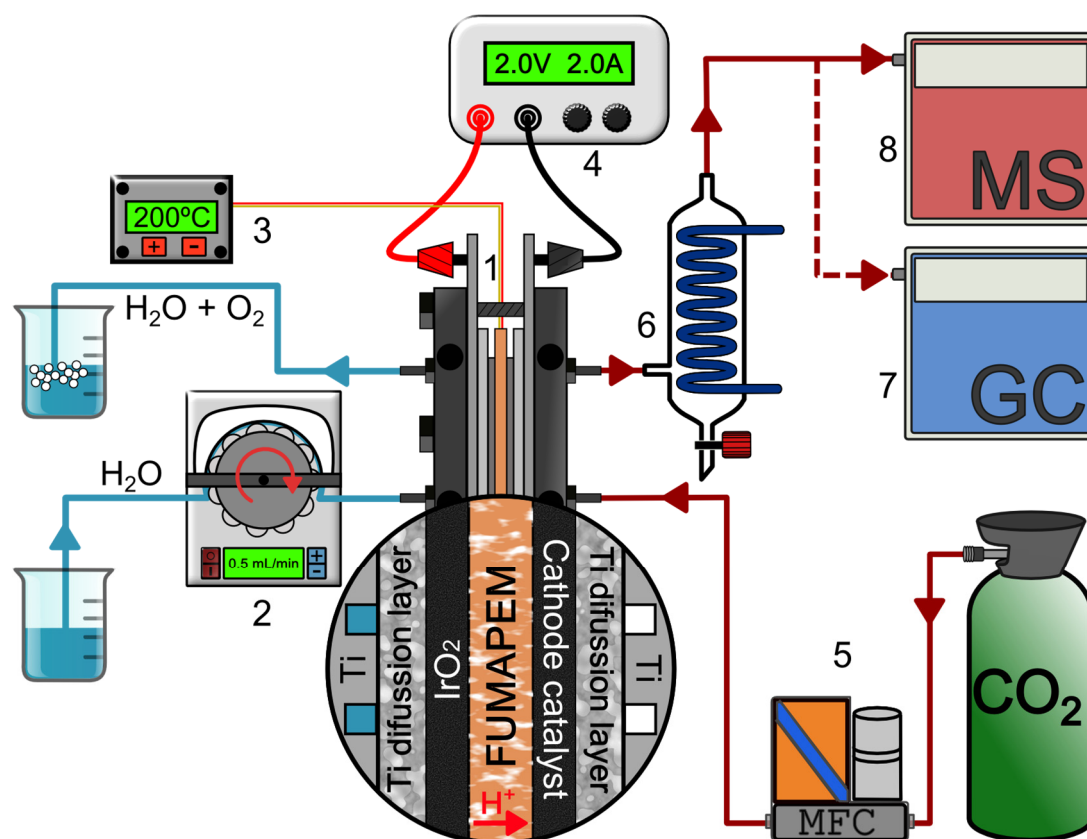


Figure 7.2. Continuous electrolysis-assisted gaseous CO₂ reduction system. (1) PEM reactor, (2) peristaltic pump and water reservoir, (3) temperature controller, (4) computer controlled power supply, (5) CO₂ source and mass flow controller (MFC), (6) water trap, (7) gas chromatograph (GC) and (8) mass spectrometer. Working temperature range of MEA is 120-200 °C.

Different type of PEM is required to handle the new system conditions since the traditional Nafion 117 membrane is not stable at high temperatures. A state of the art PEM (fumapem[®] AM membrane, fumatech, Germany; herein it is referred as fumapem) based on a polybenzimidazole copolymer was selected as new solid electrolyte media for CO₂ reduction system. This membrane,

widely employed for high-temperature PEM fuel cell (HT-PEMFC), allows proton transport at low relative humidity (%) conditions which is the actual situation inside the cell due to the high working temperature range (water is present as vapour instead of liquid). MEA composition is IrO₂ / fumaric acid / M, where M is referred to metal based catalyst in either supported or unsupported form. Finally, cell voltage is varied.

In our lab, currently preliminary tests are being performed using a wide set of MEAs. Good results are to be come in the near future. Nevertheless, it is feasible to test electrolysis-assisted CO₂ reduction and this work is in current progress. A number of parameters including catalysts and operation conditions will be examined in detail to identify highly energy efficient CO₂ mitigation strategy sourced by renewable electricity.

BIBLIOGRAPHY

1. M. CARMO, D. L. FRITZ, J. MERGE, D. STOLTEN, *INTERNATIONAL JOURNAL OF HYDROGEN ENERGY* **38**, 4901, **2013**.
2. P. MILLET, N. MBEMBA, S. A. GRIGORIEV, V. N. FATEEV, A. AUKAULOO, C. ETIEVANT, *INTERNATIONAL JOURNAL OF HYDROGEN ENERGY* **36**, 4134, **2011**.
3. P. MILLET, R. NGAMENI, S. GRIGORIEV, V. FATEEV, *INTERNATIONAL JOURNAL OF HYDROGEN ENERGY* **36**, 4156, **2011**.
4. P. MILLET, R. NGAMENI, S. GRIGORIEV, N. MBEMBA, F. BRISSET, A. RANJBARI, C. ETIEVANT, *INTERNATIONAL JOURNAL OF HYDROGEN ENERGY* **35**, 5043, **2010**.
5. T. F. JARAMILLO, K. P. JORGENSEN, J. BONDE, J. H. NIELSEN, S. HORCH, I. CHORKENDORFF, *SCIENCE* **317**, 100, **2007**.
6. H. I. KARUNADASA, E. MONTALVO, Y. SUN, M. MAJDA, J. R. LONG, C. J. CHANG, *SCIENCE* **335**, 698, **2012**.
7. A. B. LAURSEN, S. KEGNÆS, S. DAHL, I. CHORKENDORFF, *ENERGY & ENVIRONMENTAL SCIENCE* **5**, 5577, **2012**.
8. T. CORRALES-SÁNCHEZ, J. AMPURDANÉS, A. URAKAWA, *INTERNATIONAL JOURNAL OF HYDROGEN ENERGY* **39**, 20843, **2014**.
9. M. HAMDANI, R. SINGH, P. CHARTIER, *INT. J. ELECTROCHEM. SCI* **5**, 556, **2010**.
10. M. D'ARINO, F. PINNA, G. STRUKUL, *APPLIED CATALYSIS B: ENVIRONMENTAL* **53**, 161, **2004**.
11. M. A. HASNAT, I. ISHIBASHI, K. SATO, R. AGUI, T. YAMAGUCHI, K. IKEUE, M. MACHIDA, *BULLETIN OF THE CHEMICAL SOCIETY OF JAPAN* **81**, 1675, **2008**.
12. Y. NITTA, O. SUWATA, Y. IKEDA, Y. OKAMOTO, T. IMANAKA, *CATALYSIS LETTERS* **26**, 345, **1994**.
13. A. BANSODE, A. URAKAWA, *JOURNAL OF CATALYSIS* **309**, 66, **2014**.
14. A. BANSODE, B. TIDONA, P. R. VON ROHR, A. URAKAWA, *CATALYSIS SCIENCE & TECHNOLOGY* **3**, 767, **2013**.
15. A. BAZZO, A. URAKAWA, *CHEMSUSCHEM* **6**, 2095, **2013**.
16. A. FUJISHIMA, K. HONDA, *NOTES* **44**, 1971.
17. A. FUJISHIMA, K. HONDA, *NATURE* **238**, 37, **1972**.
18. T. INOUE, A. FUJISHIMA, S. KONISHI, K. HONDA, *NATURE* **277**, 637, **1979**.
19. K. OGURA, R. OOHARA, Y. KUDO, *JOURNAL OF THE ELECTROCHEMICAL SOCIETY* **152**, D213, **2005**.
20. K. OGURA, H. YANO, F. SHIRAI, *JOURNAL OF THE ELECTROCHEMICAL SOCIETY* **150**, D163, **2003**.

21. D. T. WHIPPLE, E. C. FINKE, P. J. KENIS, *ELECTROCHEMICAL AND SOLID-STATE LETTERS* **13**, B109, **2010**.
22. K. XIE, Y. ZHANG, G. MENG, J. T. IRVINE, *JOURNAL OF MATERIALS CHEMISTRY* **21**, 195, **2011**.

SHORTHANDS AND GLOSSARY

Nafion
MS RGO IC
ESEM OER MEA
BET GDL NEMCA
Vulcan PEM PTFE
TEM XRD
HER

BET: Brunauer–Emmett–Teller theory employed for the measurement of the specific surface area of a material (m^2/g)

CC: cathode catalyst

DC: direct current (mA or A)

EC: European Council

EDX: energy-dispersive X-ray spectroscopy

EEA: European Environment Agency

EPOC: electrochemical promotion of catalysis

ESEM: environmental scanning electron microscopy

GDL: gas diffusion layer

GO: graphene oxide

GR1Ti: grade 1 Titanium

HER: hydrogen evolution reaction

HHV: higher heating value (liquid water's enthalpy of dissociation, ca. 285.8 kJ/mol)

HTE: high temperature electrolyser (or electrolysis)

HTFC: high temperature fuel cell

HT-PEMFC: high temperature polymer electrolyte membrane fuel cell

IC: ion chromatograph (or chromatography)

IEA: International Energy Agency

MEA: membrane electrode assembly

MFC: mass flow controller

MID: multiple ion detection for mass spectrometry analysis

MilliQ H₂O: trademark created by Millipore Corporation to describe 'ultrapure' water in terms of resistivity (typically 18.2 M Ω ·cm at 25 °C)

MS: mass spectrometer (or spectrometry)

Nafion®: synthetic polymer with ionic properties (H⁺ transport) also called ionomer, developed by DuPont®

NEMCA: non-faradaic electrochemical modification of catalytic activity

OER: oxygen evolution reaction

ORR: oxygen reduction reaction

PEM: polymer electrolyte membrane

PEMFC: polymer electrolyte membrane fuel cell

PTFE: best known brand name is Teflon® by DuPont®

P25: titanium dioxide manufactured according to the AEROSIL® - process

RGO: reduced graphene oxide

SOEC: solid oxide electrolysis cell (or electrolyser)

SOFC: solid oxide fuel cell

TEM: transmission electron microscopy

TWSCs: thermochemical water splitting cycles

US-DOE: United States Department of Energy

UV: ultraviolet light

UVFS: ultraviolet fused silica

Vulcan-XC72®: conductive and high surface area carbon black type material

WHO: World Health Organization

XRD: x-ray diffraction

LIST OF PUBLICATIONS

JOURNAL PUBLICATIONS

Related with this thesis

“MoS₂-based materials as alternative cathode catalyst for PEM electrolysis”

Tachmajal Corrales-Sánchez, Jordi Ampurdanés and Atsushi Urakawa, *International Journal of Hydrogen Energy*, **2014**, 34, 20843

Previous journal publications

“Determination of choline and derivatives with a solid-contact ion-selective electrode based on octaamide cavitand and carbon nanotubes”

Jordi Ampurdanes, Gastón A Crespo, Alicia Maroto, M. Angeles Sarmentero, Pablo Ballester and F. Xavier Rius, *Biosensors & Bioelectronics*, **2009**, 25, 344

CONFERENCE CONTRIBUTIONS

Related with this thesis

11th European Congress on Catalysis (XI, Europacat), Lyon (France) – September 2013

Oral presentation contribution: *“Continuous Electrolysis-Assisted Nitrate Reduction”*

J. Ampurdanés and A. Urakawa

International Conference on Hydrogen Production (ICH2P'14), Fukuoka (Japan) – February 2014

Oral presentation contribution: *“Continuous Electrolysis-Assisted Nitrate Reduction”*

J. Ampurdanés and A. Urakawa

International Conference on Hydrogen Production (ICH2P'14), Fukuoka (Japan) – February 2014

Oral presentation contribution: *“MoS₂ – based catalysts as an alternative for hydrogen evolution on PEM electrolyzers”*

T. Corrales-Sánchez, J. Ampurdanés and A. Urakawa

Previous conference contributions

Mátrafüred'08 – International Conference on Electrochemical Sensors - Dobogókő (Hungary) - October 2008

Poster contribution: *“Determination of choline and derivatives using a solid-contact CNT-based ISE”*

J. Ampurdanés, G.A. Crespo, A. Maroto, M. A. Sarmentero, P. Ballester and F. X. Rius

II Workshop - Nanociencia y Nanotecnología Analíticas – Tarragona (Spain) – November 2008

Poster contribution: *“Solid-contact CNTs based electrode for the determination of trimethylammonium ions”*

J. Ampurdanés, G.A. Crespo, A. Maroto, M. A. Sarmentero, P. Ballester and F. X. Rius

CURRICULUM VITAE

AMPURDANÉS VILANOVA, JORDI

Tarragona (Spain), 16th October 2014

Date of birth 23/04/1984
Place of birth Artesa de Segre (Catalunya, Spain)
Nationality Spanish
Email jampurdanes@iciq.es , jordi.ampurdanes@gmail.com

EDUCATION AND TRAINING

07.2010-12.2014 **PhD Student**
ICIQ – Institute of Chemical Research of Catalonia
(Tarragona, Spain)
PhD Thesis: *“Novel Catalytic Material and Strategies For Hydrogen Production and Hydrogenation Reactions based on PEM Electrolysis”*
Supervisor: Dr. Atsushi Urakawa

07.2007-09.2008 **MSc. in Nanoscience and Nanotechnology**
URV - Universitat Rovira i Virgili (Tarragona, Spain)
Master Thesis: *“Development of a Solid-Contact CNT-based Electrode for the Determination of Choline and Derivatives”*
Supervisor: Prof. F. Xavier Rius Ruiz

09.2006-06.2007 **MSc. in Chemical Engineering and processes**
URV - Universitat Rovira i Virgili (Tarragona, Spain)
Master Thesis: *“Aquifer Protection for Metals Pollutants Recovery in a Gold Mine in Yanacocha (Peru)”*
Supervisor: Vicenç Claramonte

09.2002-06.2007 **BSc. in Chemical Engineering**
URV - Universitat Rovira i Virgili (Tarragona, Spain)
Final Project: “*Aquifer Protection for Metals Pollutants Recovery in a Gold Mine in Yanacocha (Peru)*”
Supervisor: Vicenç Claramonte

GRANTS

ICIQ Predoctoral Fellowship, Institute of Chemical Research of Catalonia (Tarragona, Spain).

WORK EXPERIENCE

02.2009-06.2010 I+D technician at *NTSensors*, Spin-Off associated at Universitat Rovira i Virgili (Tarragona, Spain)